PHYSICAL REVIEW D **86,** 115022 (2012)

Constraining unparticles from top physics at the Tevatron

Mamta Dahiya,[1] Sukanta Dutta,[1] and Rashidul Islam[1,2,*]

[1]*SGTB Khalsa College, University of Delhi, Delhi-110007, India*

[2]*Department of Physics and Astrophysics, University of Delhi, Delhi-110007, India*

(Received 10 July 2012; published 21 December 2012)

We study and analyze the recent observations of the top pair production $\sigma(p\bar{p} \to t\bar{t})$ at the Tevatron through flavor conserving and flavor violating channels via vector and tensor unparticles. The unparticle sector is considered with the possibility of being a color singlet or octet. The modified unparticle propagator is used to investigate the contribution of these unparticles to the observed $A_{\rm FB}^{t\bar{t}}$ (forward-backward asymmetry in top pair production) and the spin correlation at the Tevatron. We have also studied the impact of the flavor violating couplings of unparticles to the third generation quarks on (a) pair production of same sign tops/antitops $\sigma(p\bar{p} \to tt + \bar{t}\,\bar{t})$ at the Tevatron and (b) the partial top decay width for $\Gamma_{\mathcal{U}}(t \to u\mathcal{U}^V)$. We find that a large region of parameter space is consistent with the measurements of the $t\bar{t}$ production cross section, $A_{\rm FB}^{t\bar{t}}$, and spin correlation coefficient at the Tevatron, and we observe that the top decay width measurement constrains the flavor violating coupling of vector unparticles more severely than the same sign top/antitop production at the Tevatron. We also predict the best point set in the model parameter space for specific choices of $d_{\mathcal{U}}$ corresponding to $\chi^2_{\rm min}$, evaluated using the $m_{t\bar{t}}$ spectrum of $A_{\rm FB}^{t\bar{t}}$ from the data set of Run II of the Tevatron at the integrated luminosity 8.7 fb^{-1}. Our results and analysis are consistent even with unparticle theories that have broken scale invariance, as long as the infrared cutoff scale is much less than the top pair production threshold.

DOI: 10.1103/PhysRevD.86.115022 PACS numbers: 14.80.−j, 12.38.Qk, 12.60.−i, 12.90.+b

I. INTRODUCTION

The study of the top quark production and related discrepancies at the Tevatron and LHC might hold the key to new physics beyond the standard model (SM). Both the CDF and D0 collaborations have consistently measured values of $t\bar{t}$ production cross sections through various decay channels [1–3], and they are all consistent with the theoretical predictions at the next-to-next-to-leading order (NNLO) level [4,5]. On the other hand, the top quark forward-backward asymmetry is observed to be significantly larger than what the SM predicts [6–10]. The recent measurements of $A_{\rm FB}^{t\bar{t}}$ at CDF obtain a parton level asymmetry of 0.296 ± 0.067 for $m_{t\bar{t}} > 450$ GeV with 8.7 fb^{-1} of data, in contrast to the next-to-leading order (NLO) QCD prediction of 0.100 [7]. It has also been observed that in the $t\bar{t}$ rest frame, the asymmetry increases with the $t\bar{t}$ rapidity difference and with the invariant mass. If this asymmetry is true, it should indicate the presence of new physics. Hence, the study of this subject has drawn a lot of attention and various explanations have been given for the observed deviations in the context of different new physics scenarios [11–16]. Any model trying to account for the high values of $A_{\rm FB}^{t\bar{t}}$ is constrained by the SM consistency in the measured cross section and $m_{t\bar{t}}$ spectrum of $A_{\rm FB}^{t\bar{t}}$.

In the present article we examine the forward-backward (FB) asymmetry and spin correlations in top pair production at the Tevatron with the possibility of the existence of a conformally invariant hidden sector containing unparticles coupling weakly with SM fields [17]. The effective couplings of unparticles with SM fields are likely to interfere with the SM processes and hence affect the $A_{\rm FB}^{t\bar{t}}$ and the top spin correlations. Effects of unparticles on the top-antitop quark pair production process at hadron colliders and the International Linear Collider have been studied in Refs. [18–20].

We organize the paper as follows: Calculation of forward-backward asymmetry $A_{\rm FB}^{t\bar{t}}$ and that of spin correlation $C^{t\bar{t}}$ are discussed in Secs. II A and II B respectively. We review the unparticle scenario in Sec. III. Numerical results for the flavor conserving and violating interactions are given in Sec. IV. Section V analyzes the constraints to the flavor violating channels emerging from two important experimental signatures: (a) same sign top production and (b) top decay width. Section VI presents the χ^2 analysis of the model and exhibits the $m_{t\bar{t}}$ distribution of $A_{\rm FB}^{t\bar{t}}$. This section also addresses the implication of the broken scale invariance by introduction of a mass gap and, finally, summarizes the observations.

II. THE OBSERVABLES

A. Forward-backward asymmetry

The $t\bar{t}$ differential charge asymmetry at the partonic level is defined as $A_C(\cos\theta) = \frac{N_t(\cos\theta) - N_{\bar{t}}(\cos\theta)}{N_t(\cos\theta) + N_{\bar{t}}(\cos\theta)}$, where $N_t(\cos\theta) = d\sigma^{t\bar{t}}/d(\cos\theta)$, θ being the polar angle of the top quark momentum with respect to the incoming parton in the $t\bar{t}$ rest frame (which is the same as the $q\bar{q}$ rest frame for $q\bar{q} \to t\bar{t}$, the dominant production process at the Tevatron), while in the lab frame it will correspond to the polar angle between the top quark and the proton beam.

*rislam@physics.du.ac.in

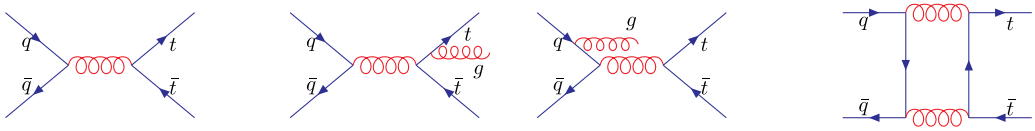

FIG. 1 (color online). QCD diagrams contributing to charge asymmetry in top pair production.

The charge conjugation invariance of the strong interaction would imply $N_t(\cos\theta) = N_{\bar{t}}(-\cos\theta)$ and the difference in the production of top quarks in the forward and backward hemispheres is equivalent to the difference in the production of top and antitop quarks in the forward hemisphere. Thus, the integrated FB asymmetry in the lab frame is equivalent to the charge asymmetry and can be written as

$$A_{\mathrm{FB}}^{t\bar{t}} = \frac{N_t(\cos\theta \geq 0) - N_t(\cos\theta \leq 0)}{N_t(\cos\theta \geq 0) + N_t(\cos\theta \leq 0)}. \quad (1)$$

Collinear initial-state radiation (ISR) makes the fundamental $q\bar{q}$ frame inaccessible in both experiment and simulation, leaving a choice between the $t\bar{t}$ rest frame or the lab ($p\bar{p}$) frame. The direction of top quarks in the lab frame can be determined using the cosine of the polar angle between the hadronically decaying top quark and the proton beam. However, the information on fundamental production asymmetry in the lab frame is diluted because of an uncontrolled longitudinal boost from the rest frame of primary $q\bar{q}$ interaction to the laboratory frame. In the $t\bar{t}$ rest frame, a measurement of the variable $\cos\theta$ in Eq. (1) requires reconstruction of the initial parton ($q\bar{q}$) rest frame, which is not accessible experimentally. Hence, instead of $\cos\theta$, the rapidity difference Δy between the top quark y_t and the antitop quark $y_{\bar{t}}$ is considered as the sensitive variable for the experimental measurement of $A_{\mathrm{FB}}^{t\bar{t}}$ in the $t\bar{t}$ rest frame. This variable (being Lorentz invariant) can be measured in the lab frame and the shape of rapidity distributions $d\sigma/dy$ in the two frames would remain the same if the boost is by a constant velocity. Experimentally, the rapidity difference Δy is calculated from the rapidity difference $y_{l_t^+(l_{\bar{t}}^-)} - y_{h_{\bar{t}}(h_t)}$ of the semileptonically decaying top and the hadronically decaying top [10], and the top rapidity in the $t\bar{t}$ rest frame comes out to be $\frac{1}{2}\Delta y$ in the limit of small p_T. The variables Δy and $\cos\theta$ are directly related by

$$y_t - y_{\bar{t}} = \Delta y = 2\tanh^{-1}\left(\frac{\cos\theta}{\sqrt{1 - \frac{4m_t^2}{\hat{s}}}}\right), \quad (2)$$

m_t being the top mass and $\hat{s}$ the square of the center-of-mass energy of the $t\bar{t}$ pair. Thus, Δy is a close estimate of the production angle in the $t\bar{t}$ frame. Also, the sign of the rapidity difference is the same as $\cos\theta$. Thus, the asymmetry in Δy is identical to the asymmetry in the top production angle $\cos\theta$ in the $t\bar{t}$ rest frame, allowing an effective measurement in the $t\bar{t}$ frame. Hence, D0 and CDF have considered the following observable which also reflects the integrated charge asymmetry in $t\bar{t}$ production at the Tevatron:

$$A_{\mathrm{FB}}^{t\bar{t}} = \frac{N[\Delta y \geq 0] - N[\Delta y \leq 0]}{N[\Delta y \geq 0] + N[\Delta y \leq 0]} = \frac{N_+ - N_-}{N_+ + N_-}, \quad (3)$$

N_+ (N_-) being the number of events with a positive (negative) rapidity difference.

Within the SM, the differential distributions of top and antitop quarks are identical at leading order in α_s. At NLO [$\mathcal{O}(\alpha_s^3)$], the dominant positive FB asymmetry is generated from the interference between the Born amplitude and two-gluon exchange (box) along with a negative asymmetry from the interference of initial state and final state gluon bremsstrahlung (Fig. 1). The inclusive charge asymmetry receives a contribution from the radiative corrections to quark-antiquark annihilation (mentioned above) and also from interference between various amplitudes contributing to quark-gluon scattering ($qg \rightarrow t\bar{t}q$ and $\bar{q}g \rightarrow t\bar{t}\,\bar{q}$), the latter contribution being much smaller than the former. Gluon-gluon fusion remains charge symmetric, and the gg initial state does not contribute to this asymmetry at any order in perturbation theory due to the fact that the gluon distribution is the same for protons and antiprotons. However, it lowers the average value. QCD predicts the size of this asymmetry to be 5% to 8% [21,22]. The measurement of the total FB asymmetry has been carried out by CDF and D0 collaborations at the Tevatron in both the laboratory frame ($p\bar{p}$ frame) and the center-of-mass frame of the top pair ($t\bar{t}$ frame) [6,9,10] (see Table I). While the other Tevatron measurements of top quark properties (e.g., production cross section) are all consistent with the SM, all of the past measurements of CDF and D0 have

TABLE I. Values of forward-backward asymmetry as measured by CDF and D0, along with the SM theoretical value.

Description	Value of $A_{\mathrm{FB}}^{t\bar{t}}$ in specific frame ($p\bar{p}$ rest frame or $t\bar{t}$ rest frame)
CDF ($L = 8.7$ fb^{-1}) (semileptonic)	$0.162 \pm .047^{[\mathrm{stat+syst}]}$ ($t\bar{t}$) [7]
CDF ($L \sim 5$ fb^{-1}) (combined)	$0.201 \pm .067^{[\mathrm{stat+syst}]}$ [8] $0.158 \pm .072^{(\mathrm{stat})} \pm .017^{(\mathrm{syst})}$ ($t\bar{t}$)
CDF ($L = 5.1$ fb^{-1}) (dileptonic)	$0.42 \pm .15^{\mathrm{stat}} \pm .05^{(\mathrm{syst})}$ ($t\bar{t}$) [9]
DØ ($L = 5.4$ fb^{-1}) (lepton + jets)	$(15.2 \pm 4.0)\%$ ($t\bar{t}$) [6]
SM (NNLO)	$0.052^{+0.000}_{-0.006}$ ($p\bar{p}$) [22]

consistently yielded a higher $A_{\rm FB}^{t\bar{t}}$ than SM prediction by more than a 2σ deviation (see Table I). CDF has also released the functional dependence of the $t\bar{t}$ rest frame asymmetry on Δy and on $m_{t\bar{t}}$ [7].

There have been many efforts [11] in the literature to explain the large excess of top asymmetry observed at the Tevatron. One challenge is to realize a model which can generate a large $A_{\rm FB}^{t\bar{t}}$ without making an appreciable change in the observed $t\bar{t}$ production cross section or invariant mass spectrum. The all-channel measurement from CDF with 4.6 fb^{-1} of data [1] is $\sigma(t\bar{t}) = 7.5 \pm 0.31(\text{stat}) \pm 0.34(\text{syst}) \pm 0.15(Z\,\text{theory})$ pb for $m_t = 172.5$ GeV, in good agreement with the SM prediction of $\sigma(t\bar{t})^{\rm NNLO}_{\rm SM} = 7.08^{+0.00+0.36}_{-0.24-0.27}$ pb for $m_t = 173$ GeV [4], and is consistent with measurements from D0 [3].

References [13,14] have compared various models in light of CDF measurements of $A_{\rm FB}^{t\bar{t}}$ and invariant mass distributions. They show that axigluon and heavy Z' models are highly constrained, while Ref. [15] further demonstrates that Z' and W' models are disfavored by the LHC measurements.

Reference [16] studies the $A_{\rm FB}^{t\bar{t}}$ in the framework of unparticles. They have only considered a colored octet vector unparticle in the s channel having flavor conserving couplings to quarks. We shall compare our results for this particular case with them.

B. Spin correlation

Due to its large mass, the top quark decays before hadronization, leading to preservation of its spin information. In the leading order in the SM, top quarks remain unpolarized because they are mainly produced by parity conserving QCD interaction. The decay of top quarks via electroweak (EW) interaction, which is negligible with respect to the strong interaction, leaves a very small effect on top polarization [23]. The angular distribution of the partial top quark decay width Γ in $t \to W^+ + b$, followed by $W^+ \to l^+ + \nu$ or $\bar{d} + u$, is correlated with the top spin axis [24,25] as follows:

$$\frac{1}{\Gamma_t}\frac{d\Gamma}{d\cos\chi_i} = \frac{1}{2}(1 + \alpha_i \cos\chi_i);$$
$$\alpha_i = \begin{cases} +1 & \text{for } l^+, \bar{d} \\ -.31 & \text{for } \bar{\nu}, u \\ -.41 & \text{for } b \end{cases}, \tag{4}$$

where Γ_t is the total top decay width and χ_i is the angle between the ith decay product and the top quark spin axis in the top quark rest frame. Since net polarization of the top quarks is negligible in leading order, the correlation between the ith decay product of the top and $\bar{i}$th decay product of the antitop can be expressed by

$$\frac{1}{\sigma_{i\bar{i}}}\frac{d^2\sigma_{i\bar{i}}}{d\cos\chi_i d\cos\bar{\chi}_{\bar{i}}} = \frac{1}{4}(1 + C^{i\bar{i}}\alpha_i\bar{\alpha}_{\bar{i}}\cos\chi_i\cos\bar{\chi}_{\bar{i}}), \tag{5}$$

with

$$C^{i\bar{i}} = \frac{\sigma_{\uparrow\uparrow} + \sigma_{\downarrow\downarrow} - \sigma_{\uparrow\downarrow} - \sigma_{\downarrow\uparrow}}{\sigma_{\uparrow\uparrow} + \sigma_{\downarrow\downarrow} + \sigma_{\uparrow\downarrow} + \sigma_{\downarrow\uparrow}}. \tag{6}$$

$\sigma_{\uparrow/\downarrow\uparrow/\downarrow}$ is the production cross section for top quark pairs where the top quark has spin up or down with respect to the top spin axis and the antitop has spin up or down with respect to the antitop spin axis.

Mahlon and Parke discussed the right choice for the spin axes of the top quark pair, since a poor choice of spin axes can lead to a small value of $C^{i\bar{i}}$ [26]. They proposed three choices for the spin axis, namely, helicity basis, beamline basis, and off-diagonal basis.

We choose the helicity basis (top quark momentum is chosen as the spin quantization axis) for our calculation. In the $t\bar{t}$ rest frame, the quarks move back-to-back and the same spin ($S = 1$) states are those with opposite helicity, so that in the helicity basis

$$C^{t\bar{t}} = \frac{\sigma_{RL} + \sigma_{LR} - \sigma_{RR} - \sigma_{LL}}{\sigma_{RR} + \sigma_{LL} + \sigma_{RL} + \sigma_{LR}}. \tag{7}$$

The dominant production mechanism for the $t\bar{t}$ pairs at the Tevatron is $qq \to t\bar{t}$ with a $J = 1$ gluon exchanged in the s channel. Near threshold, the $t\bar{t}$ pair is produced in the $S = 1$ state with the eigenstates $|++\rangle$, $\frac{1}{\sqrt{2}}(|+-\rangle + |-+\rangle)$, $|--\rangle$. Two of the three states have the opposite helicity (same spin); hence, the correlation near threshold is $C_{t\bar{t}} = 33\%$, while helicity conservation at high energy ensures that the t and $\bar{t}$ are produced with the opposite helicity and $C_{t\bar{t}} = 100\%$ at very high energies [27]. CDF has reported the value of top spin correlation in the helicity basis to be $0.60 \pm 0.50(\text{stat}) \pm 0.16(\text{syst})$ [28] and in the beam basis to be $0.042^{+0.563}_{-.562}$ [29]. The D0 measurement for the spin correlation coefficient is $-.66 < -C^{t\bar{t}} < 0.81$ in the beam basis [30]. The SM values for the same in the beam and helicity basis are -0.614 and 0.299, respectively [31].

The terms linear in $\cos\theta$ do not contribute to $C^{t\bar{t}}$ after integration over $\cos\theta$. Thus, $C^{t\bar{t}}$ and $A_{\rm FB}^{t\bar{t}}$ are sensitive to different terms. To relate the dependence of the two observables on the chiral structure of the quark couplings to any new physics sector, recently Jung *et al.* proposed a new spin-spin FB asymmetry [12] which is defined as

$$C_{\rm FB}^{t\bar{t}} \equiv C^{t\bar{t}}(\cos\theta \geq 0) - C^{t\bar{t}}(\cos\theta \leq 0) \tag{8}$$

$$= A_{\rm FB}^{t\bar{t}}(\text{opp hel}) - A_{\rm FB}^{t\bar{t}}(\text{same hel}), \tag{9}$$

while the charge asymmetry may be written as

$$A_{\rm FB}^{t\bar{t}} = A_{\rm FB}^{t\bar{t}}(\text{opp hel}) + A_{\rm FB}^{t\bar{t}}(\text{same hel}). \tag{10}$$

Since there is no contribution to $A_{\rm FB}^{t\bar{t}}$ in the SM from same helicity states, for the SM $C_{\rm FB}^{t\bar{t}} = A_{\rm FB}^{t\bar{t}}(\text{opp hel}) = A_{\rm FB}^{t\bar{t}}$.

The correlation between $C_{\rm FB}^{t\bar{t}}$ and $A_{\rm FB}^{t\bar{t}}$ can help to distinguish between various new physics scenarios.

New physics can show up both at the production of top quarks and at the decay. If the new physics contains chiral asymmetry, then it will affect the top spin correlation appreciably and also the forward-backward spin correlation asymmetry [20,32,33].

III. THE MODEL

It is known that the visible particle sector is based on theories that are free in the infrared and/or have a mass gap. In contrast, an exact conformal invariance would require the mass spectrum to be either continuous or all zero masses. Although there exist interacting conformal theories that have an infrared fixed point, such theories do not have asymptotically free in and out states and the traditional S-matrix description does not work. The theory of unparticles as a conformally invariant sector that is weakly coupled to the SM particles was proposed by Georgi [17], which was motivated by Banks-Zaks theory [34]. This assumes the existence of a hidden sector with a nontrivial infrared fixed point (e.g., Banks-Zaks type) that interacts with the SM through the exchange of a messenger field with a large mass M. Below the scale M, one can integrate out the heavy field, giving rise to the effective nonrenormalizable couplings of the form

$$\frac{C_i}{M^{d_{\rm UV}+d_{\rm SM}^i-4}}\mathcal{O}_{\rm SM}^i\mathcal{O}_{\rm UV}, \tag{11}$$

where C_i are the dimensionless coupling constants and $\mathcal{O}_{\rm SM}^i$ and $\mathcal{O}_{\rm UV}$ are, respectively, the local operators built out of SM fields and hidden sector fields having scaling dimensions $d_{\rm SM}^i$ and $d_{\rm UV}$, respectively. The hidden sector has an infrared fixed point and becomes conformal at some scale, say, $\sim\Lambda < M$. Below the energy scale Λ, the renormalizable couplings of the hidden sector fields cause dimensional transmutation. In the effective theory, the high energy operators $\mathcal{O}_{\rm UV}$ above this scale match the unparticle operators $\mathcal{O}_{\mathcal{U}}$ (the operator $\mathcal{O}_{\rm UV}$ becomes $\Lambda^{d_{\rm UV}-d_{\mathcal{U}}}\mathcal{O}_{\mathcal{U}}$) below this scale, and the interactions of Eq. (11) now take the form

$$\frac{C_i\Lambda^{d_{\rm UV}-d_{\mathcal{U}}}}{M^{d_{\rm UV}+d_{\rm SM}^i-4}}\mathcal{O}_{\rm SM}^i\mathcal{O}_{\mathcal{U}} = \frac{C_i}{\Lambda_{\mathcal{U}}^{d_{\rm SM}^i+d_{\mathcal{U}}-4}}\mathcal{O}_{\rm SM}^i\mathcal{O}_{\mathcal{U}}, \tag{12}$$

where $d_{\mathcal{U}}$ is the scaling dimension of the operator $\mathcal{O}_{\mathcal{U}}$. M, Λ, $d_{\mathcal{U}}$, and $d_{\rm UV}$ are the hidden sector parameters, while the exponent of $\Lambda_{\mathcal{U}}$ depends on the dimension of the SM operator and is given by

$$\Lambda_{\mathcal{U}}^{d_{\rm SM}^i+d_{\mathcal{U}}-4} = \frac{M^{d_{\rm UV}+d_{\rm SM}^i-4}}{\Lambda^{d_{\rm UV}-d_{\mathcal{U}}}}. \tag{13}$$

The operators with different mass dimensions are likely to couple with different strengths. The couplings C_i and the scale Λ only appear in a combination given by (12) and there is no guiding theoretical principle to fix C_i. In addition to the interaction of SM fields with unparticles which can be probed at high energy colliders (below the scale Λ), the elimination of heavy fields also induces the contact interaction among SM fields, which are suppressed by powers of M and have the effect of drowning out any unparticle effects for $d_{\mathcal{U}} \gg 1$.

Unparticle effects are detected in the colliders either through missing energy distributions or by the interference effects with SM amplitudes. But the constraints from astrophysics and cosmology [35] would render them practically undetectable in the collider experiments unless they otherwise break the scale invariance at $\gtrsim 1$ GeV. The conformal invariance may be broken at a scale μ by the Higgs unparticle coupling $H^\dagger H\mathcal{O}_{\mathcal{U}}$, which introduces a scale in the theory once the Higgs acquires a vacuum expectation value. For consistency, $\mu \leq \Lambda$ and the two scales should be well separated to give a window where the sector is conformal. Thus, for scales Λ and M to be experimentally accessible, the Higgs-scalar unparticle coupling is assumed to break scale invariance at the electroweak scale. However, if only vector unparticles are present, scale invariance is broken by higher dimensional operators, leading to the breaking of the scale invariance below the electroweak scale [36].

Initially we have not introduced the effect of the breaking scale invariance with respect to the study of the top pair production and the same sign top production at the Tevatron. Nonetheless, we have shown its effect in the evaluation of the top decay width. Introduction of such modifications to the theory does not change the cross sections appreciably if $\mu \ll 2m_t$. The phenomenological lower bound on the scale-invariance breaking scale comes from the big bang nucleosynthesis and SN 1987A where μ is required to be sufficiently large compared to the relevant energy scales $\simeq 1$ MeV and $\simeq 30$ MeV, respectively [36]. We dwell on these issues in the appropriate sections and also in Sec. VI B.

The two-point function of unparticle operators [37] is written as

$$\langle 0|\mathcal{O}_{\mathcal{U}}(x)\mathcal{O}_{\mathcal{U}}^\dagger(0)|0\rangle = \int\frac{d^4p}{(2\pi)^2}e^{-ip\cdot x}\rho(p^2), \tag{14}$$

where $\rho(p^2) = (2\pi)^2\int d\lambda\delta^4(p-p_\lambda)|\langle 0|\mathcal{O}_{\mathcal{U}}|\lambda\rangle|^2$. The spectral function $\rho(p^2)$ is determined by scale invariance to be $\rho(p^2) = A_{d_{\mathcal{U}}}\theta(p^0)\theta(p^2)(p^2)^{d_{\mathcal{U}}-2}$, where $A_{d_{\mathcal{U}}}$ is the normalization factor. This factor is fixed by identifying $\rho(p^2)$ with the $d_{\mathcal{U}}$-body phase space of massless particles to be

$$A_{d_{\mathcal{U}}} = \frac{16\pi^2\sqrt{\pi}}{(2\pi)^{2d_{\mathcal{U}}}}\frac{\Gamma(d_{\mathcal{U}}+1/2)}{\Gamma(d_{\mathcal{U}}-1)\Gamma(2d_{\mathcal{U}})}. \tag{15}$$

The scaling dimension $d_{\mathcal{U}}$ can have nonintegral values as well. With the use of the spectral function $\rho(p^2)$ and requiring scale invariance, the Feynman propagators for vector and tensor unparticles are defined to be [37]

$$\Delta_{\mu\nu}(p^2) = \frac{iA_{d_\mathcal{U}}}{2\sin(d_\mathcal{U}\pi)}(-p^2)^{d_\mathcal{U}-2}\Pi_{\mu\nu}(p),$$
$$\Delta_{\mu\nu,\rho\sigma}(p^2) = \frac{iA_{d_\mathcal{U}}}{2\sin(d_\mathcal{U}\pi)}(-p^2)^{d_\mathcal{U}-2}\mathcal{T}_{\mu\nu,\rho\sigma}(p), \tag{16}$$

where

$$\Pi^{\mu\nu}(p) = -g^{\mu\nu} + \frac{p^\mu p^\nu}{p^2},$$
$$\mathcal{T}^{\mu\nu,\rho\sigma}(p) = \frac{1}{2}\Big\{\Pi^{\mu\nu}(p)\Pi^{\nu\sigma}(p) + \Pi^{\mu\sigma}(p)\Pi^{\nu\rho}(p) - \frac{2}{3}\Pi^{\mu\nu}(p)\Pi^{\rho\sigma}(p)\Big\}, \tag{17}$$

and $(-p^2)^{d_\mathcal{U}-2}$ is interpreted as

$$(-p^2)^{d_\mathcal{U}-2} = \begin{cases} |p^2|^{d_\mathcal{U}-2} & \text{for } p^2 < 0 \\ |p^2|^{d_\mathcal{U}-2}e^{id_\mathcal{U}\pi} & \text{for } p^2 > 0. \end{cases} \tag{18}$$

Propagators are chosen such that they satisfy the relations $p_\mu\Pi^{\mu\nu}(p) = 0$, $p_\mu\mathcal{T}^{\mu\nu,\rho\sigma}(p) = 0$, and $\mathcal{T}^{\mu,\rho\sigma}_{\mu}(p) = 0$. Also, the unparticle operators are all taken to be Hermitian, ${\mathcal{O}_\mathcal{U}}^\mu$ and ${\mathcal{O}_\mathcal{U}}^{\mu\nu}$ are assumed to be transverse, and the spin-2 unparticle operator is taken to be traceless ${\mathcal{O}_\mathcal{U}}_\mu{}^\mu = 0$.

The negative sign in front of p^2 in the second term gives rise to a unique phase factor for timelike virtual unparticles but not for those that are spacelike. This leads to interesting interference effects with the SM process which will be discussed later.

Based on this template of the unparticle formalism, possible signatures of scalar, vector, and tensor unparticles at colliders and their effects on low energy phenomenology have been studied [18,19,38]. Astrophysics and cosmology also put strong constraints on unparticles [35,39]. Various theoretical aspects of unparticles have also been studied [40,41].

Grinstein *et al.* [41] have revisited the computation of two-point functions for unparticles, demanding rigid conformal invariance in the hidden sector, and shown that the unitarity of conformal algebra imposes lower bounds on scaling dimensions of the vector and tensor operators [41]. Thus, ${d_\mathcal{U}}^V \geq 3$ and ${d_\mathcal{U}}^T \geq 4$ for vector unparticles and symmetric traceless tensor unparticles, respectively. The primary vector operator ${\mathcal{O}_\mathcal{U}}^\mu$ with $\partial_\mu{\mathcal{O}_\mathcal{U}}^\mu = 0$ corresponds to particles with $du^V = 3$, while the vector unparticles corresponding to $\partial_\mu{\mathcal{O}_\mathcal{U}}^\mu \neq 0$ and $d_u > 3$ get a modified propagator

$$\Delta^{\mu\nu}(p) = \frac{-iA_{d_\mathcal{U}}}{2\sin(d_\mathcal{U}\pi)}(-p^2)^{d_\mathcal{U}-3}(p^2 g^{\mu\nu} - a p^\mu p^\nu), \tag{19}$$

with $a = 2(d_\mathcal{U} - 2)/(d_\mathcal{U} - 1)$. Note that this differs from the propagator given in Eq. (16) not only in the relative size of the terms but also by an overall extra phase factor $e^{-i\pi}$. This extra phase would affect the sign of interference terms with SM processes. In fact, this contradicts the many observations made in the literature with respect to unparticles. Similarly, the tensor unparticle propagator is modified to [42]

$$\Delta_{\mu\nu,\alpha\beta}(p^2) = \frac{A_{d_\mathcal{U}}}{2\sin(d_\mathcal{U}\pi)}(-p^2)^{d_\mathcal{U}-2}\mathcal{T}_{\mu\nu,\alpha\beta}, \tag{20}$$

where

$$\begin{aligned}\mathcal{T}_{\mu\nu,\alpha\beta}(p) &= d_\mathcal{U}(d_\mathcal{U}-1)(g_{\mu\alpha}g_{\nu\beta} + \mu \leftrightarrow \nu) \\ &+ \left[2 - \frac{d_\mathcal{U}}{2}(d_\mathcal{U}+1)\right]g_{\mu\nu}g_{\alpha\beta} - 2(d_\mathcal{U}-1)(d_\mathcal{U}-2) \\ &\times\left(g_{\mu\alpha}\frac{p_\nu p_\beta}{p^2} + g_{\mu\beta}\frac{p_\nu p_\alpha}{p^2} + \mu \leftrightarrow \nu\right) + 4(d_\mathcal{U}-2) \\ &\times\left(g_{\mu\nu}\frac{p_\alpha p_\beta}{p^2} + g_{\alpha\beta}\frac{p_\mu p_\nu}{p^2}\right) + 8(d_\mathcal{U}-2)(d_\mathcal{U}-3) \\ &\times\frac{p_\mu p_\nu p_\alpha p_\beta}{(p^2)^2}.\end{aligned} \tag{21}$$

We have considered the symmetric structure for the tensor propagator.

In this article we explore the phenomenologically viable and interesting scale invariant (not strictly conformally invariant) hidden sector where the bounds on ${d_\mathcal{U}}^V$, ${d_\mathcal{U}}^T$ are relaxed. We do investigate the sensitivity of the observables with the full conformal invariance also, though it should be kept in mind that for such large values of $d_\mathcal{U}$, the SM contact interactions (induced at scale M by the exchange of ultraheavy particles) dominate over the unparticle SM interference effects.

The relevant unparticle SM flavor conserving (FC) and flavor violating (FV) interaction Lagrangian is given in Eqs. (A3)–(A6) in Appendix A. We consider the vector and tensor unparticles with the possibility of each being a singlet or octet under $SU(3)_C$. Since gluons interact with vector unparticles through a derivative term $G_\mu{}^\alpha G^\alpha_\nu\partial^\mu\mathcal{O}^\nu_\mathcal{U}$ and not with the primary field $\mathcal{O}^\nu_\mathcal{U}$, this interaction term is suppressed by a factor of $\Lambda_\mathcal{U}$ compared to the interaction of vector unparticles with quarks. Moreover, the gluon flux at the Tevatron is low and so it is further subdued. Hence, we do not consider such interaction terms.

We compute the helicity amplitudes with appropriate color factors corresponding to the Lagrangian and present them in Appendix A. In calculating the amplitudes for unparticles, we have used the improved propagator of Eq. (19) for vector unparticles and of Eq. (20) for tensor unparticles.

The phenomenological consequences of the color octet unparticles are addressed and validated in Sec. VI B. There have been various attempts to provide a complete gauge theory of unparticles [43,44]; however, in the absence of any well-established approach to a full theory of unparticle

interactions, we study the topic from a phenomenological point of view.

IV. SENSITIVITY OF THE MODEL PARAMETERS

We perform a parton level and leading order calculation, where we have used the CTEQ6L LHApdf parton distribution function, the top mass $m_t = 173\ \mathrm{GeV}/c^2$, and $\alpha_s = \alpha_s(m_Z) = 0.13$. We evolve α_s to get $\alpha_s(2m_t)$ using CTEQ6L LHApdf. The tree-level SM cross section was obtained to be $\sigma^{\mathrm{tree}}_{\mathrm{SM}} = 4.26$ pb, which is consistent with the results available from Herwig++ [45], CalcHEP [46], and MadGraph/MadEvent [47] for the given choice of parameters. We have also matched our results with those in the existing literature [16,20].

We normalize our tree-level SM cross section to 7.08 pb to include the NNLO corrected matrix element squared [4] with $m_t = 173\ \mathrm{GeV}/c^2$. Accordingly, we normalize the SM amplitude by a factor $k = \sqrt{7.08/4.26} = \sqrt{1.663}$. The k factor is sensitive to the choice of renormalization and factorization scale but eventually it stabilizes with the inclusion of higher order corrections of the matrix element at the NNLO level [5]. As the NLO corrections in the new physics sector are not feasible within the scope of our article, we work with the LO contribution only in the unparticle physics sector. Thus, after scaling we may write the squared matrix element as

$$|\mathcal{M}^{t\bar{t}}|^2 = |k\mathcal{M}^{\mathrm{SM}}_{\mathrm{tree}}|^2 + 2(\mathcal{R}e(k\mathcal{M}^{\mathrm{SM}}_{\mathrm{tree}})^\dagger(\mathcal{M}^{\mathrm{unp}})) + |\mathcal{M}^{\mathrm{unp}}|^2. \tag{22}$$

As mentioned earlier, SM inclusive processes can generate $A^{t\bar{t}}_{\mathrm{FB}}$ which is at most 5%–8% through the radiative diagrams at NLO level. It is worth examining the additional contributions to the integrated and differential $A^{t\bar{t}}_{\mathrm{FB}}$ generated by the LO top pair production processes mediated through unparticles. The contributions of unparticles to cross section, charge asymmetry, and spin correlation coefficients come from the matrix element square term containing only unparticles and the interference of unparticles with SM QCD and electroweak matrix elements. To see the correlation between $C^{t\bar{t}}_{\mathrm{FB}}$ and $A^{t\bar{t}}_{\mathrm{FB}}$ and dependence on the chiral structure of the theory, we divide these two into same helicity and opposite helicity contributions as

$$\begin{aligned} |\mathcal{M}^{\mathrm{unp}}|^2 &= |\mathcal{M}^{\mathrm{unp}}|^2_{\text{same hel}} + |\mathcal{M}^{\mathrm{unp}}|^2_{\text{opp hel}} \\ 2\mathcal{R}e[(\mathcal{M}^{\mathrm{SM}}_{\mathrm{tree}})^\dagger \mathcal{M}^{\mathrm{unp}}] &= 2\mathcal{R}e[(\mathcal{M}^{\mathrm{SM}}_{\mathrm{tree}})^\dagger \mathcal{M}^{\mathrm{unp}}]|_{\text{same hel}} \\ &\quad + 2\mathcal{R}e[(\mathcal{M}^{\mathrm{SM}}_{\mathrm{tree}})^\dagger \mathcal{M}^{\mathrm{unp}}]|_{\text{opp hel}}. \end{aligned} \tag{23}$$

The helicity amplitudes (as given in Appendix A) involve the product of the couplings $g_i^{\mathcal{U}^{\mathrm{n}}_{(V/T)}\bar{q}q} g_j^{\mathcal{U}^{\mathrm{n}}_{(V/T)}\bar{t}t} = \lambda^{(V/T)}_{ij}$ (with i and $j \equiv L$ or R) for FC vector/tensor unparticles and g_i^{ut} for FV vector unparticles. Therefore, the observables are analyzed with the independent free parameters: the scaling dimension $d_{\mathcal{U}}$ and $\lambda^{(V/T)}_{ij}$ (g^{ut}_i) for FC vector/tensor (FV vector) unparticles. Throughout our analysis we have fixed $\Lambda_{\mathcal{U}} = 1\ \mathrm{TeV} \gg m_{t\bar{t}}$. In all of the figures showing the cross section, we plot the central values with the respective error band for CDF $\sigma^{t\bar{t}} = 7.5 \pm 0.48$ pb [1] and the SM NNLO $7.08 + 0.36 - 0.51$ pb [4]. We bound the total contribution from the SM and unparticles to the $\sigma^{t\bar{t}}$ for a given $d_{\mathcal{U}}$ at fixed $\Lambda_{\mathcal{U}} = 1$ TeV within the error bars of CDF data, which in turn gives the upper cutoff for the couplings.

A. Flavor conserving unparticles

The FC couplings for the light quarks are tightly constrained from the measurement of dijet events at the Tevatron [48]. Therefore, the FC couplings of the light quarks $g^{\mathcal{U}^{\mathrm{n}}_{(V/T)}\bar{q}q}_{(L/R)}$ with the vector and tensor unparticles are taken to be an order of magnitude smaller than those of third generation quarks or antiquarks $g^{\mathcal{U}^{\mathrm{n}}_{(V/T)}\bar{t}t}_{(L/R)}$. A detailed discussion on this can be found in Ref. [49] for $d_{\mathcal{U}} \geq 3$. We have also verified the dijet spectrum corresponding to $1 \leq d_{\mathcal{U}} \leq 3$ for most of the parameter region probed and it is consistent with the observed data. For FC processes, the products of couplings $\lambda^{(V/T)}_{ij}$ can be broadly classified into four combinations for a given $d_{\mathcal{U}}$ and Λ.

(a) $g_L^{\mathcal{U}^{\mathrm{n}}_{(V/T)}\bar{q}q} = g_L^{\mathcal{U}^{\mathrm{n}}_{(V/T)}\bar{t}t} = 0$, i.e., $\lambda^{(V/T)}_{LR} = \lambda^{(V/T)}_{RL} = \lambda^{(V/T)}_{LL} = 0$ and $\lambda^{(V/T)}_{RR} \neq 0$,

(b) $g_R^{\mathcal{U}^{\mathrm{n}}_{(V/T)}\bar{q}q} = g_R^{\mathcal{U}^{\mathrm{n}}_{(V/T)}\bar{t}t} = 0$, i.e., $\lambda^{(V/T)}_{LR} = \lambda^{(V/T)}_{RL} = \lambda^{(V/T)}_{RR} = 0$ and $\lambda^{(V/T)}_{LL} \neq 0$,

(c) $g_L^{\mathcal{U}^{\mathrm{n}}_{(V/T)}\bar{q}q} = g_R^{\mathcal{U}^{\mathrm{n}}_{(V/T)}\bar{q}q}$, $g_L^{\mathcal{U}^{\mathrm{n}}_{(V/T)}\bar{t}t} = g_R^{\mathcal{U}^{\mathrm{n}}_{(V/T)}\bar{t}t}$, i.e., $\lambda^{(V/T)}_{LL} = \lambda^{(V/T)}_{RR} = \lambda^{(V/T)}_{RL} = \lambda^{(V/T)}_{LR} = \lambda_{VV/TT}$,

(d) $g_L^{\mathcal{U}^{\mathrm{n}}_{(V/T)}\bar{q}q} = -g_R^{\mathcal{U}^{\mathrm{n}}_{(V/T)}\bar{q}q}$, $g_L^{\mathcal{U}^{\mathrm{n}}_{(V/T)}\bar{t}t} = -g_R^{\mathcal{U}^{\mathrm{n}}_{(V/T)}\bar{t}t}$, i.e., $\lambda^{(V/T)}_{LL} = \lambda^{(V/T)}_{RR} = -\lambda^{(V/T)}_{RL} = -\lambda^{(V/T)}_{LR} = \lambda_{AV/AT}$.

These four combinations correspond to the pure right-handed (RH), left-handed (LH), vector/tensor, and axial vector/axial tensor couplings, respectively. The symmetry in the helicity amplitudes given in Eqs. (A15)–(A18) and (A27)–(A30) renders the same new physics contributions for combinations (a) and (b).

1. Color singlet vector unparticles

We study the effect of the presence of color singlet unparticles on the three observables, namely, $\sigma^{t\bar{t}}$, $A^{t\bar{t}}_{\mathrm{FB}}$, and $C^{t\bar{t}}$. The variation of these observables with the product of couplings is shown in Figs. 2–4, respectively, corresponding to the specific cases.

Since there is no interference of the color singlet FC vector unparticle with QCD and the squared term of the unparticle dominates over the interference with the electroweak sector, the behavior of observables for singlet

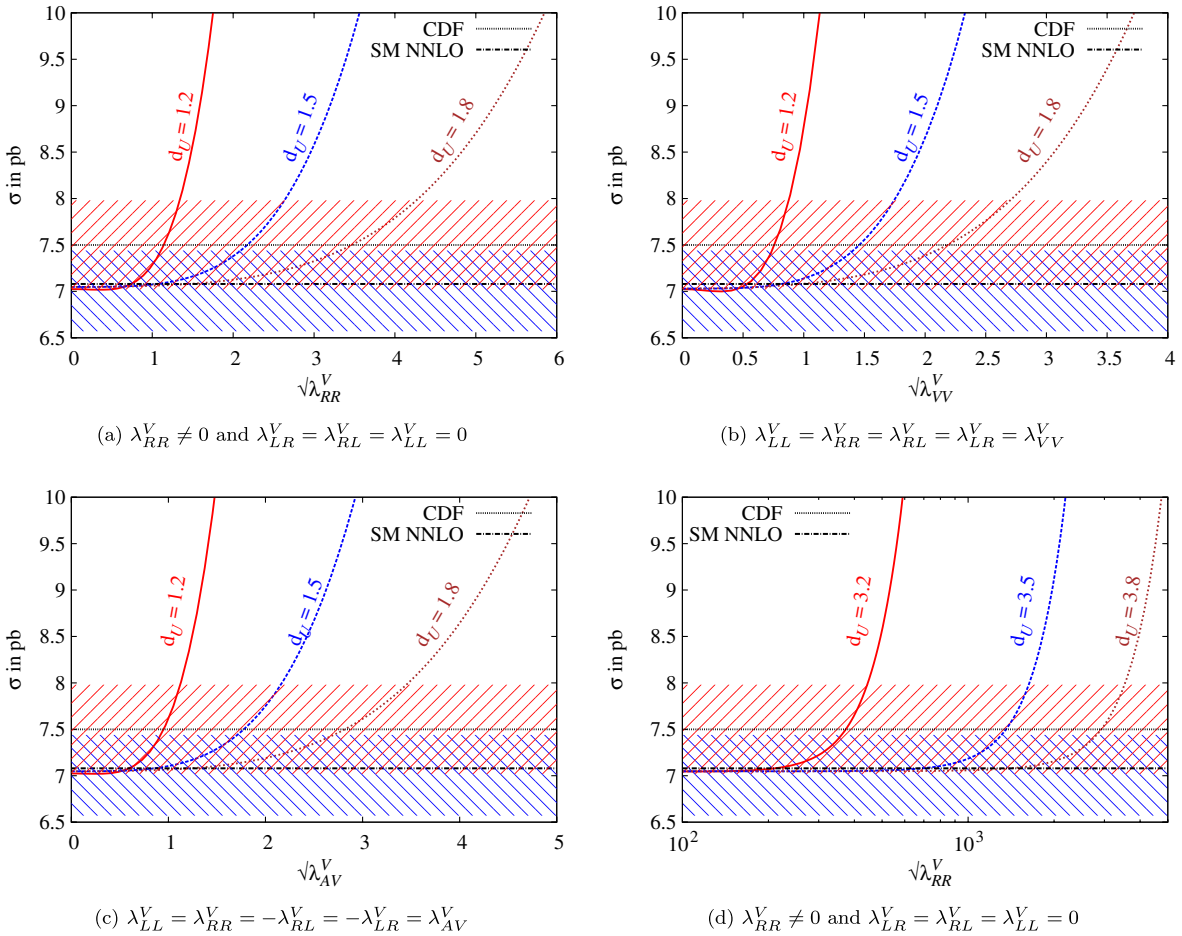

(a) $\lambda^V_{RR} \neq 0$ and $\lambda^V_{LR} = \lambda^V_{RL} = \lambda^V_{LL} = 0$

(b) $\lambda^V_{LL} = \lambda^V_{RR} = \lambda^V_{RL} = \lambda^V_{LR} = \lambda^V_{VV}$

(c) $\lambda^V_{LL} = \lambda^V_{RR} = -\lambda^V_{RL} = -\lambda^V_{LR} = \lambda^V_{AV}$

(d) $\lambda^V_{RR} \neq 0$ and $\lambda^V_{LR} = \lambda^V_{RL} = \lambda^V_{LL} = 0$

FIG. 2 (color online). Variation of the cross section $\sigma(p\bar{p} \to t\bar{t})$ with couplings $\sqrt{\lambda^V_{ij}}$ for color singlet flavor conserving vector unparticles corresponding to different values of d_U at fixed $\Lambda_U = 1$ TeV. The upper dotted line with a red band (shaded with positive slope lines) depicts the cross section 7.50 ± 0.48 pb from CDF (all channels) [1], while the lower dot-dashed line with a blue band (shaded with negative slope lines) shows the theoretical estimate 7.08 ± 0.36 pb at NNLO [4]. Panels (a), (b), and (c) show the variation of σ for d_U in the range $1 < d_U < 2$ corresponding to the different combinations of couplings [cases (a) (or b), (c), and (d) of the text, respectively]. Panel (d) depicts the variation of σ in the d_U range $3 < d_U < 4$ corresponding to the case (a) mentioned in the text.

unparticles is determined by the contribution of unparticles alone. For the FC vector singlet unparticle, the contribution of unparticles is given by

$$|\mathcal{M}^{\rm unp}_{\rm FCV}|^2_{\rm same\ hel} = B^{\rm unp}_{\rm FCV}\Big[\frac{1}{2}(1-\beta_t^2)\{(\lambda^V_{RR}+\lambda^V_{RL})^2 + (\lambda^V_{LL}+\lambda^V_{LR})^2\}s_\theta^2\Big], \tag{24}$$

$$|\mathcal{M}^{\rm unp}_{\rm FCV}|^2_{\rm opp\ hel} = B^{\rm unp}_{\rm FCV}\Big[\frac{1}{2}\{(1+\beta_t^2)[(\lambda^V_{RR})^2+(\lambda^V_{LL})^2 + (\lambda^V_{RL})^2+(\lambda^V_{LR})^2] + (1-\beta_t)^2(\lambda^V_{RR}\lambda^V_{RL} + \lambda^V_{LL}\lambda^V_{LR})\}(1+c_\theta^2) + 2\beta_t((\lambda^V_{RR})^2 + (\lambda^V_{LL})^2 - (\lambda^V_{RL})^2 - (\lambda^V_{LR})^2)c_\theta\Big], \quad \text{with}$$

$$B^{\rm unp}_{\rm FCV} = g_s^2\Big(\frac{\hat{s}}{\Lambda_U^2}\Big)^{2(d_U-1)}\Big[\frac{A_{d_U}}{2\sin(d_U\pi)}\Big]^2. \tag{25}$$

We highlight the following observations with regard to the spin correlation $C^{t\bar{t}}$ and charge asymmetry $A^{t\bar{t}}_{\rm FB}$:

(1) $A^{t\bar{t}}_{\rm FB}$ gets a contribution only from the opposite helicity amplitudes, and this contribution is proportional to $2\beta_t[(\lambda^V_{RR})^2 + (\lambda^V_{LL})^2 - (\lambda^V_{RL})^2 - (\lambda^V_{LR})^2]$. Hence, $A^{t\bar{t}}_{\rm FB}$ vanishes for $\beta_t = 0$ (i.e., when top is produced at threshold) and also for $\lambda^V_{LL} = \lambda^V_{RR} = \pm\lambda^V_{LR} = \pm\lambda^V_{RL}$, where + and − correspond to cases (c) and (d), respectively. However, the small contribution will come from interference with the electroweak part. We show the variation of $\sigma^{t\bar{t}}$ and $C^{t\bar{t}}$ for this case in Figs. 2(c) and 4(c).

(2) As β_t varies from 0 to 1, we observe that the spin correlation varies from a large negative value to a positive number. This is attributed to the fact that the opposite (same) helicity contribution increases (decreases) with increasing β_t. Also, the contribution to $\sigma^{t\bar{t}}$, $A^{t\bar{t}}_{\rm FB}$, and $C^{t\bar{t}}$ decreases with increasing

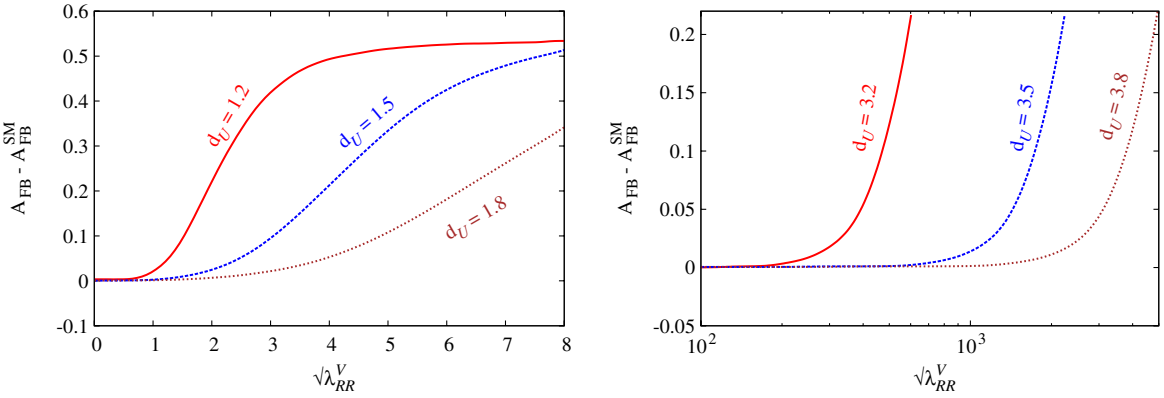

(a) $\lambda^V_{RR} \neq 0$ and $\lambda^V_{LR} = \lambda_{RL} = \lambda^V_{LL} = 0$ (b) $\lambda^V_{RR} \neq 0$ and $\lambda^V_{LR} = \lambda^V_{RL} = \lambda^V_{LL} = 0$

FIG. 3 (color online). Variation of the $A_{\rm FB} - A^{\rm SM}_{\rm FB}$ (the unparticle contribution to $A^{t\bar{t}}_{\rm FB}$) with couplings $\sqrt{\lambda^V_{RR}}$ [corresponding to case (a) of the text] for color singlet flavor conserving vector unparticles for various values of $d_{\mathcal{U}}$ at fixed $\Lambda_{\mathcal{U}} = 1$ TeV. This is evaluated using the 1d differential distribution of rapidity in the $t\bar{t}$ rest frame.

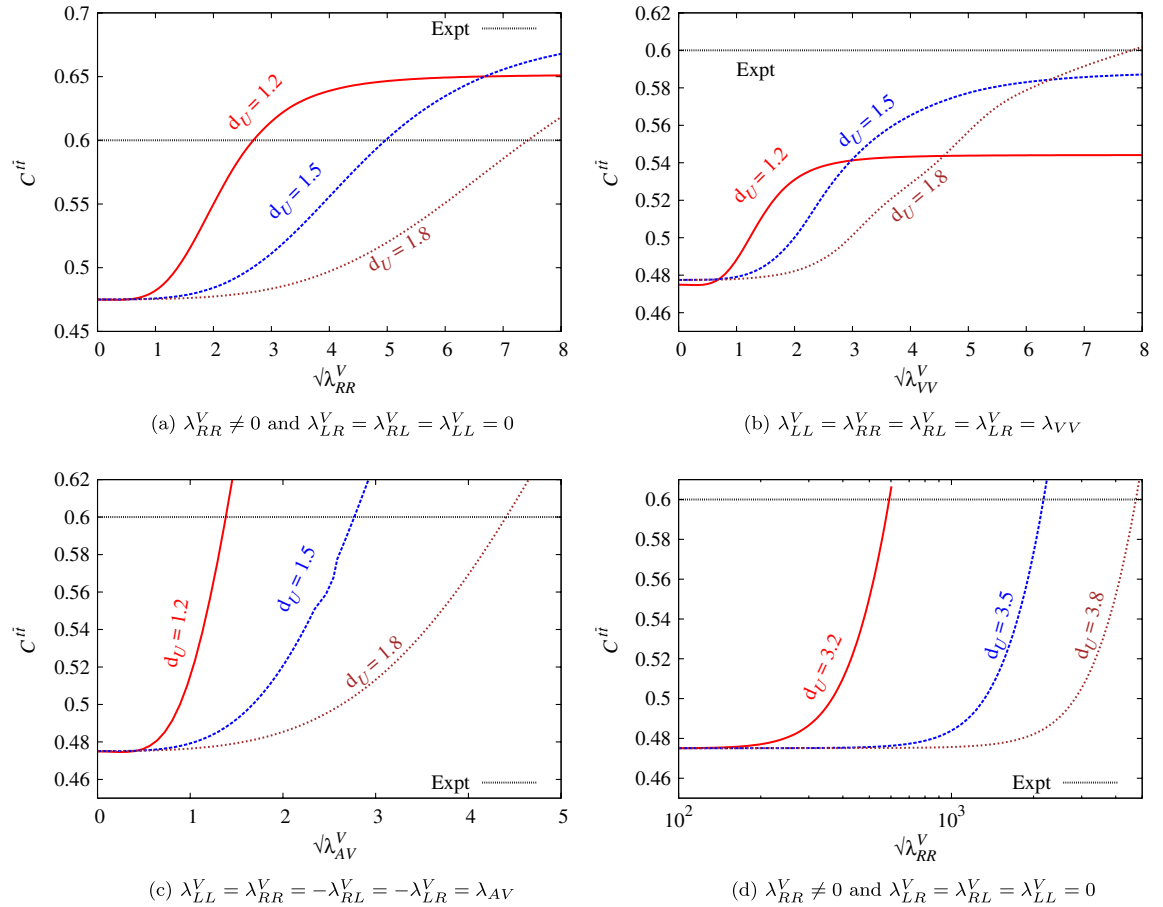

(a) $\lambda^V_{RR} \neq 0$ and $\lambda^V_{LR} = \lambda^V_{RL} = \lambda^V_{LL} = 0$ (b) $\lambda^V_{LL} = \lambda^V_{RR} = \lambda^V_{RL} = \lambda^V_{LR} = \lambda_{VV}$

(c) $\lambda^V_{LL} = \lambda^V_{RR} = -\lambda^V_{RL} = -\lambda^V_{LR} = \lambda_{AV}$ (d) $\lambda^V_{RR} \neq 0$ and $\lambda^V_{LR} = \lambda^V_{RL} = \lambda^V_{LL} = 0$

FIG. 4 (color online). Variation of the spin-correlation coefficient $C^{t\bar{t}}$ with couplings $\sqrt{\lambda^V_{ij}}$ for color singlet flavor conserving vector unparticles for various values of $d_{\mathcal{U}}$ at fixed $\Lambda_{\mathcal{U}} = 1$ TeV. The experimental value is depicted with a dot-dashed line at $0.60 \pm 0.50(\text{stat}) \pm 0.16(\text{syst})$ [28]. Panels (a), (b), and (c), respectively, correspond to cases (a), (c), and (d) for the values of $d_{\mathcal{U}}$ in the range $1 < d_{\mathcal{U}} < 2$, while panel (d) gives the variation for case (a) with $d_{\mathcal{U}}$ in the range $3 < d_{\mathcal{U}} < 4$.

$d_{\mathcal{U}}$ for a given coupling because of the term $\Lambda^{(d_{\mathcal{U}}-1)}$ in the denominator.

(3) $A_{\rm FB}^{t\bar{t}}$ and $C^{t\bar{t}}$ initially increase quadratically with the product of couplings and then become constant, since for the large couplings, the unparticle squared term takes over the SM, resulting in the cancellation of the coupling dependence in the numerator and denominator of these observables.

(4) The $C_{\rm FB}^{t\bar{t}} \approx A_{\rm FB}^{t\bar{t}} = A_{\rm FB}^{t\bar{t}}$ (opposite helicity) for FC vector unparticles as the interference term of the unparticles with the EW part is negligibly small.

These graphs exhibit that it is possible to get appreciable $A_{\rm FB}^{t\bar{t}}$ (keeping the cross section and spin correlation in agreement with the experimental values) for cases (a) and (b). This higher value of $A_{\rm FB}^{t\bar{t}}$ for the first two cases can be attributed to the complete asymmetry in the left and right couplings. We find that for the other two cases [pure vector in case (c) and pure axial vector in case (d)] there is no parameter region that agrees with the experimental value of $\sigma^{t\bar{t}}$ and at the same time gives appreciable $A_{\rm FB}^{t\bar{t}}$.

In Figs. 2(d), 3(b), and 4(d), we show the variation of $\sigma^{t\bar{t}}$, $A_{\rm FB}^{t\bar{t}}$, and $C^{t\bar{t}}$, respectively, with the coupling for $d_{\mathcal{U}} > 3$ which is allowed by the unitarity of the completely conformally invariant hidden sector. For such large values of $d_{\mathcal{U}}$, the unparticle effects are pronounced for very high values of couplings and hence the interference with the electroweak sector plays a crucial role. Note that the SM contact terms induced at large scales can also become important in this region of parameter space.

2. Color octet vector unparticle

Next we consider the possibility of vector unparticles being color octet with flavor conserving couplings. The variation of $\sigma^{t\bar{t}}$, $A_{\rm FB}^{t\bar{t}}$, and $C^{t\bar{t}}$ with couplings are shown in the Figs. 5–7, respectively. The flavor conserving octet unparticles do not interfere with the flavor singlet electroweak sector. Thus, the nature of these numbers can be explained completely on the basis of the interplay of

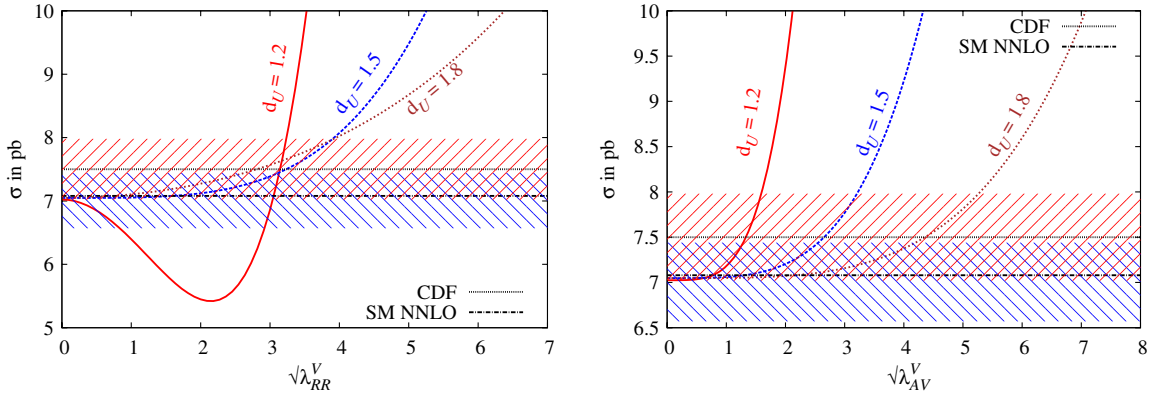

(a) $\lambda^V_{RR} \neq 0$ and $\lambda^V_{LR} = \lambda^V_{RL} = \lambda^V_{LL} = 0$

(b) $\lambda^V_{LL} = \lambda^V_{RR} = -\lambda^V_{RL} = -\lambda^V_{LR} = \lambda^V_{AV}$

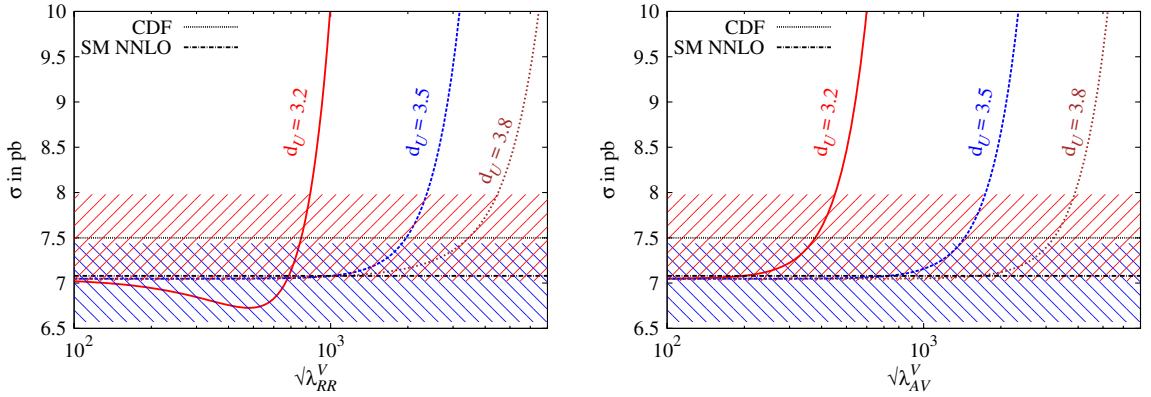

(c) $\lambda^V_{RR} \neq 0$ and $\lambda^V_{LR} = \lambda^V_{RL} = \lambda^V_{LL} = 0$

(d) $\lambda^V_{LL} = \lambda^V_{RR} = -\lambda^V_{RL} = -\lambda^V_{LR} = \lambda^V_{AV}$

FIG. 5 (color online). Variation of the cross section $\sigma(p\bar{p} \to t\bar{t})$ with couplings $\sqrt{\lambda^V_{ij}}$ for color octet flavor conserving vector unparticles corresponding to different values of $d_{\mathcal{U}}$ at fixed $\Lambda_{\mathcal{U}} = 1$ TeV. The upper dotted line with a red band (shaded with positive slope lines) depicts the cross section 7.50 ± 0.48 pb from CDF (all channels) [1], while the lower dot-dashed line with a blue band (shaded with negative slope lines) shows the theoretical estimate 7.08 ± 0.36 pb at NNLO [4]. Panels (a) and (b) show the variation of σ for cases (a) and (d) of the text for the various values of $d_{\mathcal{U}}$ in the range $1 < d_{\mathcal{U}} < 2$, while panels (c) and (d) give the same variation for the $d_{\mathcal{U}}$ values in the range $3 < d_{\mathcal{U}} < 4$.

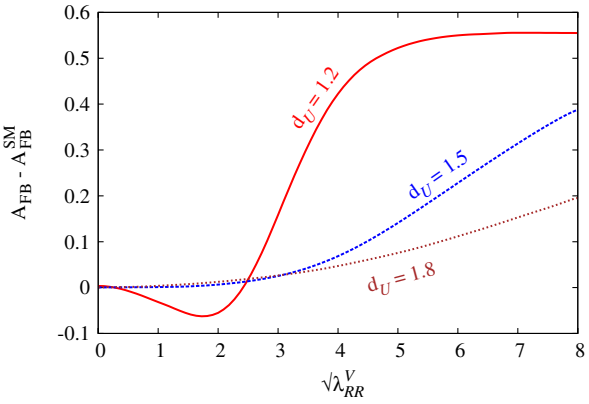

(a) $\lambda^V_{RR} \neq 0$ and $\lambda^V_{LR} = \lambda^V_{RL} = \lambda^V_{LL} = 0$

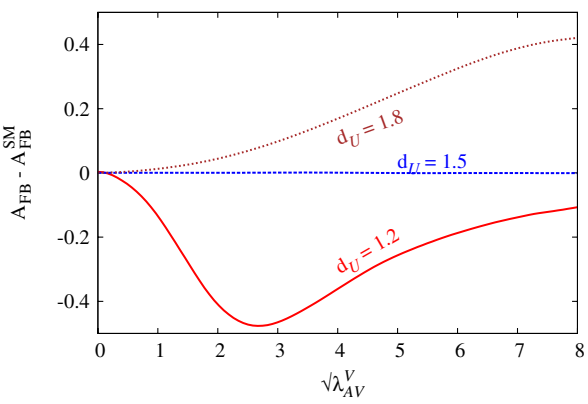

(b) $\lambda^V_{LL} = \lambda^V_{RR} = -\lambda^V_{RL} = -\lambda^V_{LR} = \lambda^V_{AV}$

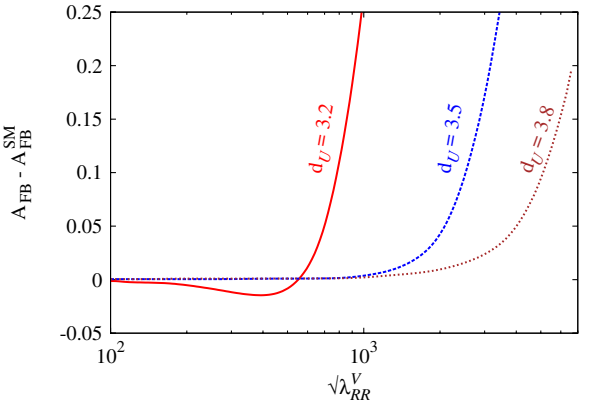

(c) $\lambda^V_{RR} \neq 0$ and $\lambda^V_{LR} = \lambda^V_{RL} = \lambda^V_{LL} = 0$

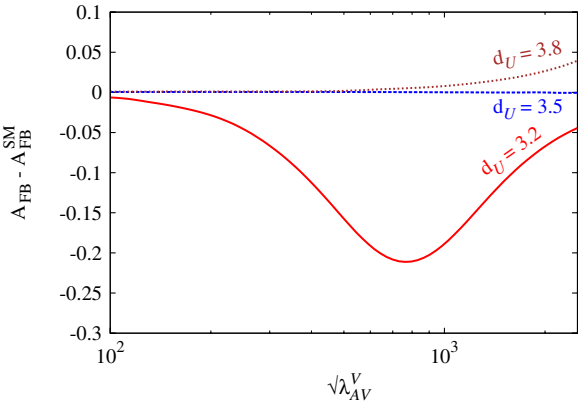

(d) $\lambda^V_{LL} = \lambda^V_{RR} = -\lambda^V_{RL} = -\lambda^V_{LR} = \lambda^V_{AV}$

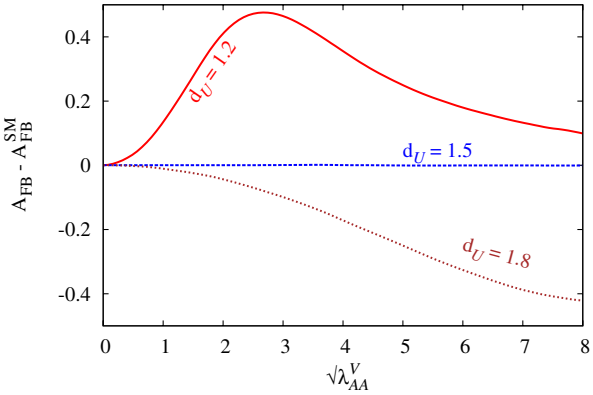

(e) $g^{\mathcal{U}_V \bar{q} q}_{L \triangleleft R}\, g^{\mathcal{U}_V \bar{t} t}_{L \triangleleft R} < 0$, the choice of coupling combination favored by the non-universal axigluon models

FIG. 6 (color online). Variation of the $A_{FB} - A_{FB}^{SM}$ (the unparticle contribution to $A_{FB}^{t\bar{t}}$) with couplings $\sqrt{\lambda^V_{ij}}$ for color octet flavor conserving vector unparticles for various values of $d_{\mathcal{U}}$ at fixed $\Lambda_{\mathcal{U}} = 1$ TeV and for different coupling combinations mentioned in the text. This is evaluated using the 1d differential distribution of rapidity in the $t\bar{t}$ rest frame.

QCD and octet unparticle helicity amplitudes. From Eqs. (18) and (19), it may be seen that the interference terms given in Eq. (23) can be rewritten as

$$[2\mathcal{M}^{\rm QCD}\mathcal{R}e(\mathcal{M}^{\rm unp}_{\rm FCV})]_{\rm same\ hel} = 2B^{\rm int}_{\rm FCV}(\lambda^V_{LL} + \lambda^V_{LR} + \lambda^V_{RL} + \lambda^V_{RR})(1 - \beta_t^2)s_\theta^2, \quad (26)$$

and

$$[2\mathcal{M}^{\rm QCD}\mathcal{R}e(\mathcal{M}^{\rm unp}_{\rm FCV})]_{\rm opp\ hel} = 2B^{\rm int}_{\rm FCV}[(\lambda^V_{LL} + \lambda^V_{RR} + \lambda^V_{LR} + \lambda^V_{RL})(1 + c_\theta^2) + 2\beta_t(\lambda^V_{LL} + \lambda^V_{RR} - \lambda^V_{RL} - \lambda^V_{LR})c_\theta], \quad (27)$$

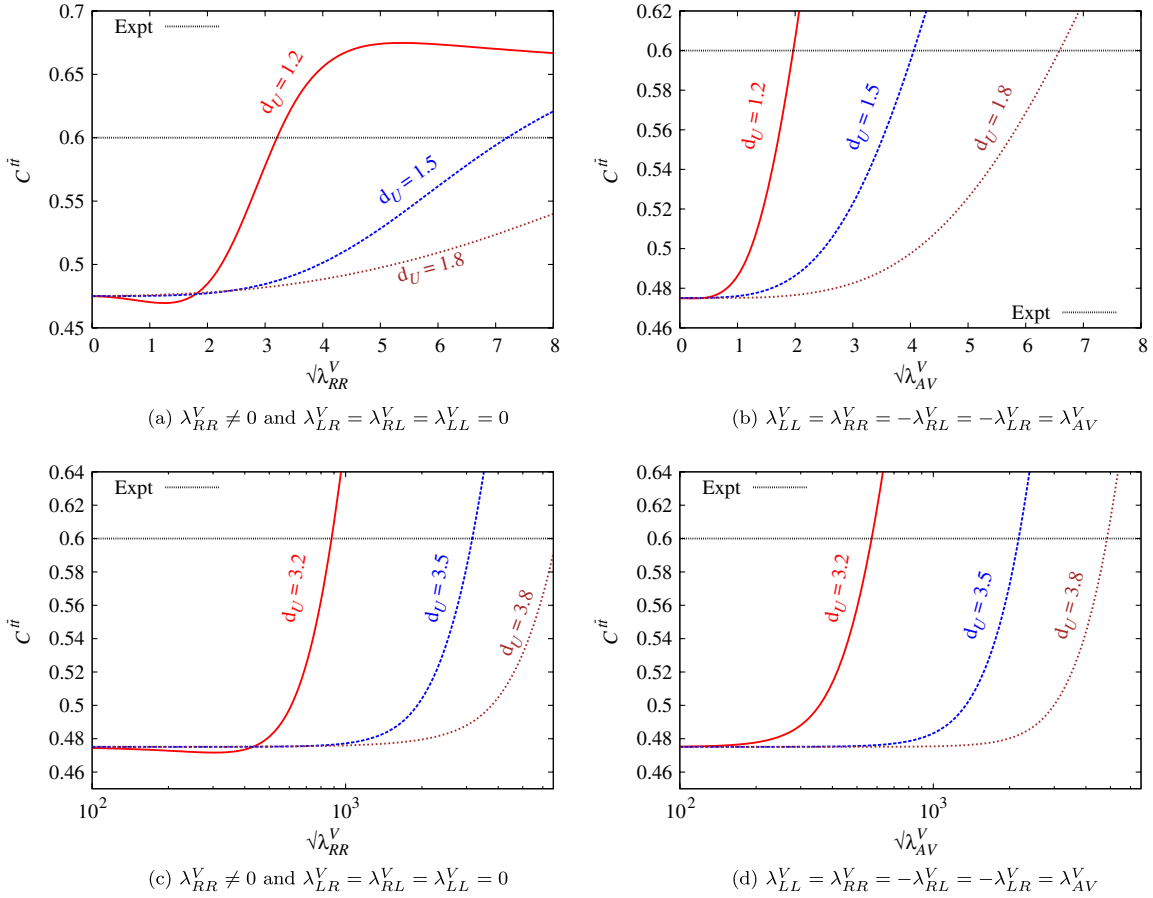

(a) $\lambda^V_{RR} \neq 0$ and $\lambda^V_{LR} = \lambda^V_{RL} = \lambda^V_{LL} = 0$

(b) $\lambda^V_{LL} = \lambda^V_{RR} = -\lambda^V_{RL} = -\lambda^V_{LR} = \lambda^V_{AV}$

(c) $\lambda^V_{RR} \neq 0$ and $\lambda^V_{LR} = \lambda^V_{RL} = \lambda^V_{LL} = 0$

(d) $\lambda^V_{LL} = \lambda^V_{RR} = -\lambda^V_{RL} = -\lambda^V_{LR} = \lambda^V_{AV}$

FIG. 7 (color online). Variation of the spin-correlation coefficient $C^{t\bar{t}}$ evaluated in the helicity basis with couplings $\sqrt{\lambda^V_{ij}}$ for color octet flavor conserving vector unparticles for various values of $d_{\mathcal{U}}$ at fixed $\Lambda_{\mathcal{U}} = 1$ TeV and for different combinations of couplings. The experimental value is depicted with a dot-dashed line at $0.60 \pm 0.50(\text{stat}) \pm 0.16(\text{syst})$ [28].

where

$$B^{\text{int}}_{\text{FCV}} = g_s^2 \left(\frac{\hat{s}}{\Lambda^2_{\mathcal{U}}}\right)^{(d_{\mathcal{U}}-1)} A_{d_{\mathcal{U}}} \left[-\frac{\cot(d_{\mathcal{U}}\pi)}{2}\right]. \quad (28)$$

The $|\mathcal{M}^{\text{unp}}_{\text{FCV}}|^2_{\text{same hel}}$ and $|M^{\text{opp}}_{\text{FCV}}|^2_{\text{same hel}}$ are the same as given in Eq. (25). Analyzing these expressions, we observe that

(1) In the interference term, unlike in the spin correlation, only the opposite helicity amplitudes contribute to $A^{t\bar{t}}_{\text{FB}}$, which is proportional to $4\beta_t(\lambda^V_{LL} + \lambda^V_{RR} - \lambda^V_{RL} - \lambda^V_{LR})$. Hence, $C^{t\bar{t}}_{\text{FB}} = A^{t\bar{t}}_{\text{FB}}$.

(2) The helicity amplitudes for unparticles and QCD are left-right symmetric. Therefore, the variation of the observables with coupling products will be the same for cases (a) and (b). We show the variation for $\sigma^{t\bar{t}}$, $A^{t\bar{t}}_{\text{FB}}$, and $C^{t\bar{t}}$ for case (a) in Figs. 5(a), 6(a), and 7(a) for the phenomenologically interesting range of $d_{\mathcal{U}}$, i.e., $1 < d_{\mathcal{U}} < 2$. The same variation for $3 < d_{\mathcal{U}} < 4$ (consistent with the conformally invariant sector) is shown in Figs. 5(a), 6(a), and 7(a), respectively. Case (c) corresponds to pure vector couplings of unparticles with quarks, which is similar to that of QCD. Hence, negligible $A^{t\bar{t}}_{\text{FB}}$ is generated only from the squared term of the EW neutral current. Case (d), on the other hand, generates appreciable $A^{t\bar{t}}_{\text{FB}}$ proportional to $16\beta_t\lambda^V_{AV}$ due to the interference of the vector (QCD) with axial vector unparticle sectors. The variation for $\sigma^{t\bar{t}}$, $A^{t\bar{t}}_{\text{FB}}$, and $C^{t\bar{t}}$ for case (d) is shown in Figs. 5(a), 6(a), and 7(a) for $1 < d_{\mathcal{U}} < 2$. The same variation for $3 < d_{\mathcal{U}} < 4$ (consistent with the conformally invariant sector) is shown in Figs. 5(d), 6(d), and 7(d), respectively.

(3) The sign of the interference term is determined by the unparticle propagator which has a nontrivial phase dependence upon $d_{\mathcal{U}}$. We may write

$$|\mathcal{M}|^2 = |\mathcal{M}^{\text{SM}}|^2 + \delta[2\mathcal{M}^{\text{QCD}}|\mathcal{R}e(\mathcal{M}^{\text{unp}})|], \quad (29)$$

where δ is negative for $n < d_{\mathcal{U}} < (n + 1/2)$, zero for $d_{\mathcal{U}} = (n + 1/2)$, and positive for $(n + 1/2) < d_{\mathcal{U}} < (n + 1)$ due to the presence of $\cot(d_{\mathcal{U}}\pi)$ (n being an integer ≥ 1). This effect is evident in Fig. 5. We observe that due to the effect of the interference, the cross section in the presence of unparticles first decreases with an increase in couplings and eventually increases with the onset of $|\mathcal{M}_{\text{unp}}|^2$ for rather large couplings.

(4) This effect is also well demonstrated for $A_{\rm FB}^{t\bar{t}}$ in Figs. 6(b) and 6(d) corresponding to case (d) where there is no contribution to $A_{\rm FB}^{t\bar{t}}$ from $|\mathcal{M}_{\rm unp}|^2$. However, for case (a), as seen from Figs. 6(a) and 6(c), the unparticle squared term overtakes the interference term and drives the $A_{\rm FB}^{t\bar{t}}$ towards a positive value with a gradual increase in the coupling strength.
It is worth mentioning that for all axigluon models, we require the light quark-axigluon and top-axigluon coupling to be of opposite sign in order to generate positive asymmetry. This is not necessary with unparticles. However, if one chooses couplings in this nonuniversal way, then $A_{\rm FB}^{t\bar{t}}$ will pick up an extra negative sign, as shown in Fig. 6(c) for $1 < d_{\mathcal{U}} < 2$. Even for $d_{\mathcal{U}} > 3$, one obtains large positive asymmetry for $3 < d_{\mathcal{U}} < 3.5$ for this choice of couplings.

Thus, with octet vector unparticle sectors having pure right- or left-handed couplings or even with axial vector couplings, there is a region in parameter space [e.g., case (a) with $d_{\mathcal{U}} = 1.2$ and case (d) with $d_{\mathcal{U}} = 1.8$] where it is possible to get appreciable positive $A_{\rm FB}^{t\bar{t}}$ keeping the $t\bar{t}$ production cross section and spin correlation consistent with experimental measurement. For higher $d_{\mathcal{U}}$ consistent with the unitarity bound of completely conformally invariant sectors, i.e., $d_{\mathcal{U}} > 3$, not enough positive $A_{\rm FB}^{t\bar{t}}$ is obtained for any $d_{\mathcal{U}}$ and coupling consistent with the $\sigma^{t\bar{t}}$.

Chen *et al.* [16] have calculated $A_{\rm FB}^{t\bar{t}}$ in the lab frame for the same case (for FC vector octet unparticles with pure right-handed coupling). Using the definition of Eq. (1) and for an identical choice of parameters, our cross section and $A_{\rm FB}^{t\bar{t}}$ are in agreement with them.

3. FC color singlet tensor unparticle

As in the case of vector unparticles, the s channel process through FC color singlet tensor unparticles interferes with the EW neutral current but not with the QCD. Therefore, pure unparticle amplitude (i.e., $|\mathcal{M}^{\rm unp}|^2$) determines the behavior of the observables. The left-right symmetry in helicity amplitudes results in almost identical behavior for the observables corresponding to cases (a) and (b), which is similar to FC vector unparticles. The same and opposite helicity contributions to $|\mathcal{M}^{\rm unp}|^2$ are given by

$$
\begin{aligned}
|\mathcal{M}^{\rm unp}_{\rm FCT}|^2_{\rm same\ hel} &= \mathcal{B}^{\rm unp}_{\rm FCT}[2\beta_t^2(1-\beta_t^2)\{(\lambda^T_{RR}+\lambda^T_{RL})^2+(\lambda^T_{LL}+\lambda^T_{LR})^2\}s_\theta^2 c_\theta^2],\\
|\mathcal{M}^{\rm unp}_{\rm FCT}|^2_{\rm opp\ hel} &= \frac{1}{2}\beta_t^2\mathcal{B}^{\rm unp}_{\rm FCT}[\{(1+\beta_t^2)((\lambda^T_{RR})^2+(\lambda^T_{LL})^2+(\lambda^T_{RL})^2+(\lambda^T_{LR})^2)\\
&\quad + 2(1-\beta_t^2)(\lambda^T_{RR}\lambda^T_{RL}+\lambda^T_{LL}\lambda^T_{LR})\}(1-3c_\theta^2+4c_\theta^4) - 4\beta_t((\lambda^T_{RR})^2+(\lambda^T_{LL})^2\\
&\quad - (\lambda^T_{RL})^2-(\lambda^T_{LR})^2)(1-2c_\theta^2)c_\theta],
\end{aligned}
\tag{30}
$$

where

$$
\mathcal{B}^{\rm unp}_{\rm FCT} = \frac{1}{16}\mathcal{C}_f^{\mathcal{U}_T^{\rm FC}}\left[g_s^2\left(\frac{\hat{s}}{\Lambda_{\mathcal{U}}^2}\right)^{2d_{\mathcal{U}}}\left[\frac{A_{d_{\mathcal{U}}}}{2\sin(d_{\mathcal{U}}\pi)}\right]^2 \times (d_{\mathcal{U}}^2)(d_{\mathcal{U}}-1)^2\right]. \tag{31}
$$

The variation of the observables' cross section $\sigma^{t\bar{t}}$ and spin correlation $C^{t\bar{t}}$ with λ_{ij}^T for different cases is shown in Figs. 8 and 9, respectively. By comparing them with the pure vector case, we observe that an additional β_t factor in the helicity amplitudes suppresses the $A_{\rm FB}^{t\bar{t}}$ for case (a) or (b) in the range of parameters which keeps the cross section and spin correlation $C^{t\bar{t}}$ in agreement with the allowed experimental values. Cases (c) and (d) do not give any contribution to $A_{\rm FB}^{t\bar{t}}$. Moreover, the order of couplings involved are much larger (keeping the $\sigma^{t\bar{t}}$ within experimental limits) compared to the vector unparticle case because the overall coupling in the tensor case has an extra factor of Λ in the denominator. Unitarity bounds the $d_{\mathcal{U}}^T$ values for the conformally invariant symmetric tensor to be $d_{\mathcal{U}}^T > 4$. However, for such values of $d_{\mathcal{U}}^T$, the unparticle effects are highly subdued, as may be seen from Figs. 8 and 9.

4. Color octet tensor unparticle

The FC tensor octet unparticles do not interfere with the electroweak neutral sector like the vector unparticles, and the behavior of the plots (shown in Figs. 10–12) is almost entirely determined by its interference with QCD. The same helicity and opposite helicity contributions to interference with QCD are given by

$$
\begin{aligned}
&2\mathcal{M}^{\rm QCD}\mathcal{R}(\mathcal{M}^{\rm unp})|_{\rm same\ hel}\\
&\quad = -4\mathcal{B}_T^{\rm int}(\lambda^T_{LL}+\lambda^T_{LR}+\lambda^T_{RL}+\lambda^T_{RR})\beta_t(1-\beta_t^2)s_\theta^2 c_\theta,
\end{aligned}
\tag{32}
$$

$$
\begin{aligned}
&2\mathcal{M}^{\rm QCD}\mathcal{R}(\mathcal{M}^{\rm unp})|_{\rm opp\ hel}\\
&= -2\mathcal{B}_T^{\rm int}\beta_t[\beta_t(\lambda^T_{LL}+\lambda^T_{RR}-\lambda^T_{LR}-\lambda^T_{RL})\\
&\quad \times(3c_\theta^2-1)+2(\lambda^T_{LL}+\lambda^T_{RR}+\lambda^T_{RL}+\lambda^T_{LR})c_\theta^3],
\end{aligned}
\tag{33}
$$

where

$$
\mathcal{B}_T^{\rm int} = \mathcal{C}_f^{\mathcal{U}_T^{\rm FC}}\left(\frac{d_{\mathcal{U}}(d_{\mathcal{U}}-1)}{4}\right) \times\left[g_s^2\left(\frac{\hat{s}}{\Lambda_{\mathcal{U}}^2}\right)^{d_{\mathcal{U}}}A_{d_{\mathcal{U}}}[\cot(d_{\mathcal{U}}\pi)]\right]. \tag{34}
$$

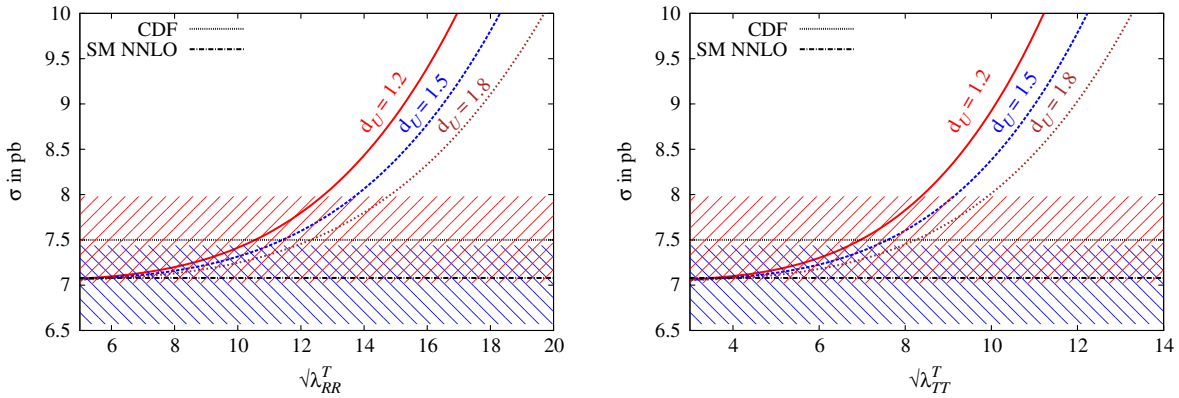

(a) $\lambda^T_{RR} \neq 0$ and $\lambda^T_{LR} = \lambda^T_{RL} = \lambda^T_{LL} = 0$

(b) $\lambda^T_{LL} = \lambda^T_{RR} = \lambda^T_{RL} = \lambda^T_{LR} = \lambda^T_{TT}$

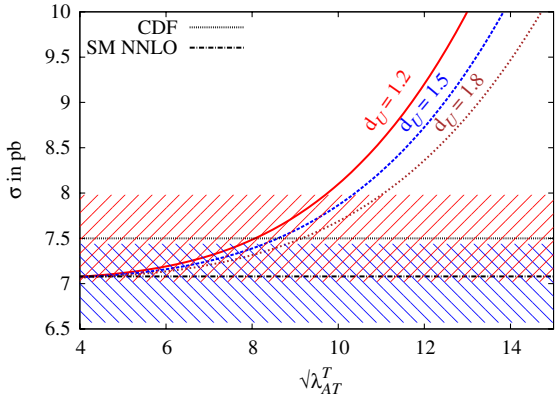

(c) $\lambda^T_{LL} = \lambda^T_{RR} = -\lambda^T_{RL} = -\lambda^T_{LR} = \lambda^T_{AT}$

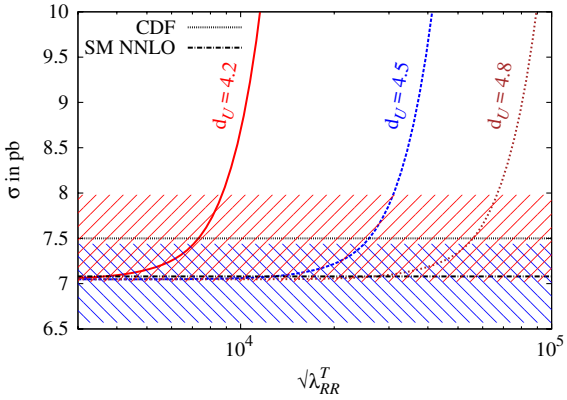

(d) $\lambda^T_{RR} \neq 0$ and $\lambda^T_{LR} = \lambda^T_{RL} = \lambda^T_{LL} = 0$

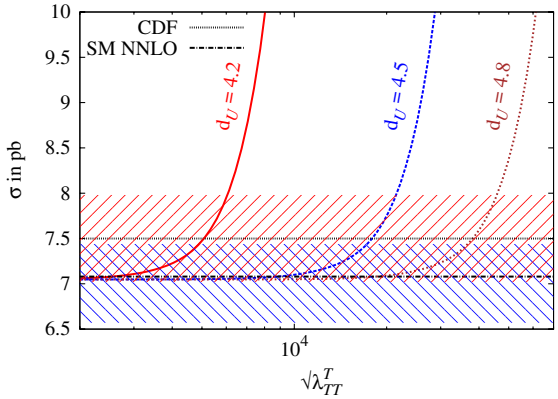

(e) $\lambda^T_{LL} = \lambda^T_{RR} = \lambda^T_{RL} = \lambda^T_{LR} = \lambda^T_{TT}$

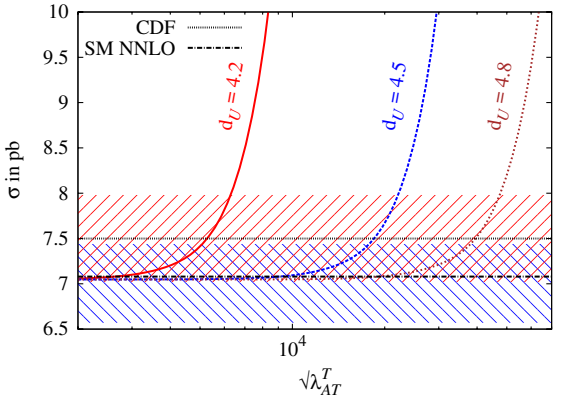

(f) $\lambda^T_{LL} = \lambda^T_{RR} = -\lambda^T_{RL} = -\lambda^T_{LR} = \lambda_{AT}$

FIG. 8 (color online). Variation of the cross section $\sigma(p\bar{p} \to t\bar{t})$ with couplings $\sqrt{\lambda^T_{ij}}$ for color singlet flavor conserving tensor unparticles corresponding to different values of $d_{\mathcal{U}}$ at fixed $\Lambda_{\mathcal{U}} = 1$ TeV and for different combinations of couplings mentioned in the text. The upper dotted line with a red band (shaded with positive slope lines) depicts the cross section 7.50 ± 0.48 pb from CDF (all channels) [1], while the lower dot-dashed line with a blue band (shaded with negative slope lines) shows a theoretical estimate 7.08 ± 0.36 pb at NNLO [4].

Here $\mathcal{C}_f^{\text{int}^{\text{FC}}_T} = 2$. Apart from an extra β_t suppression in comparison to the vector unparticles, as seen from Eq. (32), the other salient differences between the FC octet tensor and vector are

(1) Since the phase factor appearing in the tensor propagator is different from that of the vectors, the interference term contains an extra negative sign, leading to a positive $A_{\text{FB}}^{t\bar{t}}$ for $n < d_{\mathcal{U}} < (n + 1/2)$, zero for

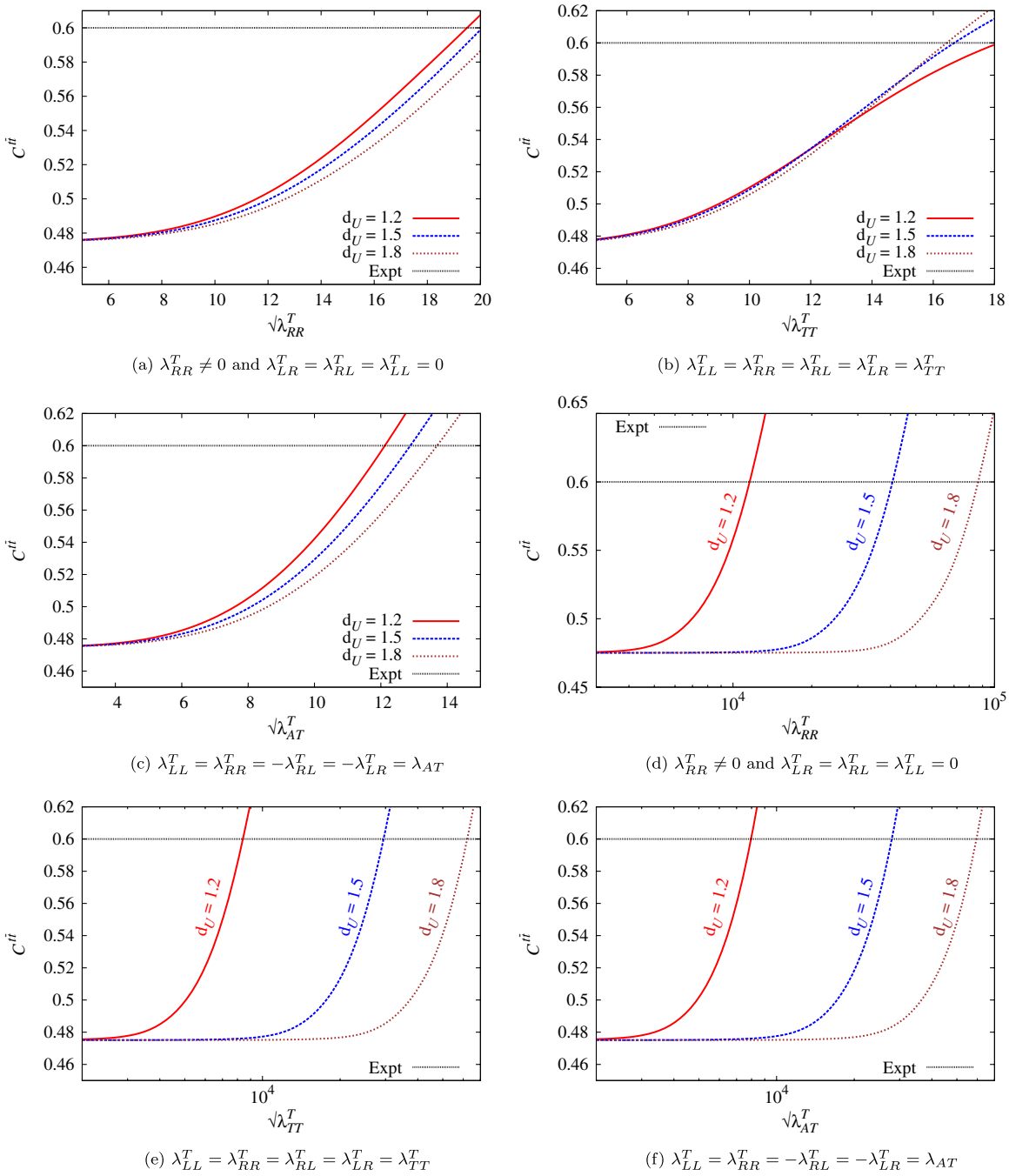

(a) $\lambda^T_{RR} \neq 0$ and $\lambda^T_{LR} = \lambda^T_{RL} = \lambda^T_{LL} = 0$

(b) $\lambda^T_{LL} = \lambda^T_{RR} = \lambda^T_{RL} = \lambda^T_{LR} = \lambda^T_{TT}$

(c) $\lambda^T_{LL} = \lambda^T_{RR} = -\lambda^T_{RL} = -\lambda^T_{LR} = \lambda_{AT}$

(d) $\lambda^T_{RR} \neq 0$ and $\lambda^T_{LR} = \lambda^T_{RL} = \lambda^T_{LL} = 0$

(e) $\lambda^T_{LL} = \lambda^T_{RR} = \lambda^T_{RL} = \lambda^T_{LR} = \lambda^T_{TT}$

(f) $\lambda^T_{LL} = \lambda^T_{RR} = -\lambda^T_{RL} = -\lambda^T_{LR} = \lambda_{AT}$

FIG. 9 (color online). Variation of the spin-correlation coefficient $C^{t\bar{t}}$ evaluated in helicity basis with couplings $\sqrt{\lambda^T}$ for color singlet flavor conserving tensor unparticles for various values of $d_{\mathcal{U}}$ at fixed $\Lambda_{\mathcal{U}} = 1$ TeV and for different combinations of couplings. The experimental value is depicted with a dot-dashed line at $0.60 \pm 0.50(\text{stat}) \pm 0.16(\text{syst})$ [28].

$d_{\mathcal{U}} = (n + 1/2)$, and negative for $(n + 1/2) < d_{\mathcal{U}} < (n + 1)$ interference with the SM. Thus, for the FC tensor octet unparticle, $A^{t\bar{t}}_{\text{FB}}$ is positive for $1 < d_{\mathcal{U}} < 1.5$ and negative for $1.5 < d_{\mathcal{U}} < 2$, which is just the opposite to that of the FC vector unparticle, as depicted in Fig. 11.

(2) Unlike the FC vector, the same helicity amplitudes also contribute to $A^{t\bar{t}}_{\text{FB}}$ for cases (a), (b), and (c), leading to $C^{t\bar{t}}_{\text{FB}} \neq A^{t\bar{t}}_{\text{FB}}$. The contribution to $A^{t\bar{t}}_{\text{FB}}$ from $|\mathcal{M}_{\text{unp}}|^2$ is zero for cases (c) and (d). The same helicity and the opposite helicity contribution to $A^{t\bar{t}}_{\text{FB}}$ vanish for the interference term in case (d). The opposite helicity contribution vanishes for case (d) (axial tensor) while it is nonzero for case (c). Thus, while an appreciable $A^{t\bar{t}}_{\text{FB}}$ contribution was coming in the FC vector octet for axial vector couplings, the same is not true for the FC tensor.

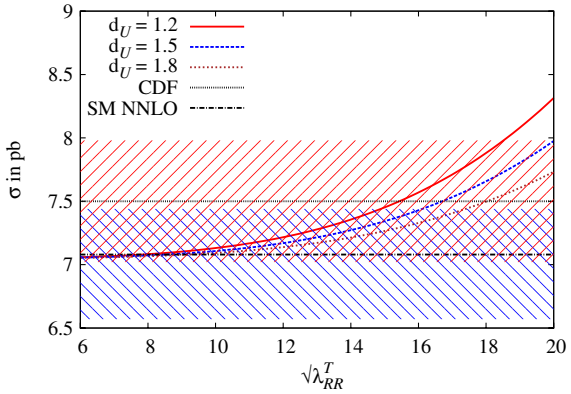

(a) $\lambda^T_{RR} \neq 0$ and $\lambda^T_{LR} = \lambda^T_{RL} = \lambda^T_{LL} = 0$

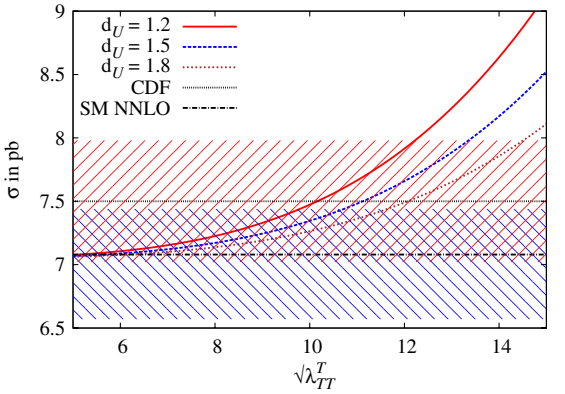

(b) $\lambda^T_{LL} = \lambda^T_{RR} = \lambda^T_{RL} = \lambda^T_{LR} = \lambda^T_{TT}$

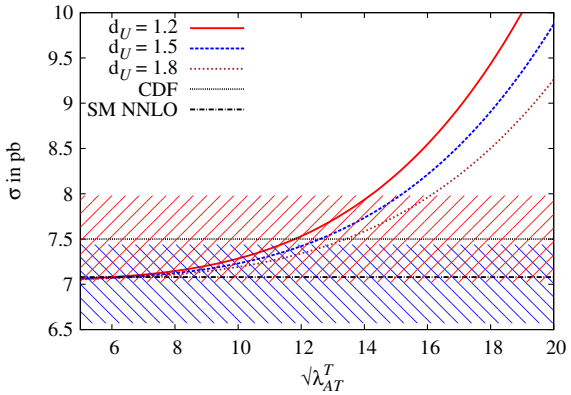

(c) $\lambda^T_{LL} = \lambda^T_{RR} = -\lambda^T_{RL} = -\lambda^T_{LR} = \lambda_{AT}$

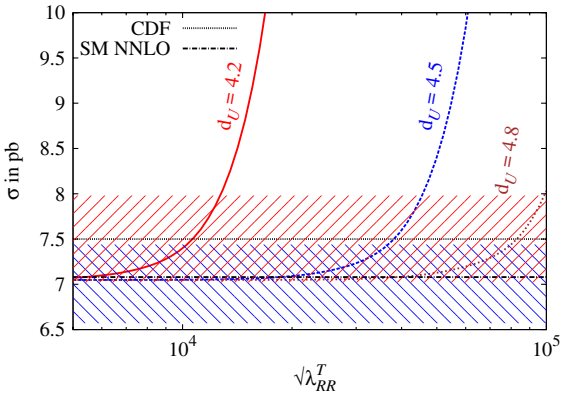

(d) $\lambda^T_{RR} \neq 0$ and $\lambda^T_{LR} = \lambda^T_{RL} = \lambda^T_{LL} = 0$

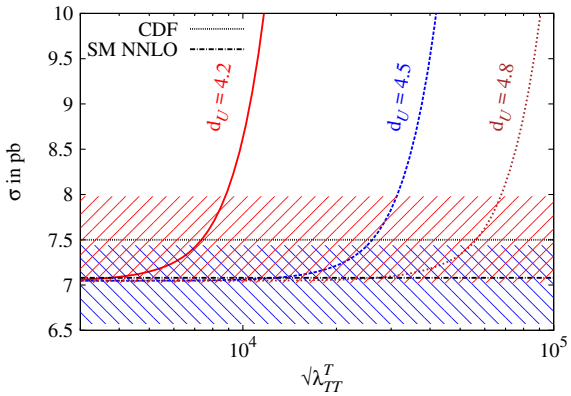

(e) $\lambda^T_{LL} = \lambda^T_{RR} = \lambda^T_{RL} = \lambda^T_{LR} = \lambda^T_{TT}$

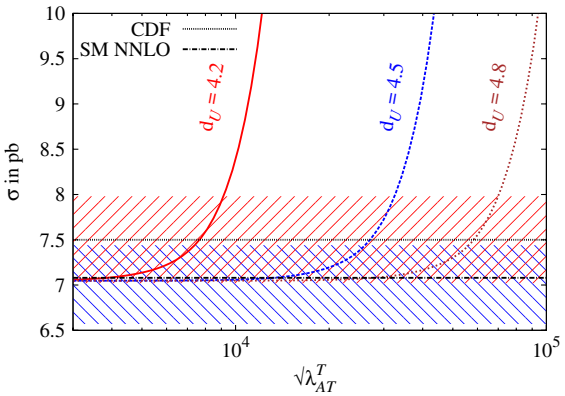

(f) $\lambda^T_{LL} = \lambda^T_{RR} = -\lambda^T_{RL} = -\lambda^T_{LR} = \lambda_{AT}$

FIG. 10 (color online). Variation of the cross section $\sigma(p\bar{p} \to t\bar{t})$ with couplings $\sqrt{\lambda^T}$ for color octet flavor conserving tensor unparticles corresponding to different values of $d_{\mathcal{U}}$ at fixed $\Lambda_{\mathcal{U}} = 1$ TeV. The upper dotted line with a red band (shaded with positive slope lines) depicts the cross section 7.50 ± 0.48 pb from CDF (all channels) [1], while the lower dot-dashed line with a blue band (shaded with negative slope lines) shows theoretical estimate 7.08 ± 0.36 pb at NNLO [4].

B. Flavor violating vector unparticle

The unparticle theory being an effective theory, it is possible to have flavor violating couplings of unparticles with quarks. The flavor violating couplings involving the first two generations of quarks and vector unparticles are tightly constrained. However, here we explore the vector unparticles which couple to the first and third generation quarks only. The top pair production mediated by these unparticles is realized through t channel processes. Hence, the second term in the propagator (19) also contributes.

Note that the vector unparticle propagator given in Eq. (16) has a pole for $d_{\mathcal{U}} = 2$ at $\hat{t} = 0$, and hence, constrains the $d_{\mathcal{U}}$ to be greater than 2 [18,50] for consistency of the theory. However, in our case $|\hat{t}|$ is quite large

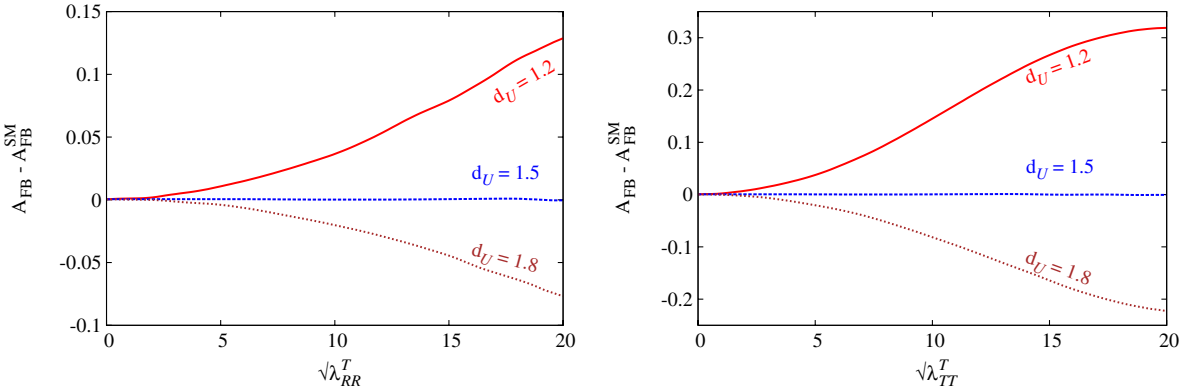

(a) $\lambda^T_{RR} \neq 0$ and $\lambda^T_{LR} = \lambda^T_{RL} = \lambda^T_{LL} = 0$ (b) $\lambda^T_{LL} = \lambda^T_{RR} = \lambda^T_{RL} = \lambda^T_{LR} = \lambda^T_{TT}$

FIG. 11 (color online). Variation of the $A_{FB} - A_{FB}^{SM}$ (the unparticle contribution to $A_{FB}^{t\bar{t}}$) with couplings $\sqrt{\lambda}^T_{ij}$ for color octet flavor conserving tensor unparticles for various values of $d_{\mathcal{U}}$ for a fixed $\Lambda = 1$ TeV. This is evaluated using the 1d differential distribution of rapidity in the $t\bar{t}$ rest frame. Panels (a) and (b) correspond to cases (a) and (c) of the text.

and we do not encounter this problem. But this kind of flavor violating coupling also initiates the top decay to unparticles, which is studied in Sec. V. This decay is only possible for $d_{\mathcal{U}} > 2$. We can overcome this constraint by introducing a small infrared cutoff which is discussed in Sec. III and later on in Sec. VI B. The implication of this broken scale invariance on the cross section, $A_{FB}^{t\bar{t}}$, and spin correlation is negligibly small as long as $\mu \ll |\hat{t}|$. This enables us to make our study of the top pair production in the region $d_{\mathcal{U}} > 1$.

Following the notation introduced in the previous subsection, the four possible couplings for a given $d_{\mathcal{U}}$ and $\Lambda_{\mathcal{U}}$ are (a) $g_L^{ut} = 0 \neq g_R^{ut}$, (b) $g_R^{ut} \neq 0 = g_L^{ut}$, (c) $g_L^{ut} = g_R^{ut} = g_V^{ut}$, and (d) $g_L^{ut} = -g_R^{ut} = g_A^{ut}$.

The t channel process involving flavor violating singlet/octet unparticles interferes with QCD and the negligibly small electroweak sector. Hence, the results can be explained by the flavor violating unparticle new physics sector and its interference with QCD. Writing separately the same and opposite helicity contributions to these terms,

$$|\mathcal{M}^{\text{unp}}|^2_{\text{same hel}} = c_f^{sq} g_s^2 \mathcal{B}^2_{\text{FVV}} \times \left[\frac{1}{2}\{(g_R^{ut})^4 + (g_L^{ut})^4\}(1-\beta_t^2)(1+A_t)^2 s_\theta^2 + 4(g_L^{ut} g_R^{ut})^2 \times \{(1+\beta_t^2)(1+A_t^2) + (1+\beta_t^2)A_t^2 c_\theta^2 + 4\beta_t A_t + 2(1+\beta_t^2+2\beta_t A_t)A_t c_\theta\}\right], \quad (35)$$

$$|\mathcal{M}^{\text{unp}}|^2_{\text{opp hel}} = c_f^{sq} g_s^2 \mathcal{B}^2_{\text{FVV}}\left[4(g_L^{ut} g_R^{ut})^2(1-\beta_t^2)A_t^2 s_\theta^2 + 2\{(g_R^{ut})^4 + (g_L^{ut})^4\} \times \left\{(1+A_t)^2\beta_t c_\theta + \frac{1}{4}(1+\beta_t^2)(1+A_t)^2(1+c_\theta^2)\right\}\right], \quad (36)$$

$$2\mathcal{M}^{\text{QCD}}\mathcal{R}e(\mathcal{M}^{\text{unp}})|_{\text{same hel}} = c_f^{\text{int}} g_s^2 \mathcal{B}_{\text{FVV}}[\{(g_L^{ut})^2 + (g_R^{ut})^2\}(1-\beta_t^2)(1+A_t)s_\theta^2], \quad (37)$$

and

$$2\mathcal{M}^{\text{QCD}}\mathcal{R}e(\mathcal{M}^{\text{unp}})|_{\text{opp hel}} = 2c_f^{\text{int}} g_s^2 \mathcal{B}_{\text{FVV}}[\{(g_L^{ut})^2 + (g_R^{ut})^2\}(1+A_t) \times (1+c_\theta^2+2\beta_t c_\theta)], \quad (38)$$

with

$$\mathcal{B}_{\text{FVV}} = \left(\frac{1}{\Lambda_{\mathcal{U}}^2}\right)^{(d_{\mathcal{U}}-1)}\left[\frac{A_{d_{\mathcal{U}}}}{2\sin(d_{\mathcal{U}}\pi)}\right](-\hat{t})^{(d_{\mathcal{U}}-2)}\hat{s};$$

$$A_t = \frac{am_t^2}{4\hat{t}} \quad \text{and} \quad a = \frac{2(d_{\mathcal{U}}-2)}{(d_{\mathcal{U}}-1)}.$$

Here $c_f^{sq} = 9(2)$ for FV singlet (octet) while $c_f^{\text{int}} = 4$ $(-2/3)$ for the FV singlet (octet).

The inherent symmetry of the helicity amplitudes makes the contribution to the observables identical for cases (a) and (b) and similarly for cases (c) and (d). Figures 13–16 give the variation of cross section $\sigma^{t\bar{t}}$, charge asymmetry $A_{FB}^{t\bar{t}}$, and spin correlation coefficient $C^{t\bar{t}}$ corresponding to the color singlet FV coupling, while the same variations for the flavor violating color octet are given in Figs. 17–20. The salient features of these flavor violating unparticles are as follows:

(1) Unlike the FC vector, the explicit and implicit dependence of $\hat{t}$ in the matrix element and in A_t, respectively, restrains the straightforward simplification of the matrix element squared as a polynomial in c_θ.
The contribution to $A_{FB}^{t\bar{t}}$ as well as $\sigma^{t\bar{t}}$ comes from both same and opposite helicity amplitudes.

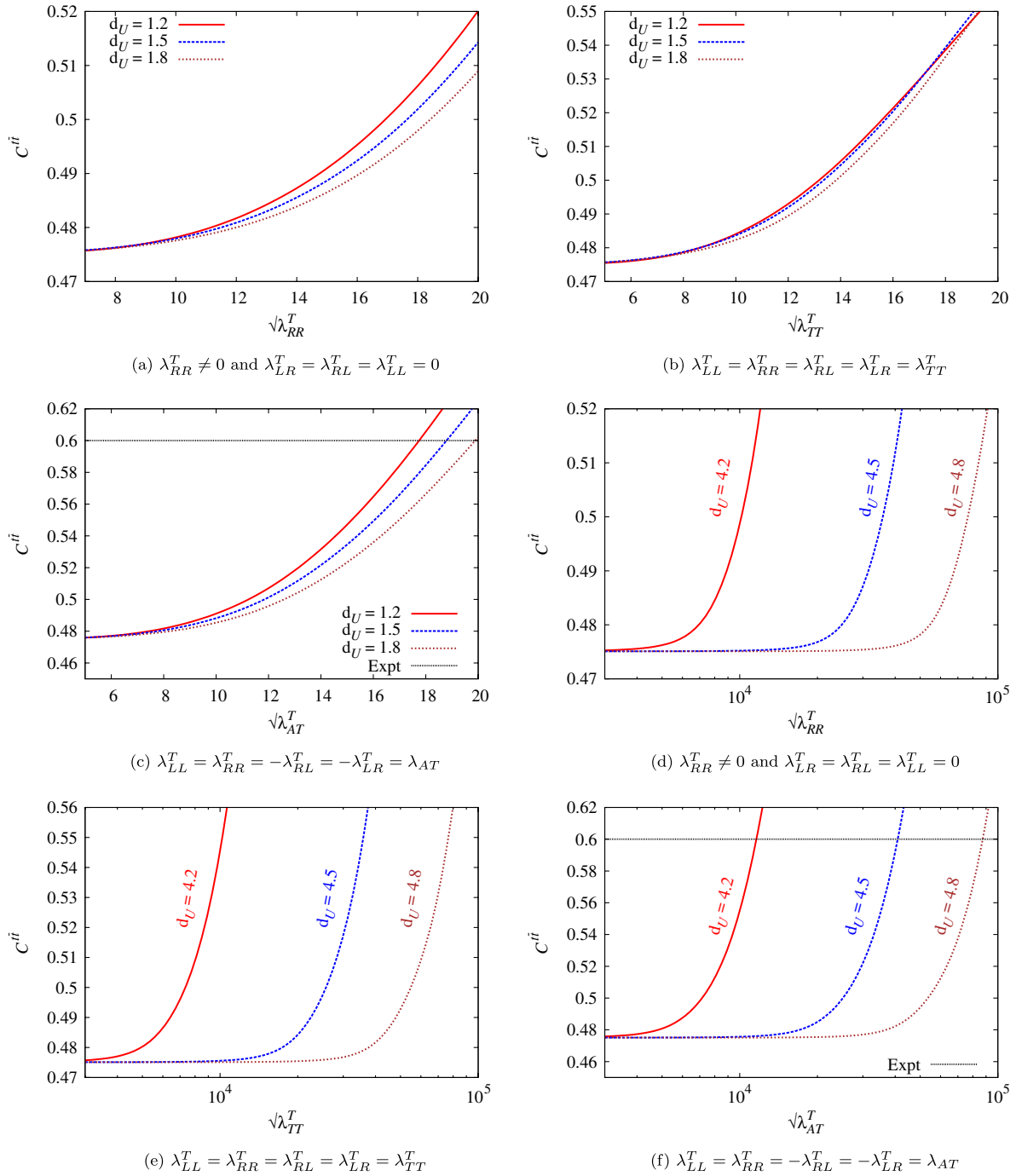

(a) $\lambda^T_{RR} \neq 0$ and $\lambda^T_{LR} = \lambda^T_{RL} = \lambda^T_{LL} = 0$

(b) $\lambda^T_{LL} = \lambda^T_{RR} = \lambda^T_{RL} = \lambda^T_{LR} = \lambda^T_{TT}$

(c) $\lambda^T_{LL} = \lambda^T_{RR} = -\lambda^T_{RL} = -\lambda^T_{LR} = \lambda_{AT}$

(d) $\lambda^T_{RR} \neq 0$ and $\lambda^T_{LR} = \lambda^T_{RL} = \lambda^T_{LL} = 0$

(e) $\lambda^T_{LL} = \lambda^T_{RR} = \lambda^T_{RL} = \lambda^T_{LR} = \lambda^T_{TT}$

(f) $\lambda^T_{LL} = \lambda^T_{RR} = -\lambda^T_{RL} = -\lambda^T_{LR} = \lambda_{AT}$

FIG. 12 (color online). Variation of the spin-correlation coefficient $C^{t\bar{t}}$ evaluated in the helicity basis with couplings $\sqrt{\lambda^T_{ij}}$ for color octet flavor conserving tensor unparticles for various values of $d_{\mathcal{U}}$ at fixed $\Lambda_{\mathcal{U}} = 1$ TeV and for different coupling combinations as mentioned in the text. The experimental value is depicted with a dot-dashed line at $0.60 \pm 0.50(\text{stat}) \pm 0.16(\text{syst})$ [28].

Therefore, C^t_{FB} is not the same as $A^{t\bar{t}}_{\text{FB}}$ when the flavor violating couplings are present.

(2) $\hat{t} = m_t^2 - (\hat{s}/2)(1 - \beta_t c_\theta)$ is always negative and $\sin(d_{\mathcal{U}}\pi)$ is negative for $(2n-1) < d_{\mathcal{U}} < (2n)$ but positive for $(2n) < d_{\mathcal{U}} < (2n+1)$. Finally, the sign of the color factor decides the sign of the contribution of the interference term of the FV vector unparticle with QCD. Thus, the interference term will be negative (positive) for the FV singlet (octet) for $1 < d_{\mathcal{U}} < 2$ but the sign will be reversed for $2 < d_{\mathcal{U}} < 3$. However, the negative values for the singlet are visible only for very small couplings, since with large couplings $|\mathcal{M}^{\text{unp}}|^2$ contribution overshadows the interference term, and hence the cross section, $A^{t\bar{t}}_{\text{FB}}$, and spin correlation for the FV singlet first decrease and then increase.

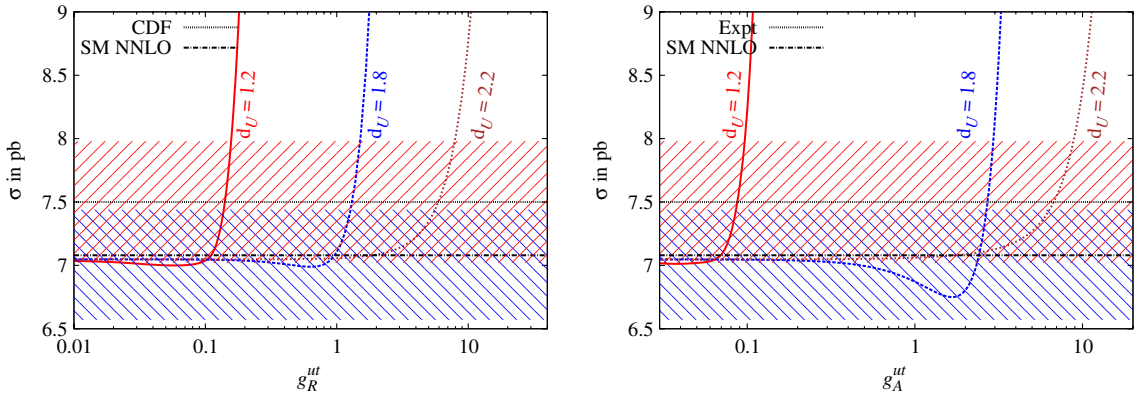

(a) $g_L^{ut} = 0 \neq g_R^{ut}$ (b) $g_R^{ut} = -g_L^{ut} = g_A^{ut}$

FIG. 13 (color online). Variation of the cross section $\sigma(p\bar{p} \to t\bar{t})$ with couplings g_i^{ut} for color singlet flavor violating vector unparticles corresponding to different values of $d_{\mathcal{U}}$ in the range $1 < d_{\mathcal{U}} < 3$ at fixed $\Lambda_{\mathcal{U}} = 1$ TeV. The upper dotted line with a red band (shaded with positive slope lines) depicts the cross section 7.50 ± 0.48 pb from CDF (all channels) [1], while the lower dot-dashed line with a blue band (shaded with negative slope lines) shows the theoretical estimate 7.08 ± 0.36 pb at NNLO [4].

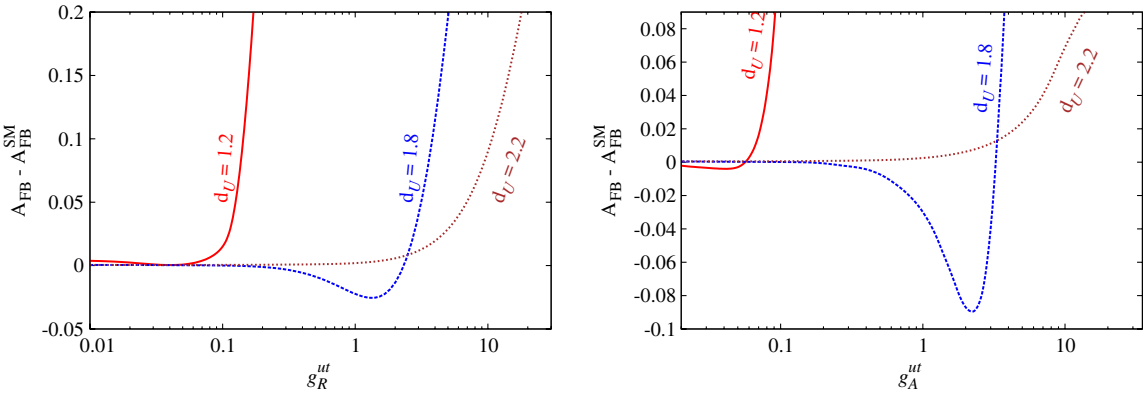

(a) $g_L^{ut} = 0 \neq g_R^{ut}$ (b) $g_R^{ut} = -g_L^{ut} = g_A^{ut}$

FIG. 14 (color online). Variation of the unparticle contribution to charge asymmetry $A_{FB} - A_{FB}^{SM}$ with couplings g_i^{ut} in the presence of flavor violating color singlet vector unparticles for various values of $d_{\mathcal{U}}$ in the range $1 < d_{\mathcal{U}} < 3$ at fixed $\Lambda_{\mathcal{U}} = 1$ TeV. This is evaluated using the 1d differential distribution of rapidity in the $t\bar{t}$ rest frame.

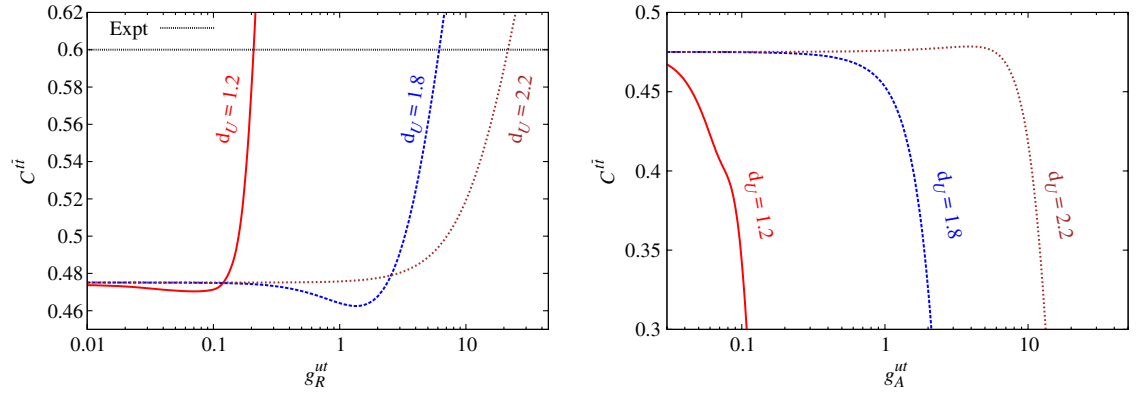

(a) $g_L^{ut} = 0 \neq g_R^{ut}$ (b) $g_R^{ut} = -g_L^{ut} = g_A^{ut}$

FIG. 15 (color online). Variation of the spin correlation coefficient $C^{t\bar{t}}$ with couplings g_i^{ut} in the presence of flavor violating color singlet vector unparticles for various values of $d_{\mathcal{U}}$ in the range $1 < d_{\mathcal{U}} < 3$ at fixed $\Lambda_{\mathcal{U}} = 1$ TeV. The experimental value is depicted with a dot-dashed line at $0.60 \pm 0.50(\text{stat}) \pm 0.16(\text{syst})$ [28].

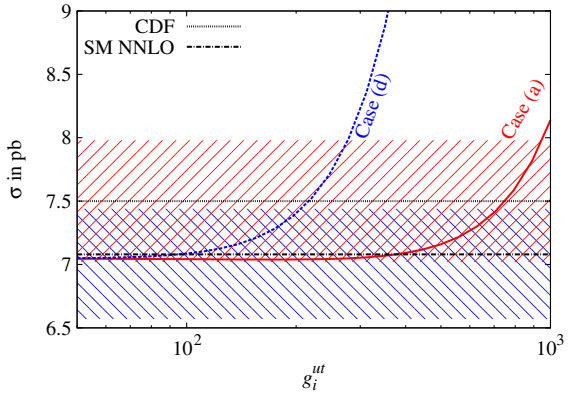

(a) g_i^{ut} variation of $\sigma^{t\bar{t}}$ for cases (a) $g_L^{ut} = 0 \neq g_R^{ut}$ and (d) $g_R^{ut} = -g_L^{ut} = g_A^{ut}$ with $d_{\mathcal{U}} = 3.2$

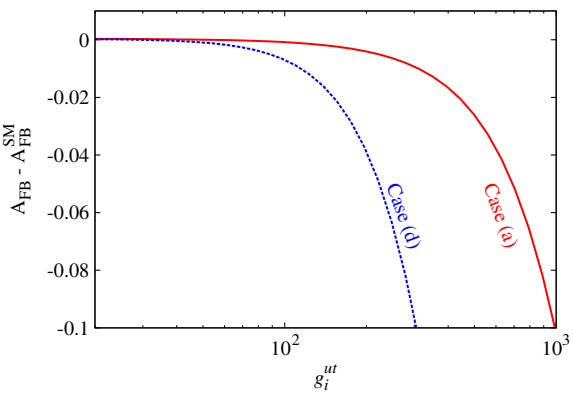

(b) g_i^{ut} variation of $A_{FB} - A_{FB}^{SM}$ for cases (a) $g_L^{ut} = 0 \neq g_R^{ut}$ and (d) $g_R^{ut} = -g_L^{ut} = g_A^{ut}$ with $d_{\mathcal{U}} = 3.2$

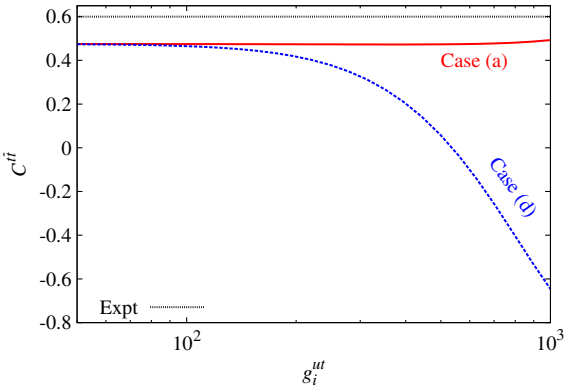

(c) g^{ut} variation of $C^{t\bar{t}}$ for cases (a) and (d) with $d_{\mathcal{U}} = 3.2$

FIG. 16 (color online). Variation of the cross section $\sigma(p\bar{p} \to t\bar{t})$, the unparticle contribution to charge asymmetry $A_{\mathrm{FB}} - A_{\mathrm{FB}}^{\mathrm{SM}}$, and spin correlation coefficient $C^{t\bar{t}}$ with couplings g_i^{ut} for color singlet flavor violating vector unparticles at fixed $d_{\mathcal{U}} = 3.2$ and $\Lambda_{\mathcal{U}} = 1$ TeV, corresponding to cases (a) and (d) mentioned in the text. In plot (a), the upper dotted line with a red band (shaded with positive slope lines) depicts the cross section 7.50 ± 0.48 pb from CDF (all channels) [1], while the lower dot-dashed line with a blue band (shaded with negative slope lines) shows the theoretical estimate 7.08 ± 0.36 pb at NNLO [4]. Plot (b) is evaluated using the 1d differential distribution of rapidity in the $t\bar{t}$ rest frame. In plot (c), the expertimental value is depicted with a dot-dashed line at $0.60 \pm 0.50(\mathrm{stat}) \pm 0.16(\mathrm{syst})$ [28].

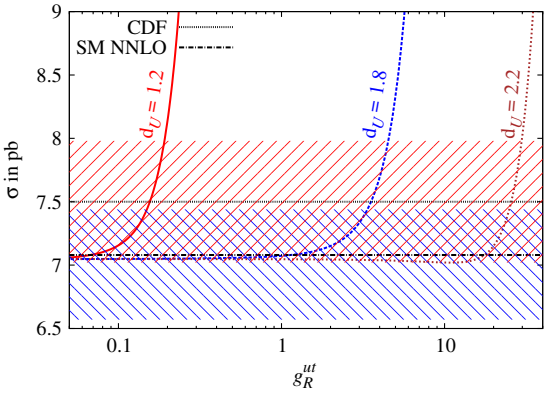

(a) $g_L^{ut} = 0 \neq g_R^{ut}$

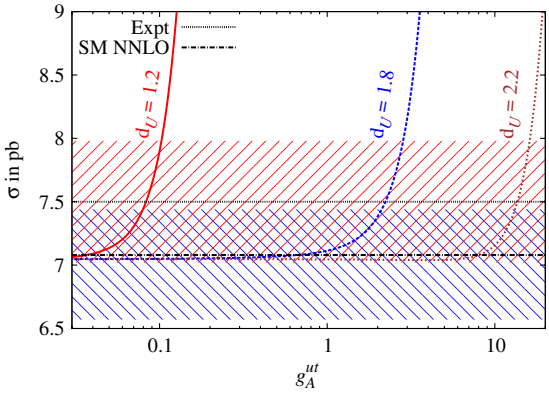

(b) $g_R^{ut} = -g_L^{ut} = g_A^{ut}$

FIG. 17 (color online). Variation of the cross section $\sigma(p\bar{p} \to t\bar{t})$ with couplings g_i^{ut} for color octet flavor violating vector unparticles for various values of $d_{\mathcal{U}}$ in the range $1 < d_{\mathcal{U}} < 3$ at fixed $\Lambda_{\mathcal{U}} = 1$ TeV and for cases (a) [or (b)] and (d) [or (c)] mentioned in the text. The upper dotted line with a red band (shaded with positive slope lines) depicts the cross section 7.50 ± 0.48 pb from CDF (all channels) [1], while the lower dot-dashed line with a blue band (shaded with negative slope lines) shows the theoretical estimate 7.08 ± 0.36 pb at NNLO [4].

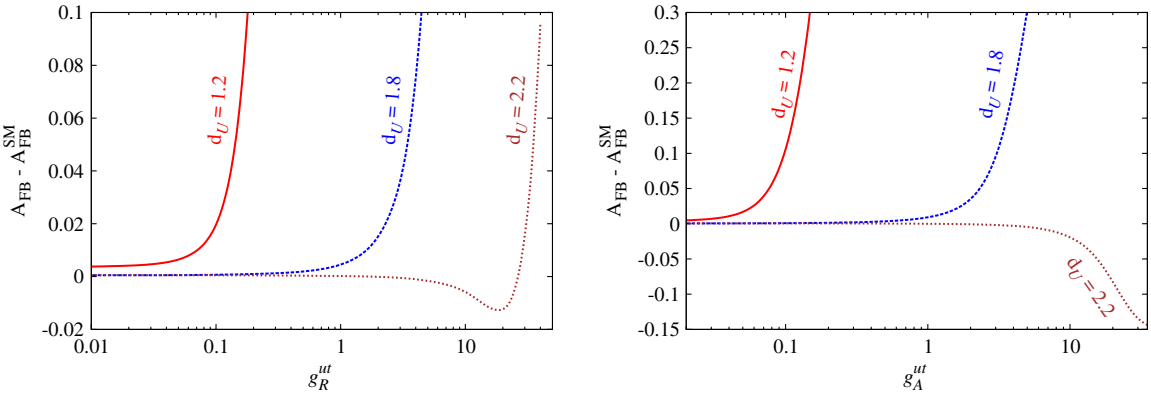

(a) $g_L^{ut} = 0 \neq g_R^{ut}$ (b) $g_R^{ut} = -g_L^{ut} = g_A^{ut}$

FIG. 18 (color online). Variation of the unparticle contribution to charge asymmetry A_{FB}^{SM} with couplings g_i^{ut} in the presence of flavor violating color octet vector unparticles for various values of $d_{\mathcal{U}}$ in the range $1 < d_{\mathcal{U}} < 3$ at fixed $\Lambda_{\mathcal{U}} = 1$ TeV and for the cases (a) [or (b)] and (d) [or (c)]. This is evaluated using the 1d differential distribution of rapidity in the $t\bar{t}$ rest frame.

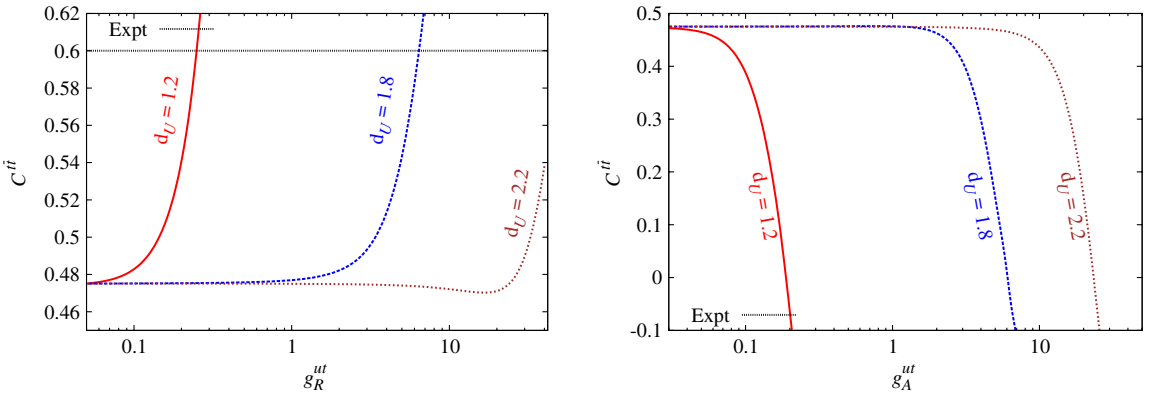

(a) $g_L^{ut} = 0 \neq g_R^{ut}$ (b) $g_R^{ut} = -g_L^{ut} = g_A^{ut}$

FIG. 19 (color online). Variation of the spin correlation coefficient $C^{t\bar{t}}$ with couplings g_i^{ut} in the presence of flavor violating color octet vector unparticles for various values of $d_{\mathcal{U}}$ in the range $1 < d_{\mathcal{U}} < 3$ at fixed $\Lambda_{\mathcal{U}} = 1$ TeV and for cases (a) [or (b)] and (d) [or (c)] mentioned in the text. The experimental value is depicted with a dot-dashed line at $0.60 \pm 0.50(\text{stat}) \pm 0.16(\text{syst})$ [28].

Since $-1 < m_t^2/(4\hat{t}) \leq 0$, it implies $|A_t| \leq 1$, and the factor $(1 + A_t)$ is always positive. Thus, even though a flips sign from positive for $1 < d_{\mathcal{U}} < 2$ to negative for $2 < d_{\mathcal{U}} < 3$, it does not affect the sign of the interference term for the $d_{\mathcal{U}}$ values considered.

Thus, for couplings to be within the range that gives $\sigma^{t\bar{t}}$ consistent with the CDF value, the FV singlet vector unparticle gives favorable $A_{FB}^{t\bar{t}}$ only for $d_{\mathcal{U}}$ close to 1. On the other hand, the octet gives favorable values for the entire range $1 < d_{\mathcal{U}} < 2$. For $2 < d_{\mathcal{U}} < 3$, the octet gives negative $A_{FB}^{t\bar{t}}$ for allowed values of couplings, while the singlet gives very low values.

V. FV COUPLINGS: SAME SIGN TOPS AND TOP DECAY WIDTH

As we have introduced the FV neutral current via non-diagonal coupling for the fermion-fermion unparticle involving the first and third generations, this coupling is likely to have its bearings on the same sign top quark production and top decay width [51].

A. Same sign top production

Recently, an inclusive search of same sign tops at CMS disfavored the flavor conserving neutral current (FCNC) solution in the Z' model for the $A_{FB}^{t\bar{t}}$ anomaly at the Tevatron [52]. The SM contribution is highly suppressed and any affirmative signal would indicate a presence of new physics. The unparticle theory through their FV couplings also generates the same sign tops $p\bar{p} \to tt$ via t and u channel Feynman diagrams. We compute the parton level helicity amplitudes for $uu \to tt$ which are given in Appendix A 5.

As mentioned earlier, we have performed our analysis with $\Lambda_{\mathcal{U}} = 1$ TeV to probe the physics at the Tevatron, where the partonic c.m. energy $\ll 1$ TeV. However, to examine the physics at the LHC and validate the same model, we need to enhance this scale at least to $\Lambda_{\mathcal{U}} = 10$ TeV. In this light at present, we only see the

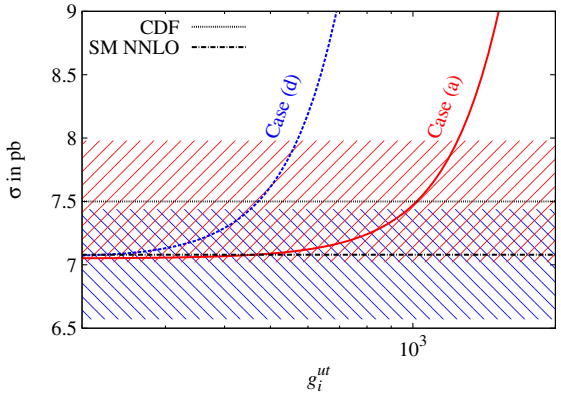

(a) g_i^{ut} variation of $\sigma^{t\bar{t}}$ for cases (a) $g_L^{ut} = 0 \neq g_R^{ut}$ and (d) $g_R^{ut} = -g_L^{ut} = g_A^{ut}$ with $d_{\mathcal{U}} = 3.2$

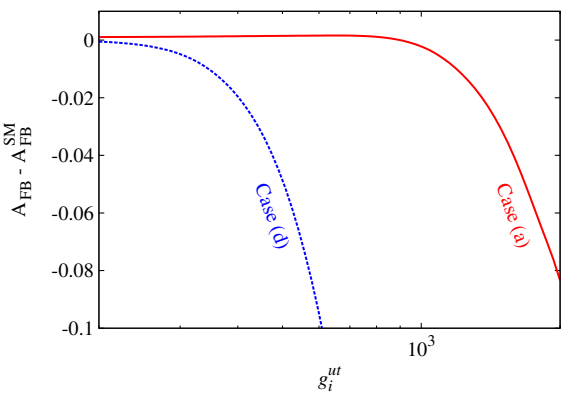

(b) g_i^{ut} variation of $A_{FB} - A_{FB}^{SM}$ for cases (a) $g_L^{ut} = 0 \neq g_R^{ut}$ and (d) $g_R^{ut} = -g_L^{ut} = g_A^{ut}$ with $d_{\mathcal{U}} = 3.2$

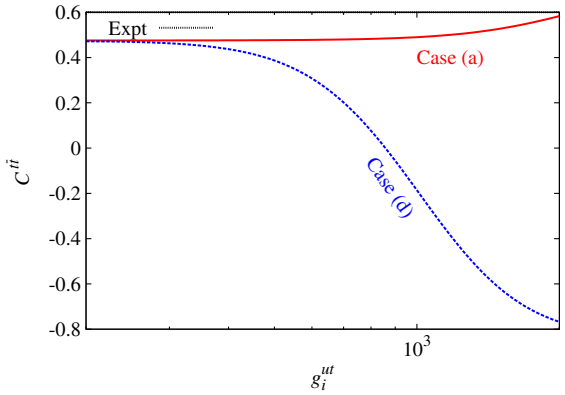

(c) g_i^{ut} variation of $C^{t\bar{t}}$ for cases (a) $g_L^{ut} = 0 \neq g_R^{ut}$ and (d) $g_R^{ut} = -g_L^{ut} = g_A^{ut}$ with $d_{\mathcal{U}} = 3.2$

FIG. 20 (color online). Variation of the cross section $\sigma(p\bar{p} \to t\bar{t})$, the unparticle contribution to charge asymmetry $A_{\rm FB} - A_{\rm FB}^{\rm SM}$, and the spin correlation coefficient $C^{t\bar{t}}$ with couplings g_i^{ut} for color octet flavor violating vector unparticles at fixed $d_{\mathcal{U}} = 3.2$ and $\Lambda_{\mathcal{U}} = 1$ TeV corresponding to cases (a) and (d) mentioned in the text. In plot (a), the upper dotted line with a red band (shaded with positive slope lines) depicts the cross section 7.50 ± 0.48 pb from CDF (all channels) [1], while the lower dot-dashed line with a blue band (shaded with negative slope lines) shows the theoretical estimate 7.08 ± 0.36 pb at NNLO [4]. Plot (b) is evaluated using the 1d differential distribution of rapidity in the $t\bar{t}$ rest frame. In plot (c), the experimental value is depicted with a dot-dashed line at $0.60 \pm 0.50(\text{stat}) \pm 0.16(\text{syst})$ [28].

effect of the unparticle physics at the Tevatron and check their cross-validity among various processes. Same sign top production was also constrained by the Tevatron [53]. The CDF data were based on a same sign dilepton search and their observations are summarized in Table II of Ref. [53]. They predicted the upper limits at 95% C.L., on the production cross section $\sigma(p\bar{p} \to tt + \bar{t}\,\bar{t})$ times branching ratio $\text{BR}(W \to l\nu)^2$ for all distinct chirality modes: left-left (LL) to be 54 fb, right-right (RR) to be 51 fb, and left-right (LR) to be 51 fb, assuming only one nonzero mode at one time. We present the 95% C.L. contours for varying $d_{\mathcal{U}}$ on the $|g_L^{ut}| - |g_R^{ut}|$ plane using the result from the LL mode, assuming that there is a remarkable difference in efficiency or shape among the contributions from the LL, LR, or RR modes. The contours corresponding to color singlets and octets are shown in Figs. 21(a) and 21(b), respectively.

We expect that with the change of the scale $\Lambda_{\mathcal{U}}$, we will be able to probe the same parameter region for the LHC. This work is currently in progress.

B. Top decay width

The total decay width of top quarks is one of the fundamental properties of top physics. It is measured with precision from the partial decay width $\Gamma(t \to Wb)$ in the t channel of the single top quark production and from $t\bar{t}$ events. Recently, the top total width was measured to be $\Gamma_t = 1.99^{+0.69}_{-0.55}$ GeV corresponding to 2.3 fb^{-1} data by the D0 Collaboration [54]. The SM contribution to the top decay width at NLO in α_s is given as

$$\Gamma_{\rm SM}(t \to Wb) = \frac{G_F m_t^3}{8\pi\sqrt{2}} |V_{tb}|^2 \left(1 - \frac{M_W^2}{m_t^2}\right)^2 \left(1 + 2\frac{M_W^2}{m_t^2}\right) \times \left[1 - \frac{2\alpha_s}{3\pi}\left(\frac{2\pi^2}{3} - \frac{5}{2}\right)\right]. \quad (39)$$

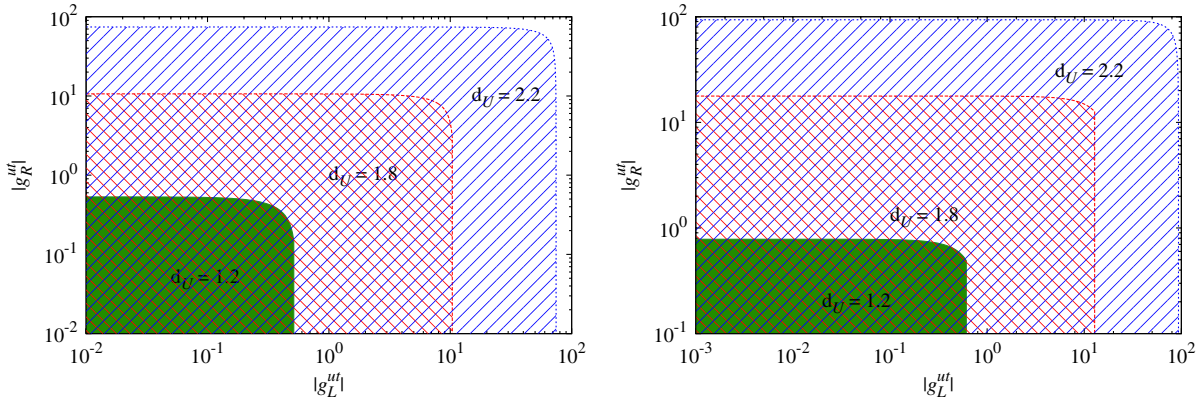

(a) Flavor Violating Singlet Vector Unparticle (b) Flavor Violating Octet Vector Unparticle

FIG. 21 (color online). Exclusion contours at 95% C.L. corresponding to the cross section $\sigma(p\bar{p} \to tt + \bar{t}\bar{t}) = 54$ fb [52] on the $|g_L^{ut}| - |g_R^{ut}|$ plane for a given $d_{\mathcal{U}}$ and $\Lambda_{\mathcal{U}} = 1$ TeV. The value of the couplings bounded by the enclosed region (for a specific $d_{\mathcal{U}}$ value) are allowed.

Computing with $\alpha_s(M_Z) = 0.118$, $G_F = 1.16637 \times 10^{-5}$ GeV^{-2}, $M_W = 80.399$ GeV, $|V_{tb}| = 1$, and $m_t = 173$ GeV, we find $\Gamma_{\rm SM} = (t \to Wb)_{\rm SM} = 1.34$ GeV.

In the unparticle sector, this was first introduced by Georgi [17] where he considered the flavor violating derivative coupling of the scalar unparticles given as $i\lambda\Lambda^{-d_{\mathcal{U}}}\bar{u}\gamma_\mu(1-\gamma_5)t\partial^\mu\mathcal{O}_{\mathcal{U}} + \text{H.c.}$ The FV vector unparticle initiates a new channel for a top decaying to an unparticle and a lighter quark q. We compute the partial decay width $\Gamma_{\mathcal{U}}(t \to q\mathcal{U}^V)$ as given in Appendix B. This

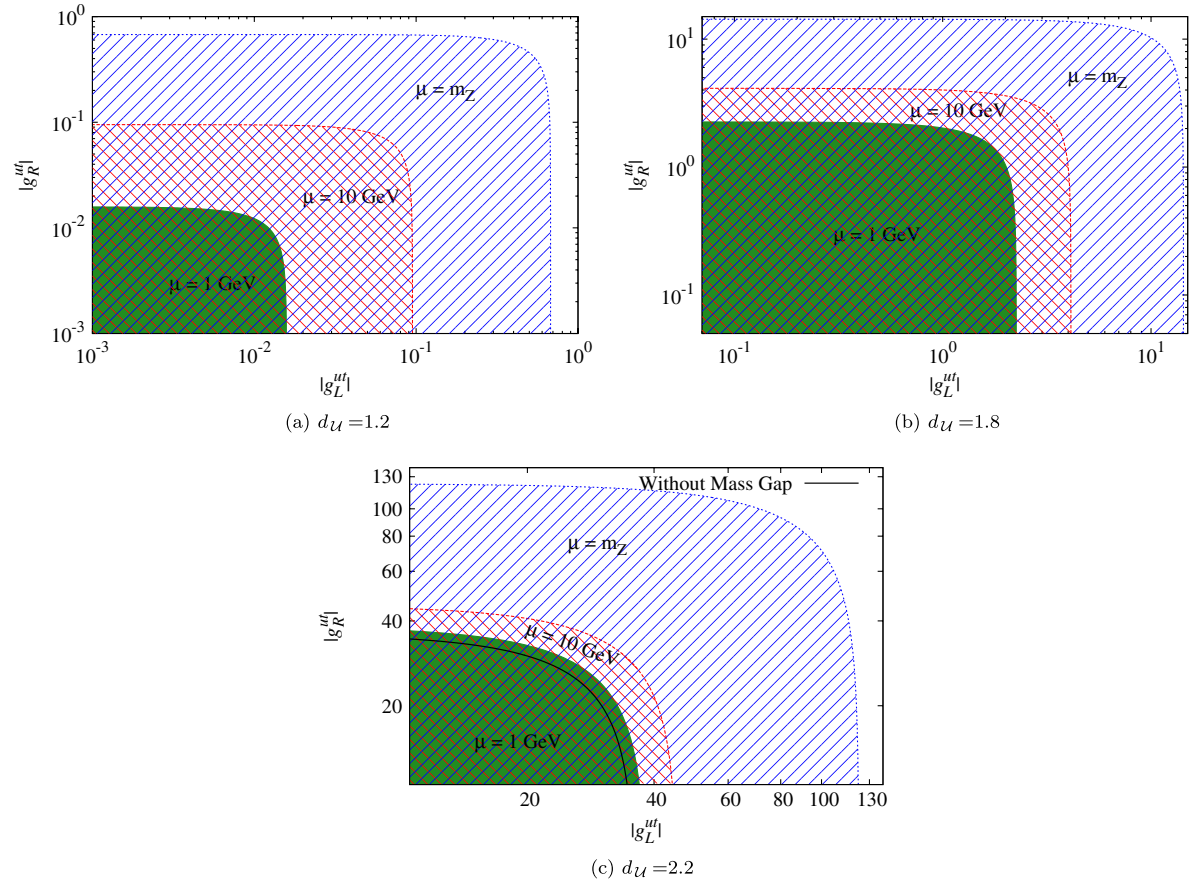

(a) $d_{\mathcal{U}}$ =1.2 (b) $d_{\mathcal{U}}$ =1.8

(c) $d_{\mathcal{U}}$ =2.2

FIG. 22 (color online). Exclusion contours at 95% C.L. corresponding to $\Gamma_t = 1.99^{+0.69}_{-0.55}$ GeV [54] on the $|g_L^{ut}| - |g_R^{ut}|$ plane for flavor violating octet vector unparticles with a given mass gap μ and $\Lambda_{\mathcal{U}} = 1$ TeV. The values of the couplings bounded by the enclosed region (for a specific mass μ value) are allowed. In panel (c), the black contour line corresponds to $\mu = 0$ GeV.

decay width diverges for $d_{\mathcal{U}} < 2$ while for $d_{\mathcal{U}} > 2$ it is given as

$$\Gamma_t = \Gamma_{\rm SM} + \frac{N_C}{6}\frac{A_{d_{\mathcal{U}}}}{4\pi^2} g_s^2[(g_L^{\mathcal{U}_V^n tq})^2 + (g_R^{\mathcal{U}_V^n tq})^2]\left(\frac{m_t^2}{\Lambda_{\mathcal{U}}^2}\right)^{d_{\mathcal{U}}-1} \times \frac{m_t}{4}\left[\frac{a-4+(a+2)d_{\mathcal{U}}}{(d_{\mathcal{U}}-2)(d_{\mathcal{U}}-1)d_{\mathcal{U}}(d_{\mathcal{U}}+1)}\right]. \quad (40)$$

However, if the scale invariance is broken at a scale $\mu \neq 0$, one can evaluate the decay width in the region $1 < d_{\mathcal{U}} < 2$. As mentioned earlier inclusion of such a mass gap also protects the theory from realizing a continuous spectrum of unparticles through the decay process. Introduction of such a scale, however, does not modify the cross sections for $\mu \ll m_{t\bar{t}}$. We depict the exclusion contours with various choices of the breaking scales at 1 GeV, 10 GeV, and at $m_Z = 91.18$ GeV, corresponding to the color octet unparticles on the $|g_L^{ut}| - |g_R^{ut}|$ plane. These contours show the allowed range of these couplings constrained from the observed total top decay width $\Gamma_t = \Gamma_{\rm SM} + \Gamma_{\mathcal{U}}$ by D0. The nature and behavior of the contribution from the color singlet flavor violating unparticles are similar to that of the octet. Therefore, we do not provide the corresponding contours separately. We find from Fig. 22 that the parameter region which contributes considerably to $t\bar{t}$ events, along with large positive $A_{\rm FB}^{t\bar{t}}$, shrinks, and hence is much more constrained. We also observe that the increase in the scale invariance breaking scale relaxes the bound on the couplings.

VI. ANALYSIS AND SUMMARY

A. $m_{t\bar{t}}$ distribution of $A_{\rm FB}^{t\bar{t}}$

We scan our parameters and perform a χ^2 analysis for both FC and FV cases and predict the set of best parameters which can possibly explain the $A_{\rm FB}^{t\bar{t}}$ anomaly. To perform this analysis, we take into account the $A_{\rm FB}^{t\bar{t}}$ distribution over $m_{t\bar{t}}$ bins from the full Run II Tevatron data set [7]. We define the χ^2 as

$$\chi^2 = \sum_{i=1}^{n} \frac{(\mathcal{O}_i^{th} - \mathcal{O}_i^{\rm exp})^2}{(\delta\mathcal{O}_i^{\rm exp})^2}, \quad (41)$$

where i is the $m_{t\bar{t}}$ bin index; $\mathcal{O}_i$th, $\mathcal{O}_i^{\rm exp}$, and $\delta\mathcal{O}_i^{\rm exp}$ are the SM + model estimate, experimental measurement, and its error in the corresponding ith bin, respectively. Following Ref. [7], we quote and use the experimental data based on the complete data set of Run II at an integrated luminosity 8.7 fb^{-1} (given in Table II) to compute $\chi^2_{\rm min}$. The first column is the bin size while the second and third columns of Table II give experimentally observed values of $A_{\rm FB}^{t\bar{t}}$ in each of these bins with its error and the expected number from NLO (QCD + EW) with backgrounds, respectively. We also add the observed cross section as an eighth observable in Eq. (41) $\sigma(p\bar{p} \to t\bar{t}) = 7.5 \pm 0.31({\rm stat}) \pm 0.34({\rm syst}) \pm 0.15(Z\,{\rm theory})$ pb [1]. The two-dimensional parameter space $[(\sqrt{\lambda_{LL}}, \sqrt{\lambda_{RR}})$ for FC cases and (g_L^{ut}, g_R^{ut}) for the FV case] for fixed $d_{\mathcal{U}}$ and $\Lambda_{\mathcal{U}}$ is scanned leading to the minimum value of the $\chi^2 \equiv \chi^2_{\rm min}$.

At $\chi^2_{\rm min}$ the corresponding parameter points are likely to be the best possible model parameters in the unparticle physics at $\Lambda_{\mathcal{U}} = 1$ TeV, which are consistent with all the observations. The fourth through seventh columns in Table II exhibit the $m_{t\bar{t}}$ spectrum of $A_{\rm FB}^{t\bar{t}}$, corresponding to the four distinct cases of best-fit model parameters. In Fig. 23, we plot histograms showing the $m_{t\bar{t}}$ spectrum of $A_{\rm FB}^{t\bar{t}}$ for all four cases. We have shown and compared the slope of our best-fit line with that from the experimental data in this figure and Table II.

B. Effect of mass gap

In our study, we have not introduced any infrared cutoff in the theory of unparticles modulo top decay width. The existence of massless fields in a theory gives rise to severe modification in the low energy phenomenology which is successfully explained by the SM alone. To be precise, if there is no cutoff in the theory of unparticles there would be

TABLE II. The first three columns give the bin limits of the $m_{t\bar{t}}$, the observed $A_{\rm FB}^{t\bar{t}}$ with error, and the NLO (QCD + EW) generated $A_{\rm FB}^{t\bar{t}}$, respectively [7]. The next four consecutive columns provide the differential $A_{\rm FB}^{t\bar{t}}$, corresponding to the model parameters (given in Fig. 23) leading to $\chi^2_{\rm min}$ at fixed $\Lambda_{\mathcal{U}} = 1$ TeV. The penultimate line gives the $\chi^2_{\rm min}$ for respective cases. The last line in the table gives the slope of the best-fit line with the simulated data.

$m_{t\bar{t}}$	$A_{\rm FB}^{t\bar{t}}$ ($\pm$ stat)	NLO (QCD + EW) $t\bar{t}$ + bkg	FC vector singlet case (a)	FC vector octet case (a)	FC tensor octet case (d)	FV vector octet case (a)
$<$400 GeV/c^2	-0.006 ± 0.031	0.012	0.03	0.03	0.03	0.03
400–450 GeV/c^2	0.065 ± 0.040	0.023	0.05	0.05	0.06	0.05
450–500 GeV/c^2	0.118 ± 0.051	0.022	0.06	0.06	0.07	0.07
500–550 GeV/c^2	0.159 ± 0.069	0.041	0.09	0.10	0.10	0.10
550–600 GeV/c^2	0.118 ± 0.088	0.066	0.13	0.13	0.15	0.14
600–700 GeV/c^2	0.273 ± 0.103	0.065	0.21	0.26	0.29	0.27
$\geq$700 GeV/c^2	0.306 ± 0.136	0.107	0.28	0.34	0.41	0.39
$\chi^2_{\rm min}$	…	…	2.80	3.16	3.36	3.65
Slope of best-fit line	$(8.9 \pm 2.3) \times 10^{-4}$	$(2.2 \pm 2.3) \times 10^{-4}$	6.7×10^{-4}	8.8×10^{-4}	1×10^{-3}	9.8×10^{-4}

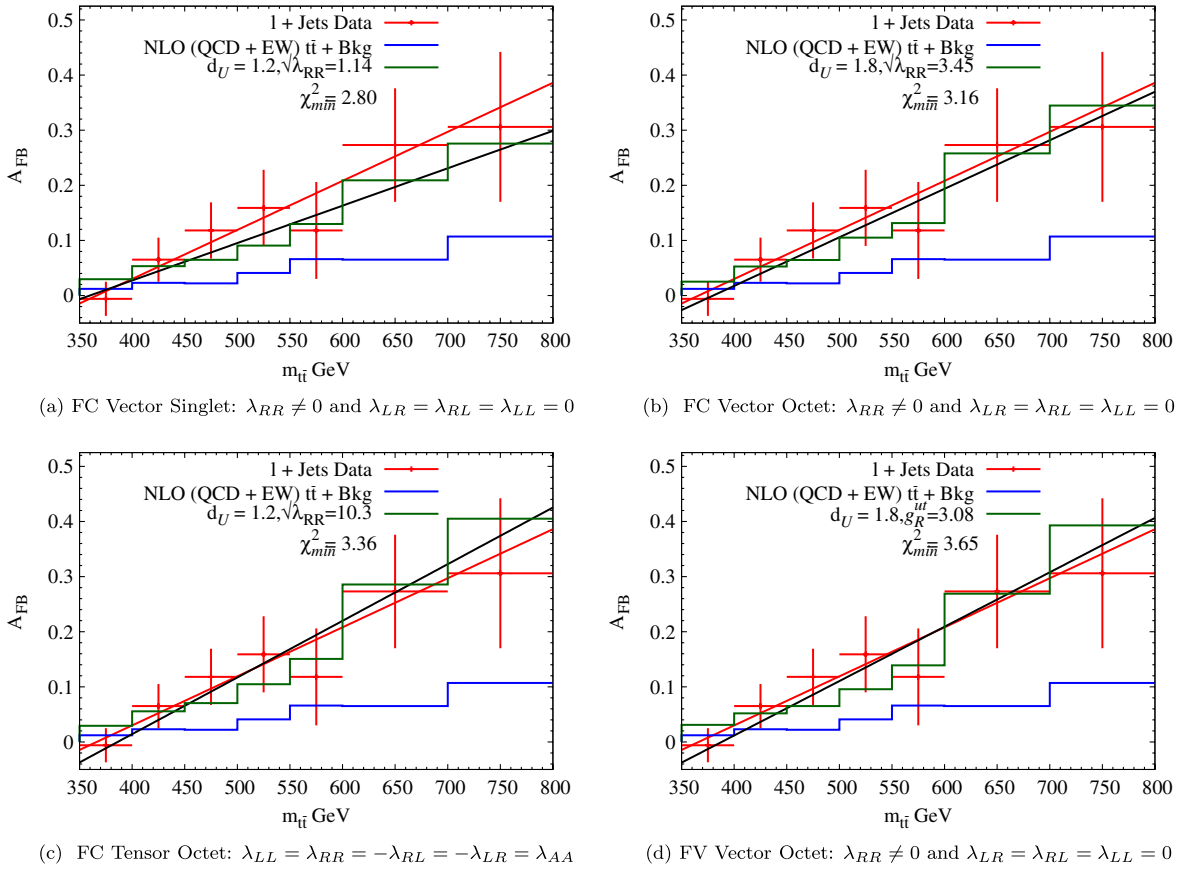

(a) FC Vector Singlet: $\lambda_{RR} \neq 0$ and $\lambda_{LR} = \lambda_{RL} = \lambda_{LL} = 0$

(b) FC Vector Octet: $\lambda_{RR} \neq 0$ and $\lambda_{LR} = \lambda_{RL} = \lambda_{LL} = 0$

(c) FC Tensor Octet: $\lambda_{LL} = \lambda_{RR} = -\lambda_{RL} = -\lambda_{LR} = \lambda_{AA}$

(d) FV Vector Octet: $\lambda_{RR} \neq 0$ and $\lambda_{LR} = \lambda_{RL} = \lambda_{LL} = 0$

FIG. 23 (color online). $m_{t\bar{t}}$ distribution of $A_{\mathrm{FB}}^{t\bar{t}}$ at χ^2_{min} for the four favorable point sets in parameter space at fixed $\Lambda_{\mathcal{U}} = 1$ TeV. The histograms corresponding to the best-fit model parameters are shown by green steps and the experimental data points are shown with their errors in red, while the SM NLO (QCD + EW) with backgrounds are shown in the blue shaded histogram. The red straight line in all graphs is the best-fit line with the experimental data from Ref. [7], while the black straight line depicts the best-fit line with the model (unparticles) plus SM NLO (QCD + EW) with background data.

massive production of color singlet/octet unparticles in colliders.

A standard way to treat the breaking of conformal symmetry is to introduce a mass gap in the spectral density and thereby remove modes with energy less than the infrared cutoff scale μ in the spectral density. Thus, the propagator for vector unparticles given in Eq. (19) will be modified to

$$\Delta^{\mu\nu}(p) = \frac{-iA_{d_{\mathcal{U}}}}{2\sin(d_{\mathcal{U}}\pi)}[-(p^2-\mu^2)]^{d_{\mathcal{U}}-2} \times \left(-g^{\mu\nu} + a\frac{p^\mu p^\nu}{p^2}\right), \tag{42}$$

with

$$[(-(p^2-\mu^2)]^{d_{\mathcal{U}}-2} = \begin{cases} |p^2-\mu^2|^{d_{\mathcal{U}}-2} & \text{for } p^2 < \mu^2 \\ |p^2-\mu^2|^{d_{\mathcal{U}}-2} e^{id_{\mathcal{U}}\pi} & \text{for } p^2 > \mu^2. \end{cases} \tag{43}$$

It reduces to (19) in the limit $\mu \to 0$. From Eq. (43) it follows that one can ignore the existence of the mass gap as long as all the momentum invariants involved with the unparticle propagators are much larger than the conformal symmetry breaking scale. For $\mu = 1$ GeV, 10 GeV, and m_Z, the effects are negligibly small. Since the minimum of these momentum invariants in the case of top pair production is the threshold $m_{t\bar{t}}$, the suppression of the partonic cross section can be at most $(1-\mu^2/\hat{s}_{\mathrm{min}})^{d_{\mathcal{U}}-2} = (1-\mu^2/m_{t\bar{t}}^2)^{d_{\mathcal{U}}-2}$ and $(1-\mu^2/\hat{t}_{\mathrm{min}})^{d_{\mathcal{U}}-2} = (1-\mu^2/m_{t\bar{t}}^2)^{d_{\mathcal{U}}-2}$ for s and t channel processes, respectively. We have checked the stability and consistency of our results corresponding to the above-mentioned choices of the breaking scales for all s and t channel processes.

Similarly, computation of the same sign top pair production mediated by the flavor violating unparticles does not have any impact due to introduction of the breaking scale, as long as the scale is sufficiently smaller than the same sign top pair threshold $\simeq 350$ GeV.

The presence of FV couplings leads to a decay process like $t \to u + \mathcal{U}$ which diverges for $d_{\mathcal{U}} > 2$ [18,50] unless one introduces a mass gap. Therefore, the adoption of scale invariance breaking is inevitable in the region $1 < d_{\mathcal{U}} < 2$ for the top pair production and same sign top pair production processes induced by FV

couplings. However, once scale invariance is broken at a scale μ, the states with momenta $p^2 < \mu^2$ are removed from phase space, resulting in a finite and positive decay width even for $d_{\mathcal{U}} < 2$ [36].

Introduction of color octet unparticles is likely to produce them in plenty at hadron colliders through $q\bar{q} \to \mathcal{U}^{V/T} + \mathcal{U}^{V/T}$ and $gg \to \mathcal{U}^{V/T} + \mathcal{U}^{V/T}$. These processes mediate through s and t channels. Gluon flux being low at the Tevatron, production of such colored unparticles from a gluon-gluon initial state may not have a large bearing in our analysis. Production of colored scalar unparticles has been studied by Cacciapaglia *et al.* [43]. There they showed that the pair production cross section of color scalar unparticles is suppressed by a factor of $(2\text{-}d_{\mathcal{U}})$ with respect to the particle pair production. One would expect the production of the vector unparticles to follow suit with respect to the vector particles. But then these channels are also constrained by an observed dijet cross section at the Tevatron. The upper limit on the allowed cross section through these processes translates to an upper bound on the couplings of the respective light quark with colored vector/tensor unparticles.

Throughout our study, including the χ^2 analysis of $m_{t\bar{t}}$ distribution of $A_{\rm FB}^{t\bar{t}}$, the cross sections depend on the product of couplings $g_i^{\mathcal{U}^{\mathbf{n}}_{(V/T)}\bar{q}q} g_j^{\mathcal{U}^{\mathbf{n}}_{(V/T)}\bar{t}t} = \lambda_{ij}^{(V/T)}$ involving light quarks and top quarks with flavor conserving color vector/tensor unparticles. In light of our assumption $g_{(L/R)}^{\mathcal{U}^{\mathbf{n}}_{(V/T)}\bar{q}q} \ll g_{(L/R)}^{\mathcal{U}^{\mathbf{n}}_{(V/T)}\bar{t}t}$ (mentioned in Sec. IVA), our analysis is consistent with respect to the observation from the dijet cross section.

Although the introduction of flavor violating interactions involving colored unparticles, up quarks, and top quarks in a $\hat{t}$ channel process does not encounter these shortcomings, it can still copiously produce unparticles in the colliders via top decay. The contribution of the decay channel to the partial top decay width constrains this coupling for $d_{\mathcal{U}} > 2$.

However, all of these problems can be eased out if we can model the color unparticle theory by requiring it to have an infrared cutoff. Fairly large μ is likely to suppress the copious production of color unparticles through all channels discussed here. Even this allows us to constrain the couplings from the decay process $t \to u + \mathcal{U}^V$ in the region $1 < d_{\mathcal{U}} < 2$ corresponding to a specific choice of μ from the measurement of the top decay width.

C. Observations and conclusions

We have studied the interactions of vector and tensor color singlet/octet unparticles in the top sector at the Tevatron through FC and FV couplings. In this way, we have made an attempt to address the existing anomaly in the $A_{\rm FB}^{t\bar{t}}$ at the Tevatron, keeping the cross section and spin correlation of $t\bar{t}$ consistent with the data. We have also studied the contribution of these unparticles to the top decay width and the same sign top pair production induced by FV couplings.

We summarize our observations here:

(1) In the range of $d_{\mathcal{U}}$ allowed by completely conformal theory, i.e., $d_{\mathcal{U}} > 3$, appreciable positive $A_{\rm FB}^{t\bar{t}}$ is obtained, albeit for very high values of unparticle couplings which may not be in the perturbative regime.

In Fig. 24, we show the behavior of the cross section for the process $q\bar{q} \to t\bar{t}$ as a function of the parton center-of-mass energy $\sqrt{\hat{s}} \equiv m_{t\bar{t}}$, varying from the threshold value to 1 TeV. Investigating the perturbative nature of the couplings for the fully conformal theory in Fig. 24(a), we plot the behavior corresponding to the maximum allowed interaction strengths such that unitarity is not violated until 1 TeV. These upper limits on the interaction

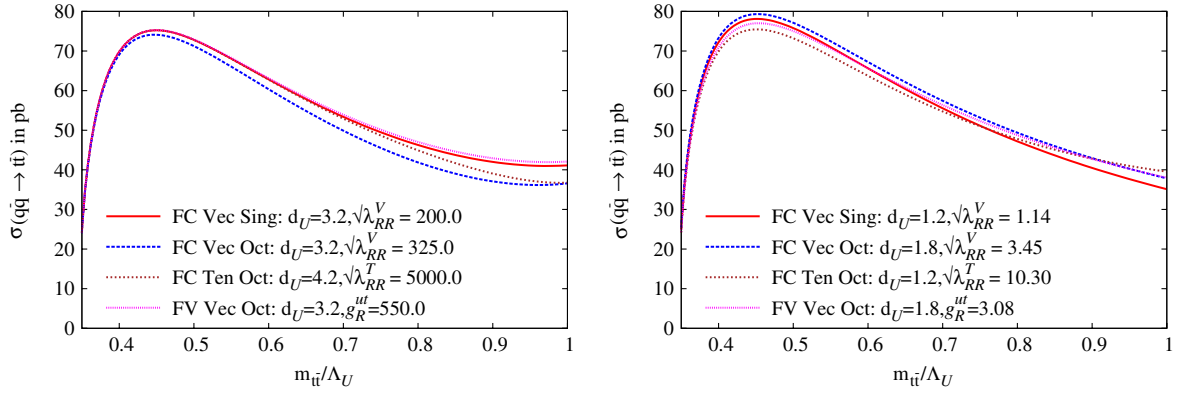

(a) $d_{\mathcal{U}}$ values allowed by completely conformal theory

(b) Four favorable point sets based on $\chi^2_{\rm min}$

FIG. 24 (color online). Variation of the cross section for the process $q\bar{q} \to t\bar{t}$ with $\sqrt{\hat{s}} \equiv m_{t\bar{t}}$ in units of $\Lambda_{\mathcal{U}}$. Panel (a) gives the behavior corresponding to the maximum allowed interaction strengths such that unitarity is not violated until 1 TeV. Panel (b) shows the $\sqrt{\hat{s}}$ variation for the four focus points identified in Fig. 23, illustrating that the parameter values that explain the $A_{\rm FB}^{t\bar{t}}$ anomaly preserve unitarity.

strengths may be read off directly from the figure, e.g., the interaction strength $\sqrt{\lambda^V_{RR}}/(\Lambda_\mathcal{U})^{d_\mathcal{U}-1} < 200\ (\mathrm{TeV})^{1-d_\mathcal{U}}$ in the case of a FC vector singlet. For a given $d_\mathcal{U}$, this limit can translate into an upper bound on the coupling for fixed $\Lambda_\mathcal{U}$ or a lower bound on $\Lambda_\mathcal{U}$ for a fixed $\sqrt{\lambda^V_{RR}}$. These values contribute to the cross section $\sigma^{t\bar{t}}$ within the experimental limits but are unable to explain the observed large value of $A^{t\bar{t}}_{\mathrm{FB}}$. Further, as mentioned earlier, at such high values of $d_\mathcal{U}$, the SM contact interactions cannot be ignored. Hence, these values of $d_\mathcal{U}$ are not phenomenologically interesting.

(2) The $A^{t\bar{t}}_{\mathrm{FB}}$ anomaly in top pair production can be explained by the process mediated by FC vector color singlet unparticles when only the RH (or LH) couplings are present [i.e., case (a) or (b) in our article]. When $1 < d_\mathcal{U} < 2$, one gets appreciable positive $A^{t\bar{t}}_{\mathrm{FB}}$, keeping the other observables, namely, $\sigma^{t\bar{t}}$ and $C^{t\bar{t}}$, within the CDF observed values. $A^{t\bar{t}}_{\mathrm{FB}}$ is higher for values closer to $d_\mathcal{U} = 1$.

(3) In the case of a FC vector color octet, cases (a) and (b) give favorable values of $A^{t\bar{t}}_{\mathrm{FB}}$ for a large range of $d_\mathcal{U}$ values in the region $1 < d_\mathcal{U} < 2$ and for the couplings that do not modify the cross section and spin correlation appreciably from the SM values. The higher the value of $d_\mathcal{U}$, the smaller the value of $A^{t\bar{t}}_{\mathrm{FB}}$ is for a given coupling. If the FC octet unparticles have axial vector couplings [case(d)] then positive $A^{t\bar{t}}_{\mathrm{FB}}$ is obtained only for $1.5 < d_\mathcal{U} < 2$. To explain the $A^{t\bar{t}}_{\mathrm{FB}}$ anomaly for $d_\mathcal{U}$ values in the region $1 < d_\mathcal{U} < 1.5$ for case (d), one has to assume that couplings of unparticles with light quarks are of opposite sign to those with top quarks, just like in the case of axigluon models. With this nonuniversal choice of couplings, appreciable positive $A^{t\bar{t}}_{\mathrm{FB}}$ may be obtained even for $3 < d_\mathcal{U} < 3.5$.

(4) With unparticle operators assumed to be vectors having FC couplings, whether they are singlet or octet under $SU(3)_C$, the spin FB asymmetry $C^{t\bar{t}}_{\mathrm{FB}} = A^{t\bar{t}}_{\mathrm{FB}}$.

(5) Additional factors of β_t and $\Lambda_\mathcal{U}^{-2}$ in the cross section suppress the tensor unparticle effects compared to vector unparticles. Assuming the tensor unparticle to be a FC singlet, there is no parameter space that can explain the $A^{t\bar{t}}_{\mathrm{FB}}$ anomaly while at the same time keeping the other observables within the experimental limits. If, however, tensor unparticles are color octets, appreciable $A^{t\bar{t}}_{\mathrm{FB}}$ is obtained for cases (a) and (c) with $1 < d_\mathcal{U} < 1.5$ (the closer $d_\mathcal{U}$ is to 1, the higher $A^{t\bar{t}}_{\mathrm{FB}}$ is). Moreover, with the presence of tensor unparticles, $C^{t\bar{t}}_{\mathrm{FB}} \neq A^{t\bar{t}}_{\mathrm{FB}}$.

(6) In the presence of FV couplings of vector unparticles involving first and third generation quarks only, color octet unparticles give the appreciable positive $A^{t\bar{t}}_{\mathrm{FB}}$ for $1 < d_\mathcal{U} < 2$. A color singlet gives sufficiently positive $A^{t\bar{t}}_{\mathrm{FB}}$ only for values of $d_\mathcal{U}$ very close to 1. With both same and opposite helicity amplitudes contributing to $A^{t\bar{t}}_{\mathrm{FB}}$ in the presence of FV couplings, $A^{t\bar{t}}_{\mathrm{FB}} \neq C^{t\bar{t}}_{\mathrm{FB}}$.

(7) We observe that although a large parameter region in the FV sector is consistent with CDF and D0 data, it gets constrained from the same sign top/antitop production.

Considering the recent measurement of the top decay width, the parameter region shrinks to a large extent. Unparticles are likely to escape the detection accounting for the missing energy and transverse momentum or they will show up as a pair of light quark jets/leptons. Then one could compare these processes with the experimentally constrained FCNC partial decay width $t \to Z + \text{jet}$, which is $\leq 3.7\%$ from CDF [55] and $\leq 3.2\%$ from DØ [56], respectively. However, the partial decay width of $t \to \mathcal{U}u$ is expected to be larger than $t \to Z + \text{jet}$, as its phase space allows the continuum spectrum for unparticles unlike the Z boson.

(8) Our results and analysis are consistent with the inception of a nonzero infrared cutoff as long as $\mu^2 \ll$ momentum invariants involving unparticles in all $\hat{s}$, $\hat{t}$, and $\hat{u}$ channels at the parton level.

(9) We have identified some focus points of the model which can explain the $A^{t\bar{t}}_{\mathrm{FB}}$ anomaly (given in Table II) based on the χ^2 analysis performed with two independent parameters of the theory $d_\mathcal{U}$ and the coupling $\sqrt{\lambda_{ij}}/g_i^{ut}$ for a given $\Lambda_\mathcal{U}$. Following the scanning of the unconstrained parameter region, we computed the χ^2_{min} with respect to the deviation from the experimentally observed $m_{t\bar{t}}$ distribution of $A^{t\bar{t}}_{\mathrm{FB}}$ spread over seven bins at the Tevatron for fixed $\Lambda_\mathcal{U} = 1$ TeV. We find that all four points corresponding to the χ^2_{min} neither conflict with the other measured observables of $p\bar{p} \to t\bar{t}$, nor do they transgress the allowed upper limit of the same sign top pair production cross section and the observed total top decay width.

We investigated further and established that all of these focus points preserved the unitarity which is illustrated in Fig. 24(b).

(10) The new physics effect can either show up at the top pair production or in the top decay channels. However, in an experiment, the top and antitop are reconstructed from all observed decay products using the SM template which contains the SM tWb vertices. Therefore, unparticle induced decay channels of top/antitop to the visible spectrum and missing energy will add up to the cross section reported in the experiment. We have, in this article, considered the unpartcle contribution only to the top pair production with SM decay of the top/

antitop. The total cross section, including the additional top/antitop decay via unparticles, is likely to reach the present upper bound of the allowed one sigma band at much lower values of the couplings in comparison to those shown in Figs. 2, 5, 8, 10, 13, 16(a), and 17.

(11) The inclusion of the down sector in the Lagrangian (A4) induces the $bq\mathcal{U}$ vertices in various modes of B decay and in the $b\bar{b}$ production at the hadron colliders. Since our analysis involves the flavor violation among the first and third generation quarks, the flavor violating couplings from rare decay modes $B^0 \to K^0\bar{K}^0$ and $B^{\pm,0} \to \phi\pi^{\pm,0}$ (which have only $b \to d$ penguin contributions in the SM) constrain the left chiral $bd\mathcal{U}$ couplings [57]. The study of the CP phase of B meson mixing also constrains the left chiral vector unparticle current [58]. $SU(2)$ gauge invariance would then impose the constraints on the left chiral couplings in the up quark sector as well. Thus, the case with the pure right-handed couplings remains unconstrained. Therefore, our analysis for the flavor violating focus point which arises from the combination involving $g_L^{ut} = 0$ and $g_R^{ut} \neq 0$ remains unconstrained by the B physics.

It is worthwhile to probe the contribution of unparticles at the LHC and correlate findings from the top sector at the Tevatron. We expect that the present and forthcoming measurements with higher luminosity data for top pair cross section, charge asymmetry, and spin correlation will severely constrain the parameter space of flavor conserving and violating unparticle interactions. In addition, the $m_{t\bar{t}}$ distribution of the cross section [59,60] and charge asymmetry will constrain the new physics possibilities. With the improved b-tagging efficiency, the unparticle contribution to the $b\bar{b}$ production is likely to influence the model analysis. The contribution of unparticles to the light quark dijet production is likely to put an upper bound on the flavor conserving light quark-unparticle interaction strength [61–63].

Recently, the measurement of same sign top pairs by CMS has ruled out the favored Z' model of $A_{\rm FB}^{t\bar{t}}$ [52]. Therefore, one expects that the same sign top pair production through unparticles will narrow down the allowed flavor violating parameter space. In the same spirit, the impact of the constraints on the FCNC decays of top quarks observed by ATLAS [64] and CMS [65] needs to be studied in this model.

Presently, this analysis and an estimate of the unparticle contribution to all of these processes for the LHC is in progress.

ACKNOWLEDGMENTS

The authors would like to thank D. Choudhury, Mukesh Kumar, and A. Goyal for fruitful discussions. We acknowledge partial support from DST, India under Grant No. SR/S2/HEP-12/2006. S. D. and R. I. would like to acknowledge the UGC research award and CSIR JRF, respectively, for partial financial support. M. D. would like to thank the IUCAA, Pune for hospitality while part of this work was completed. We also thank RECAPP, HRI for local hospitality where this work was initiated. We would like to thank D. Ghosh and M. Perez-Victoria for valuable comments.

APPENDIX A: COMPUTATION OF HELICITY AMPLITUDES

The generalized Lagrangian for the SM and the $J = 1, 2$ neutral current via color singlets and octets is given as

$$\mathcal{L}_{\rm QCD} = -g_s\{T^a\}_{ji}A_\mu^a\sum_f \bar{q}_{fj}\gamma^\mu q_{fi}, \tag{A1}$$

where g_s is the QCD coupling, f is the flavor index, and i, j are the color indices.

$$\mathcal{L}_{\rm NC} = -\sum_f \bar{q}_f\gamma^\mu\left[eQ_fA_\mu + \frac{e}{s_Wc_W}(T_f^3P_L - s_W^2Q_f)Z_\mu\right]q_f, \tag{A2}$$

where e = electromagnetic coupling, Q_f = charge of quark q_f in units of e, $s_W = \sin\theta_W$, $c_W = \cos\theta_W$, and θ_W = Weinberg angle.

$$\mathcal{L}_{J=1}^{(s)} = \frac{g_s}{\Lambda_{\mathcal{U}}^{d_{\mathcal{U}}-1}}\sum_{\substack{\alpha=L,R\\ \mathbf{n}=1,8}} g_\alpha^{\mathcal{U}_V^{\mathbf{n}}\bar{q}q}\{T_{\mathbf{n}}^a\}_{ji}\mathcal{O}_\mu^{\mathbf{n},a}\sum_f \bar{q}_{fj}\gamma^\mu P_\alpha q_{fi} + \text{H.c.}, \tag{A3}$$

$$\mathcal{L}_{J=1}^{(t)} = \frac{g_s}{\Lambda_{\mathcal{U}}^{d_{\mathcal{U}}-1}}\sum_{\substack{\alpha=L,R\\ \mathbf{n}=1,8}} \mathcal{O}_\mu^{\mathbf{n},a}\{T_{\mathbf{n}}^a\}_{ji}[g_\alpha^{\mathcal{U}_V^{\mathbf{n}}\bar{t}u}\bar{t}_j\gamma^\mu P_\alpha q_{fi} + g_\alpha^{\mathcal{U}_V^{\mathbf{n}}\bar{b}u}\bar{b}_j\gamma^\mu P_\alpha q_{fi} + \text{H.c.}], \tag{A4}$$

$$\mathcal{L}_{J=2}^{(s)} = \frac{-g_s}{4\Lambda_{\mathcal{U}}^{d_{\mathcal{U}}}}\sum_{\substack{\alpha=L,R\\ \mathbf{n}=1,8}} g_\alpha^{\mathcal{U}_T^{\mathbf{n}}\bar{q}q}\{T_{\mathbf{n}}^a\}_{ji}\mathcal{O}_{\mu\nu}^{\mathbf{n},a} \times \sum_f \bar{q}_{fj}i(\gamma_\mu\partial_\nu + \gamma_\nu\partial_\mu)P_\alpha q_{fi} + \text{H.c.}, \tag{A5}$$

$$\mathcal{L}_{J=2}^{(t)} = \frac{-g_s}{4\Lambda_{\mathcal{U}}^{d_{\mathcal{U}}}}\sum_{\substack{\alpha=L,R\\ \mathbf{n}=1,8}} \mathcal{O}_{\mu\nu}^{\mathbf{n},a}\{T_{\mathbf{n}}^a\}_{ji}i[g_\alpha^{\mathcal{U}_T^{\mathbf{n}}\bar{t}u}\bar{t}_j(\gamma_\mu\partial_\nu + \gamma_\nu\partial_\mu)P_\alpha q_{fi} + g_\alpha^{\mathcal{U}_T^{\mathbf{n}}\bar{b}u}\bar{b}_j(\gamma_\mu\partial_\nu + \gamma_\nu\partial_\mu)P_\alpha q_{fi} + \text{H.c.}]. \tag{A6}$$

The matrix element is computed in this appendix, fixing the color flow of the particles involved in the process $q\bar{q} \to t\bar{t}$ as follows:

$$\{q(p_q)\}_i\{\bar{q}(p_{\bar{q}})\}_j \to \{t(p_t)\}_k\{\bar{t}(p_{\bar{t}})\}_l. \tag{A7}$$

The matrix elements corresponding to the given Lagrangian in Eqs. (A1)–(A6) are

$$\sum_i i\mathcal{M}_i = i\mathcal{M}_1(\mathrm{QCD}) + i\mathcal{M}_2(\mathrm{NC}) + i\mathcal{M}_3(\hat{s}; J=1; \mathbf{1}) + i\mathcal{M}_4(\hat{s}; J=1; \mathbf{8}) + i\mathcal{M}_5(\hat{t}; J=1; \mathbf{1}) + i\mathcal{M}_6(\hat{t}; J=1; \mathbf{8}) + i\mathcal{M}_7(\hat{s}; J=2; \mathbf{1}) + i\mathcal{M}_8(\hat{s}; J=2; \mathbf{8}) + i\mathcal{M}_9(\hat{t}; J=2; \mathbf{1}) + i\mathcal{M}_{10}(\hat{t}; J=2; \mathbf{8}), \quad \text{(A8)}$$

$$\begin{aligned}
\sum_i i\mathcal{M}_i = {} & C_{\mathbf{QCD}}[\bar{v}(p_{\bar{q}}, \lambda_{\bar{q}})_i i\gamma^\mu u(p_q, \lambda_q)_l]\frac{-ig_{\mu\nu}}{\hat{s}}[\bar{u}(p_t, \lambda_t)_k i\gamma^\nu v(p_{\bar{t}}, \lambda_{\bar{t}})_j] \\
& + C_{\mathbf{NC}}[\bar{v}(p_{\bar{q}}, \lambda_{\bar{q}})_i i\gamma^\mu u(p_q, \lambda_q)_l]\frac{-ig_{\mu\nu}}{\hat{s}}[\bar{u}(p_t, \lambda_t)_k i\gamma^\nu v(p_{\bar{t}}, \lambda_{\bar{t}})_j] \\
& + C_{\mathbf{NC}}[\bar{v}(p_{\bar{q}}, \lambda_{\bar{q}})_i i\gamma^\mu (T_q^3 P_L - s_W^2 Q_q) u(p_q, \lambda_q)_l]\frac{-ig_{\mu\nu}}{\hat{s} - m_Z^2 + im_Z\Gamma_Z}[\bar{u}(p_t, \lambda_t)_k i\gamma^\nu (T_t^3 P_L - s_W^2 Q_t) v(p_{\bar{t}}, \lambda_{\bar{t}})_j] \\
& + \sum_{\mathbf{n}\equiv\mathbf{1},\mathbf{8}} C_{\mathbf{n}}^s\Big[\bar{v}(p_{\bar{q}}, \lambda_{\bar{q}})_i \frac{i\gamma^\mu}{\Lambda^{d_\mathcal{U}-1}}(g_L^{\mathcal{U}_V^{\mathbf{n}}\bar{q}q} P_L + g_R^{\mathcal{U}_V^{\mathbf{n}}\bar{q}q} P_R) u(p_q, \lambda_q)_l\Big]\frac{iA_{d_\mathcal{U}}(-\hat{s})^{d_\mathcal{U}-2}}{2\sin(d_\mathcal{U}\pi)}\Big[g_{\mu\nu} - a\frac{(p_q+p_{\bar{q}})^\mu (p_q+p_{\bar{q}})^\nu}{(p_q+p_{\bar{q}})^2}\Big] \\
& \times\Big[\bar{u}(p_t, \lambda_t)_k \frac{i\gamma^\nu}{\Lambda^{d_\mathcal{U}-1}}(g_L^{\mathcal{U}_V^{\mathbf{n}}\bar{t}t} P_L + g_R^{\mathcal{U}_V^{\mathbf{n}}\bar{t}t} P_R) v(p_{\bar{t}}, \lambda_{\bar{t}})_j\Big] - \sum_{\mathbf{n}\equiv\mathbf{1},\mathbf{8}} C_{\mathbf{n}}^t\Big[\bar{v}(p_{\bar{q}}, \lambda_{\bar{q}})_i \frac{i\gamma^\mu}{\Lambda^{d_\mathcal{U}-1}}(g_L^{\mathcal{U}_V^{\mathbf{n}}\bar{t}\bar{q}} P_L + g_R^{\mathcal{U}_V^{\mathbf{n}}\bar{t}\bar{q}} P_R) v(p_{\bar{t}}, \lambda_{\bar{t}})_j\Big] \\
& \times\frac{iA_{d_\mathcal{U}}(-\hat{t})^{d_\mathcal{U}-2}}{2\sin(d_\mathcal{U}\pi)}\Big[g_{\mu\nu} - a\frac{(p_q-p_t)^\mu (p_q-p_t)^\nu}{(p_q-p_t)^2}\Big]\Big[\bar{u}(p_t, \lambda_t)_k \frac{i\gamma^\nu}{\Lambda^{d_\mathcal{U}-1}}(g_L^{\mathcal{U}_V^{\mathbf{n}}tq} P_L + g_R^{\mathcal{U}_V^{\mathbf{n}}tq} P_R) q(p_q, \lambda_q)_l\Big] \\
& + \sum_{\mathbf{n}\equiv\mathbf{1},\mathbf{8}} C_{\mathbf{n}}^s\Big[\bar{v}(p_{\bar{q}}, \lambda_{\bar{q}})_i \frac{-i[\gamma^\mu (p_q-p_{\bar{q}})^\nu + \gamma^\nu (p_q-p_{\bar{q}})^\mu]}{4\Lambda^{d_\mathcal{U}}}(g_L^{\mathcal{U}_T^{\mathbf{n}}\bar{q}q} P_L + g_R^{\mathcal{U}_T^{\mathbf{n}}\bar{q}q} P_R) u(p_q, \lambda_q)_l\Big]\frac{iA_{d_\mathcal{U}}(-\hat{s})^{d_\mathcal{U}-2}}{2\sin(d_\mathcal{U}\pi)}\mathcal{T}_{\mu\nu,\alpha\beta} \\
& \times\Big[\bar{u}(p_t, \lambda_t)_k \frac{i[\gamma^\alpha (p_t-p_{\bar{t}})^\beta + \gamma^\beta (p_t-p_{\bar{t}})^\alpha]}{4\Lambda^{d_\mathcal{U}}}(g_L^{\mathcal{U}_T^{\mathbf{n}}\bar{t}t} P_L + g_R^{\mathcal{U}_T^{\mathbf{n}}\bar{t}t} P_R) v(p_{\bar{t}}, \lambda_{\bar{t}})_j\Big] \\
& - \sum_{\mathbf{n}\equiv\mathbf{1},\mathbf{8}} C_{\mathbf{n}}^t\Big[\bar{v}(p_{\bar{q}}, \lambda_{\bar{q}})_i \frac{-i[\gamma^\mu (p_t+p_q)^\nu + \gamma^\nu (p_t+p_q)^\mu]}{4\Lambda^{d_\mathcal{U}}}(g_L^{\mathcal{U}_T^{\mathbf{n}}\bar{t}\bar{q}} P_L + g_R^{\mathcal{U}_T^{\mathbf{n}}\bar{t}\bar{q}} P_R) v(p_{\bar{t}}, \lambda_{\bar{t}})_j\Big]\frac{iA_{d_\mathcal{U}}(-\hat{t})^{d_\mathcal{U}-2}}{2\sin(d_\mathcal{U}\pi)} \\
& \times\mathcal{T}_{\mu\nu,\alpha\beta}\Big[\bar{u}(p_t, \lambda_t)_k \frac{i[\gamma^\alpha (p_{\bar{q}}+p_{\bar{t}})^\beta + \gamma^\beta (p_{\bar{q}}+p_{\bar{t}})^\alpha]}{4\Lambda^{d_\mathcal{U}}}(g_L^{\mathcal{U}_T^{\mathbf{n}}tq} P_L + g_R^{\mathcal{U}_T^{\mathbf{n}}tq} P_R) q(p_q, \lambda_q)_l\Big]. \quad \text{(A9)}
\end{aligned}$$

Here $C_{\mathbf{n}}^{\mathbf{s}}$ is the color propagator for the color octet vectors/tensors in the s channel and $C_{\mathbf{n}}^t$ is the color propagator for the color octet ($n \equiv 8$) and singlet ($n \equiv 1$) vectors/tensors in the t channel. To compute the squared and interference terms with these color propagators, we provide the color factors in the following table. We compute the helicity amplitudes in the center-of-mass frame $q\bar{q}$. The momentum assignments are

$$\begin{aligned}
p_q &= \frac{\sqrt{\hat{s}}}{2}(1, 0, 0, 1), \\
p_{\bar{q}} &= \frac{\sqrt{\hat{s}}}{2}(1, 0, 0, -1), \\
p_t &= \frac{\sqrt{\hat{s}}}{2}(1, \beta_t s_\theta, 0, \beta_t c_\theta), \\
p_{\bar{t}} &= \frac{\sqrt{\hat{s}}}{2}(1, -\beta_t s_\theta, 0, -\beta_t c_\theta),
\end{aligned} \quad \text{(A10)}$$

where $s_\theta \equiv \sin\theta$; $c_\theta \equiv \cos\theta$, $\beta_t = \sqrt{1 - \frac{4m_t^2}{\hat{s}}}$ and θ is the angle between q and t momenta.

1. Helicity amplitudes for $q\bar{q} \to t\bar{t}$ in the standard model

The helicity amplitudes for $q\bar{q} \to t\bar{t}$ in the standard model are given by

$$\mathcal{M}_{1,2}(+\,-\,\pm\pm) = \mp g_R[g_L + g_R]\frac{1}{2}\sqrt{1-\beta_t^2}\, s_\theta, \quad \text{(A11)}$$

$$\mathcal{M}_{1,2}(+\,-\,\pm\mp) = \pm g_R[g_L(1 \mp \beta_t) + g_R(1 \pm \beta_t)]\frac{1}{2}(1 \pm c_\theta), \quad \text{(A12)}$$

$$\mathcal{M}_{1,2}(-\,+\,\pm\pm) = \mp g_L[g_L + g_R]\frac{1}{2}\sqrt{1-\beta_t^2}\, s_\theta, \quad \text{(A13)}$$

$$\mathcal{M}_{1,2}(-\,+\,\pm\mp) = \mp g_L[g_L(1 \mp \beta_t) + g_R(1 \pm \beta_t)]\frac{1}{2}(1 \mp c_\theta). \quad \text{(A14)}$$

In the above, if the helicity amplitudes are gluon mediating, then they are in units of g_s^2; if they are photon mediating, then they are in units of $(eQ_q)(eQ_t)$; if they are Z-boson mediating, then they are in units of

$(e/s_W c_W)^2 s/(s - m_Z^2)$. Here for the gluon and photon mediating process, $g_L = g_R = 1$, whereas for the Z-boson mediating process, $g_L = T_q^3 - s_W^2 Q_q$, $g_R = -s_W^2 Q_q$.

2. Helicity amplitudes for $q\bar{q} \to t\bar{t}$ via flavor conserving vector unparticles

The helicity amplitudes mediated by the flavor conserving vector unparticle $\mathcal{M}_{3,4}(\hat{s}; J = 1; \mathbf{n})$ in units of $g_s^2(-1)^{d_\mathcal{U}-3}\frac{A_{d_\mathcal{U}}}{2\sin(d_\mathcal{U}\pi)}[\frac{\hat{s}}{\Lambda_\mathcal{U}^2}]^{d_\mathcal{U}-1}$ are given by

$$\mathcal{M}_{3,4}(+\,-\,\pm\pm) = \mp g_R^{\mathcal{U}_V^{\mathbf{n}}\bar{q}q}[g_L^{\mathcal{U}_V^{\mathbf{n}}\bar{t}t} + g_R^{\mathcal{U}_V^{\mathbf{n}}\bar{t}t}]\frac{1}{2}\sqrt{1-\beta_t^2}s_\theta, \tag{A15}$$

$$\mathcal{M}_{3,4}(+\,-\,\pm\mp) = \pm g_R^{\mathcal{U}_V^{\mathbf{n}}\bar{q}q}[g_L^{\mathcal{U}_V^{\mathbf{n}}\bar{t}t}(1 \mp \beta_t) + g_R^{\mathcal{U}_V^{\mathbf{n}}\bar{t}t}(1 \pm \beta_t)]\frac{1}{2}(1 \pm c_\theta), \tag{A16}$$

$$\mathcal{M}_{3,4}(-\,+\,\pm\pm) = \mathcal{M}_{3,4}(+\,-\,\pm\pm)|_{L\leftrightarrow R}, \tag{A17}$$

$$\mathcal{M}_{3,4}(-\,+\,\pm\mp) = \mathcal{M}_{3,4}(+\,-\,\mp\pm)|_{L\leftrightarrow R}. \tag{A18}$$

3. Helicity amplitudes for $q\bar{q} \to t\bar{t}$ via flavor violating vector unparticles

The following helicity amplitudes $\mathcal{M}_{5,6}(\hat{t}; J = 1; \mathbf{n})$ are given in units of $g_s^2\frac{A_{d_\mathcal{U}}}{2\sin(d_\mathcal{U}\pi)}[\frac{\hat{t}}{\Lambda_\mathcal{U}^2}]^{d_\mathcal{U}-1}\frac{\hat{s}}{\hat{t}}$:

$$\mathcal{M}_{5,6}(+\,+\,\pm\pm) = \pm g_L^{\mathcal{U}_V^{\mathbf{n}}\bar{t}q} g_R^{\mathcal{U}_V^{\mathbf{n}}\bar{t}q'}(1 \pm \beta_t) \times \left[1 \pm a\frac{m_t^2}{4\hat{t}}(1 \pm c_\theta)\right], \tag{A19}$$

$$\mathcal{M}_{5,6}(+\,+\,\pm\mp) = g_L^{\mathcal{U}_V^{\mathbf{n}}\bar{t}q} g_R^{\mathcal{U}_V^{\mathbf{n}}\bar{t}q'} a\frac{m_t^2}{4\hat{t}}\sqrt{1-\beta_t^2}s_\theta, \tag{A20}$$

$$\mathcal{M}_{5,6}(+\,-\,\pm\pm) = -g_R^{\mathcal{U}_V^{\mathbf{n}}\bar{t}q} g_R^{\mathcal{U}_V^{\mathbf{n}}\bar{t}q'}\sqrt{1-\beta_t^2}\frac{1}{2}s_\theta\left[1 + a\frac{m_t^2}{4\hat{t}}\right], \tag{A21}$$

TABLE III. Color factors for the interference and the squared terms of s and t channels for color singlet and octet vectors and tensors.

Color factor $q(p_q)_i\bar{q}(p_{\bar{q}})_j \to t(p_t)_k\bar{t}(p_{\bar{t}})_l$	FC octet $\{j,i\}\{k,l\}$ s chan. $C_\mathbf{8}^s = C_\mathbf{QCD}$	FV octet $\{i,k\}\{l,j\}$ t chan. $C_\mathbf{8}^t$	FC singlet $\{j,i\}\{k,l\}$ s chan. $C_\mathbf{1}^s = C_\mathbf{NC}$	FV singlet $\{i,k\}\{l,j\}$ t chan. $C_\mathbf{1}^t$
Int. with QCD	2	$-2/3$	0	4
Int. with NC	0	0	9	3
Squared term	2	2	9	9

$$\mathcal{M}_{5,6}(+\,-\,\pm\mp) = -g_R^{\mathcal{U}_V^{\mathbf{n}}\bar{t}q} g_R^{\mathcal{U}_V^{\mathbf{n}}\bar{t}q'}(1 \pm \beta_t)\frac{1}{2}(1 \pm c_\theta) \times \left[1 + a\frac{m_t^2}{4\hat{t}}\right], \tag{A22}$$

$$\mathcal{M}_{5,6}(-\,+\,\pm\pm) = \mathcal{M}_{5,6}(+\,-\,\mp\mp)|_{L\leftrightarrow R}, \tag{A23}$$

$$\mathcal{M}_{5,6}(-\,+\,\pm\mp) = \mathcal{M}_{5,6}(+\,-\,\mp\pm)|_{L\leftrightarrow R}, \tag{A24}$$

$$\mathcal{M}_{5,6}(-\,-\,\pm\pm) = \mathcal{M}_{5,6}(+\,+\,\mp\mp)|_{L\leftrightarrow R}, \tag{A25}$$

$$\mathcal{M}_{5,6}(-\,-\,\pm\mp) = \mathcal{M}_{5,6}(+\,+\,\mp\pm)|_{L\leftrightarrow R}. \tag{A26}$$

4. Helicity amplitudes for $q\bar{q} \to t\bar{t}$ via flavor conserving tensor unparticles

The following helicity amplitudes $\mathcal{M}_{7,8}(\hat{s}; J = 2; \mathbf{n})$ are given in units of $g_s^2(-1)^{d_\mathcal{U}-2}\frac{A_{d_\mathcal{U}}}{2\sin(d_\mathcal{U}\pi)}[\frac{\hat{s}}{4\Lambda_\mathcal{U}^2}]^{d_\mathcal{U}}4d_\mathcal{U}(d_\mathcal{U}-1)$:

$$\mathcal{M}_{7,8}(+\,-\,\pm\pm) = \mp g_R^{\mathcal{U}_T^{\mathbf{n}}\bar{q}q}[g_L^{\mathcal{U}_T^{\mathbf{n}}\bar{t}t} + g_R^{\mathcal{U}_T^{\mathbf{n}}\bar{t}t}]\beta_t\sqrt{1-\beta_t^2}s_\theta c_\theta, \tag{A27}$$

$$\mathcal{M}_{7,8}(+\,-\,\pm\mp) = g_R^{\mathcal{U}_T^{\mathbf{n}}\bar{q}q}[g_L^{\mathcal{U}_T^{\mathbf{n}}\bar{t}t}(1 \mp \beta_t) + g_R^{\mathcal{U}_T^{\mathbf{n}}\bar{t}t} \times (1 \pm \beta_t)]\frac{1}{2}\beta_t(1 \pm c_\theta)(1 \mp 2c_\theta), \tag{A28}$$

$$\mathcal{M}_{7,8}(-\,+\,\pm\pm) = \mathcal{M}_{7,8}(+\,-\,\pm\pm)|_{L\leftrightarrow R}, \tag{A29}$$

$$\mathcal{M}_{7,8}(-\,+\,\pm\mp) = \mathcal{M}_{7,8}(+\,-\,\mp\pm)|_{L\leftrightarrow R}. \tag{A30}$$

5. Helicity amplitudes for $qq \to tt$ via flavor violating vector unparticles

The following helicity amplitudes of the t channel diagram are given in units of $g_s^2\frac{A_{d_\mathcal{U}}}{2\sin(d_\mathcal{U}\pi)}[\frac{\hat{t}}{\Lambda_\mathcal{U}^2}]^{d_\mathcal{U}-1}\frac{\hat{s}}{\hat{t}}$. The symbol a is defined in (19).

$$\mathcal{M}^t_{++\pm\pm} = -g_R^{qt} g_R^{qt}(1 \pm \beta_t)\left[1 + a\frac{m_t^2}{p^2}\frac{1}{2}(1 \pm c_\theta)\right], \tag{A31}$$

$$\mathcal{M}^t_{++\pm\mp} = g_R^{qt} g_R^{qt}\sqrt{1-\beta_t^2}\frac{1}{2}s_\theta a\frac{m_t^2}{p^2}, \tag{A32}$$

$$\mathcal{M}^t_{-+\pm\pm} = \mp g_L^{qt} g_R^{qt}\sqrt{1-\beta_t^2}\frac{1}{2}s_\theta\left[1 + a\frac{m_t^2}{p^2}\right], \tag{A33}$$

$$\mathcal{M}^t_{-+\pm\mp} = \pm g_L^{qt} g_R^{qt}(1 \mp \beta_t)\frac{1}{2}(1 \mp c_\theta)\left[1 + a\frac{m_t^2}{p^2}\right], \tag{A34}$$

$$\mathcal{M}^t_{+-\pm\pm} = \mathcal{M}^t_{-+\pm\pm}|_{L\to R}, \quad \text{(A35)}$$

$$\mathcal{M}^t_{+-\pm\mp} = \mathcal{M}^t_{-+\mp\pm}|_{L\to R}, \quad \text{(A36)}$$

$$\mathcal{M}^t_{--\pm\pm} = \mathcal{M}^t_{++\mp\mp}|_{L\to R}, \quad \text{(A37)}$$

$$\mathcal{M}^t_{--\pm\mp} = -\mathcal{M}^t_{++\mp\pm}|_{L\to R}. \quad \text{(A38)}$$

The following helicity amplitudes of the u channel diagram are given in units of $g_s^2 \frac{A_{d_\mathcal{U}}}{2\sin(d_\mathcal{U}\pi)}[\frac{\hat{t}}{\Lambda_\mathcal{U}^2}]^{d_\mathcal{U}-1}\frac{\hat{s}}{\hat{u}}$.

$$\mathcal{M}^u_{++\pm\pm} = -\mathcal{M}^t\,{+}\,{+}\,\pm\,\pm|_{\theta\to\pi+\theta}, \quad \text{(A39)}$$

$$\mathcal{M}^u_{++\pm\mp} = -\mathcal{M}^t\,{+}\,{+}\,\pm\,\mp|_{\theta\to\pi+\theta}, \quad \text{(A40)}$$

$$\mathcal{M}^u_{-+\pm\pm} = -\mathcal{M}^t\,{-}\,{+}\,\pm\,\pm|_{\theta\to\pi+\theta}, \quad \text{(A41)}$$

$$\mathcal{M}^u_{-+\pm\mp} = \mathcal{M}^t\,{-}\,{+}\,\pm\,\mp|_{\theta\to\pi+\theta}, \quad \text{(A42)}$$

$$\mathcal{M}^u_{+-\pm\pm} = \mathcal{M}^u_{-+\pm\pm}|_{L\to R}, \quad \text{(A43)}$$

$$\mathcal{M}^u_{+-\pm\mp} = \mathcal{M}^u_{-+\mp\pm}|_{L\to R}, \quad \text{(A44)}$$

$$\mathcal{M}^u_{--\pm\pm} = \mathcal{M}^u_{++\mp\mp}|_{L\to R}, \quad \text{(A45)}$$

$$\mathcal{M}^u_{--\pm\mp} = -\mathcal{M}^u_{++\mp\pm}|_{L\to R}. \quad \text{(A46)}$$

APPENDIX B: PARTIAL DECAY WIDTH FOR $t \to q\mathcal{U}$ VIA FLAVOR VIOLATING VECTOR UNPARTICLES

The matrix element of $t \to q\mathcal{U}$ is given by $\mathcal{M} = g_s\Lambda_\mathcal{U}^{1-d_\mathcal{U}}\bar{u}(p_q)\gamma^\mu(g_L^{\mathcal{U}^n_V tq}P_L + g_R^{\mathcal{U}^n_V tq}P_R)u(p_t)\epsilon_\mu(p_\mathcal{U})$. Averaging over spin and color, the matrix element squared reads as

$$\overline{|\mathcal{M}|^2} = \frac{N_C}{6}\frac{2g_s^2}{\Lambda_\mathcal{U}^{2(d_\mathcal{U}-1)}}[(g_L^{\mathcal{U}^n_V tq})^2 + (g_R^{\mathcal{U}^n_V tq})^2]m_t p_q^0\left[\frac{(a+2)m_t - 4p_q^0}{(m_t - 2p_q^0)}\right]. \quad \text{(B1)}$$

The differential decay width for the top decaying to an unparticle and quark is given as

$$\begin{aligned} d\Gamma &= \frac{N_C}{6}\frac{\overline{|\mathcal{M}|^2}}{2m_t}\frac{A_{d_\mathcal{U}}}{16\pi^3}\frac{p_q^0 dp_q^0 d\Omega}{(m_t^2 - 2m_t p_q^0)^{2-d_\mathcal{U}}} \\ &= \frac{N_C}{6}\frac{g_s^2}{\Lambda_\mathcal{U}^{2(d_\mathcal{U}-1)}}\frac{A_{d_\mathcal{U}}}{16\pi^3}[(g_L^{\mathcal{U}^n_V tq})^2 + (g_R^{\mathcal{U}^n_V tq})^2]\left[\frac{(a+2)m_t^2 - 4m_t p_q^{0^{3-d_\mathcal{U}}}}{(m_t^2 - 2m_t p_q^0)}\right](p_q^0)^2\theta(m_t - 2p_q^0)dp_q^0 d\Omega \quad \text{(B2)} \\ &= \frac{N_C}{6}\frac{A_{d_\mathcal{U}}}{4\pi^2}g_s^2[(g_L^{\mathcal{U}^n_V tq})^2 + (g_R^{\mathcal{U}^n_V tq})^2]\left(\frac{m_t^2}{\Lambda_\mathcal{U}^2}\right)^{d_\mathcal{U}-1}m_t[(a+2) - 4x](1-2x)^{d_\mathcal{U}-3}x^2\theta(1-2x)dx. \end{aligned}$$

In (B2) we have taken $x = p_q^0/m_t$. Integrating (B2) with respect to x in the limit $[0, 1/2]$, we get the total decay width of a top quark for $d_\mathcal{U} > 2$. The color factor $N_C = 3, 4$ for singlet and octet unparticles, respectively. Upon introduction of the mass gap $\mu \neq 0$ Eq. (B2) becomes

$$\begin{aligned} d\Gamma = \frac{N_C}{6}\frac{A_{d_\mathcal{U}}}{4\pi^2}g_s^2[(g_L^{\mathcal{U}^n_V tq})^2 + (g_R^{\mathcal{U}^n_V tq})^2]\left(\frac{m_t^2}{\Lambda_\mathcal{U}^2}\right)^{d_\mathcal{U}-1}m_t[(a+2) - 4x](1-2x-x_0)^{d_\mathcal{U}-2} \\ \times\frac{x^2}{(1-2x)}\theta(1-2x-x_0)dx, \end{aligned} \quad \text{(B3)}$$

where $x_0 = \mu^2/m_t^2$. Evaluating the integral in the limit of $[0, (1-x_0)/2]$, we get the partial top decay width in the region $d_\mathcal{U} > 1$.

[1] CDF Collaboration, CDF, Note No. 9913, http://www-cdf.fnal.gov/physics/new/top/confNotes/cdf9913 ttbarx-s4invfb.ps.

[2] T. Aaltonen *et al.* (CDF Collaboration), Phys. Rev. D **82**, 052002 (2010); **83**, 071102 (2011); **84**, 031101 (2011).

[3] V. M. Abazov *et al.* (D0 Collaboration), Phys. Rev. D **84**, 012008 (2011); Phys. Lett. B **704**, 403 (2011).

[4] N. Kidonakis, Phys. Rev. D **82**, 114030 (2010); arXiv:1105.3481.

[5] P. Baernreuther, M. Czakon, and A. Mitov, Phys. Rev. Lett. **109**, 132001 (2012).

[6] V. M. Abazov *et al.* (D0 Collaboration), Phys. Rev. D **84**, 112005 (2011).
[7] CDF Collaboration, CDF, Note No. 10807, http://www-cdf.fnal.gov/physics/new/top/2012/LepJe_AFB_Winter2012/CDF10807.pdf.
[8] CDF Collaboration, CDF, Note No. 10584, 2011, http://www-cdf.fnal.gov/physics/new/top/2011/AfbComb/Afb_combo_5invfb.pdf.
[9] CDF Collaboration, CDF, Note No. 10436, http://www-cdf.fnal.gov/physics/new/top/2011/DilAfb/cdfpubnote.pdf.
[10] T. Aaltonen *et al.* (CDF Collaboration), Phys. Rev. D **83**, 112003 (2011).
[11] O. Antunano, J. H. Kuhn, and G. Rodrigo, Phys. Rev. D **77**, 014003 (2008); P. Ferrario and G. Rodrigo, J. Phys. Conf. Ser. **171**, 012091 (2009); S. Jung, H. Murayama, A. Pierce, and J. D. Wells, Phys. Rev. D **81**, 015004 (2010); Q.-H. Cao, D. McKeen, J. L. Rosner, G. Shaughnessy, and C. E. M. Wagner, Phys. Rev. D **81**, 114004 (2010); V. Barger, W.-Y. Keung, and C.-T. Yu, Phys. Rev. D **81**, 113009 (2010); J. Cao, Z. Heng, L. Wu, and J. M. Yang, Phys. Rev. D **81**, 014016 (2010); B. Xiao, Y.-k. Wang, and S.-h. Zhu, Phys. Rev. D **82**, 034026 (2010); A. Djouadi, G. Moreau, F. Richard, and R. K. Singh, Phys. Rev. D **82**, 071702 (2010); Y.-k. Wang, B. Xiao, and S.-h. Zhu, Phys. Rev. D **82**, 094011 (2010); R. S. Chivukula, E. H. Simmons, and C.-P. Yuan, Phys. Rev. D **82**, 094009 (2010); D.-W. Jung, P. Ko, and J. S. Lee, Phys. Lett. B **701**, 248 (2011); D. Choudhury, R. M. Godbole, S. D. Rindani, and P. Saha, Phys. Rev. D **84**, 014023 (2011); S. Jung, A. Pierce, and J. D. Wells, Phys. Rev. D **83**, 114039 (2011); C. Delaunay, O. Gedalia, Y. Hochberg, G. Perez, and Y. Soreq, J. High Energy Phys. 08 (2011) 031; D. Krohn, T. Liu, J. Shelton, and L.-T. Wang, Phys. Rev. D **84**, 074034 (2011); N. Craig, C. Kilic, and M. J. Strassler, Phys. Rev. D **84**, 035012 (2011); R. Foot, Phys. Rev. D **83**, 114013 (2011); E. R. Barreto, Y. A. Coutinho, and J. Sa Borges, Phys. Rev. D **83**, 054006 (2011); A. R. Zerwekh, Phys. Lett. B **704**, 62 (2011); K. M. Patel and P. Sharma, J. High Energy Phys. 04 (2011) 085; K. Blum, C. Delaunay, O. Gedalia, Y. Hochberg, S. J. Lee, Y. Nir, G. Perez, and Y. Soreq, Phys. Lett. B **702**, 364 (2011); B. Bhattacherjee, S. S. Biswal, and D. Ghosh, Phys. Rev. D **83**, 091501 (2011); E. L. Berger, Q.-H. Cao, C.-R. Chen, C. S. Li, and H. Zhang, Phys. Rev. Lett. **106**, 201801 (2011); Y. Bai, J. L. Hewett, J. Kaplan, and T. G. Rizzo, J. High Energy Phys. 03 (2011) 003; J. Cao, L. Wang, L. Wu, and J. M. Yang, Phys. Rev. D **84**, 074001 (2011); B. Xiao, Y.-K. Wang, Z.-Q. Zhou, and S.-h. Zhu, Phys. Rev. D **83**, 057503 (2011); K. Cheung and T.-C. Yuan, Phys. Rev. D **83**, 074006 (2011); G. Marques-Tavares and M. Schmaltz, Phys. Rev. D **84**, 054008 (2011); S. Jung, A. Pierce, and J. D. Wells, Phys. Rev. D **84**, 091502 (2011); G. Bevilacqua, M. Czakon, C. G. Papadopoulos, and M. Worek, Phys. Rev. D **84**, 114017 (2011); M. Frank, A. Hayreter, and I. Turan, Phys. Rev. D **84**, 114007 (2011); J. Baglio, M. Beccaria, A. Djouadi, G. Macorini, E. Mirabella, N. Orlando, F. M. Renard, and C. Verzegnassi, Phys. Lett. B **705**, 212 (2011); D. Y. Shao, C. S. Li, J. Wang, J. Gao, H. Zhang, and H. X. Zhu, Phys. Rev. D **84**, 054016 (2011); E. Alvarez, L. Da Rold, J. I. S. Vietto, and A. Szynkman, J. High Energy Phys. 09 (2011) 007; L. Vecchi, J. High Energy Phys. 10 (2011) 003; G. Zhu, Phys. Lett. B **703**, 142 (2011); X.-P. Wang, Y.-K. Wang, B. Xiao, J. Xu, and S.-h. Zhu, Phys. Rev. D **83**, 115010 (2011); J. A. Aguilar-Saavedra and M. Perez-Victoria, Phys. Lett. B **705**, 228 (2011); S. Knapen, Y. Zhao, and M. J. Strassler, Phys. Rev. D **86**, 014013 (2012); E. Gabrielli, M. Raidal, and A. Racioppi, arXiv:1112.5885; P. Ko, Y. Omura, and C. Yu, Nuovo Cimento Soc. Ital. Fis. C **035N3**, 245 (2012); S. Chatrchyan *et al.* (CMS Collaboration), Phys. Lett. B **709**, 28 (2012); L. Wang, L. Wu, and J. M. Yang, Phys. Rev. D **85**, 075017 (2012); E. L. Berger, Q.-H. Cao, C.-R. Chen, J.-H. Yu, and H. Zhang, arXiv:1111.3641; N. Kosnik, I. Dorsner, J. Drobnak, S. Fajfer, and J. F. Kamenik, Proc. Sci., EPS-HEP (2011) 380 [arXiv:1111.0477]; K. Yan, J. Wang, D. Y. Shao, and C. S. Li, Phys. Rev. D **85**, 034020 (2012); J. N. Ng and P. T. Winslow, J. High Energy Phys. 02 (2012) 140; K. Kolodziej, Phys. Lett. B **710**, 671 (2012); J. H. Kuhn and G. Rodrigo, J. High Energy Phys. 01 (2012) 063; J. Cao, K. Hikasa, L. Wang, L. Wu, and J. M. Yang, Phys. Rev. D **85**, 014025 (2012); P. Ko, Y. Omura, and C. Yu, J. High Energy Phys. 01 (2012) 147; H. Davoudiasl, T. McElmurry, and A. Soni, Phys. Rev. D **85**, 054001 (2012); S. S. Biswal, S. Mitra, R. Santos, P. Sharma, R. K. Singh, and M. Won, Phys. Rev. D **86**, 014016 (2012); E. L. Berger, Q.-H. Cao, C.-R. Chen, J.-H. Yu, and H. Zhang, Phys. Rev. Lett. **108**, 072002 (2012); J. A. Aguilar-Saavedra, Nuovo Cimento Soc. Ital. Fis. C **035N3**, 167 (2012); B. Grinstein, C. W. Murphy, D. Pirtskhalava, and P. Uttayarat, arXiv:1203.2183; D. Duffty, Z. Sullivan, and H. Zhang, Phys. Rev. D **85**, 094027 (2012); P. Ko, Y. Omura, and C. Yu, arXiv:1205.0407; S. Y. Ayazi, S. Khatibi, and M. Mohammadi Najafabadi, arXiv:1205.3311; K. Hagiwara and J. Nakamura, arXiv:1205.5005; B. C. Allanach and K. Sridhar, Phys. Rev. D **86**, 075016 (2012); K. Hagiwara, J. Kanzaki, and Y. Takaesu, arXiv:1205.5173; D. Pagani, Proc. Sci., CORFU (2011) 027; G. Dupuis and J. M. Cline, arXiv:1206.1845.
[12] D.-W. Jung, P. Ko, J. S. Lee, and S.-h. Nam, Phys. Lett. B **691**, 238 (2010).
[13] J. Shu, K. Wang, and G. Zhu, Phys. Rev. D **85**, 034008 (2012).
[14] M. I. Gresham, I.-W. Kim, and K. M. Zurek, Phys. Rev. D **83**, 114027 (2011).
[15] J. A. Aguilar-Saavedra and M. Perez-Victoria, J. High Energy Phys. 09 (2011) 097; Phys. Rev. D **84**, 115013 (2011).
[16] C.-H. Chen, G. Cvetic, and C. S. Kim, Phys. Lett. B **694**, 393 (2011).
[17] H. Georgi, Phys. Rev. Lett. **98**, 221601 (2007).
[18] D. Choudhury and D. K. Ghosh, Int. J. Mod. Phys. A **23**, 2579 (2008).
[19] A. T. Alan and N. K. Pak, Europhys. Lett. **84**, 11001 (2008); A. T. Alan, N. K. Pak, and A. Senol, Europhys. Lett. **83**, 21001 (2008); H.-F. Li, H.-l. Li, Z.-G. Si, and Z.-J. Yang, Commun. Theor. Phys. **51**, 707 (2009); B. Sahin, Balk. Phys. Lett. **18N5**, 28 (2010); I. Sahin, Eur. Phys. J. C **60**, 431 (2009); T. M. Aliev, O. Cakir, and

K. O. Ozansoy, Phys. Lett. B **670**, 336 (2009); T. M. Aliev and K. O. Ozansoy, arXiv:0905.1597.
[20] M. Arai, N. Okada, and K. Smolek, Phys. Rev. D **79**, 074019 (2009).
[21] J. H. Kuhn and G. Rodrigo, Phys. Rev. D **59**, 054017 (1999); Phys. Rev. Lett. **81**, 49 (1998); M. T. Bowen, S. D. Ellis, and D. Rainwater, Phys. Rev. D **73**, 014008 (2006); L. G. Almeida, G. F. Sterman, and W. Vogelsang, Phys. Rev. D **78**, 014008 (2008); V. Ahrens, A. Ferroglia, M. Neubert, B. D. Pecjak, and L. L. Yang, Phys. Rev. D **84**, 074004 (2011); W. Bernreuther and Z.-G. Si, Phys. Rev. D **86**, 034026 (2012).
[22] N. Kidonakis, Phys. Rev. D **84**, 011504 (2011).
[23] W. Beenakker, A. Denner, W. Hollik, R. Mertig, T. Sack, and D. Wackeroth, Nucl. Phys. B **411**, 343 (1994); C. Kao, G. A. Ladinsky, and C. P. Yuan, Int. J. Mod. Phys. A **12**, 1341 (1997).
[24] A. Brandenburg, Phys. Lett. B **388**, 626 (1996); Eur. Phys. J. C **33**, s469 (2004); K. Melnikov and M. Schulze, Phys. Lett. B **700**, 17 (2011); S. J. Parke, Nuovo Cimento Soc. Ital. Fis. C **035N3**, 111 (2012).
[25] V. M. Abazov *et al.* (D0 Collaboration), Phys. Rev. Lett. **108**, 032004 (2012); G. Aad *et al.* (ATLAS Collaboration), Phys. Rev. Lett. **108**, 212001 (2012).
[26] G. Mahlon and S. J. Parke, Phys. Lett. B **411**, 173 (1997); Phys. Rev. D **53**, 4886 (1996).
[27] T. Stelzer and S. Willenbrock, Phys. Lett. B **374**, 169 (1996).
[28] T. Aaltonen *et al.* (CDF Collaboration), Phys. Rev. D **83**, 031104 (2011).
[29] CDF Collaboration, CDF, Note No. 10719-CONF, http://www-cdf.fnal.gov/physics/new/top/2011; V. M. Abazov *et al.* (D0 Collaboration), Phys. Lett. B **702**, 16 (2011).
[30] K. Bloom (D0 Collaboration), arXiv:1109.3691.
[31] W. Bernreuther and Z.-G. Si, Nucl. Phys. B **837**, 90 (2010).
[32] C. Kao, Phys. Lett. B **348**, 155 (1995); C.-S. Li, R. J. Oakes, J. M. Yang, and C. P. Yuan, Phys. Lett. B **398**, 298 (1997); S. Gopalakrishna, T. Han, I. Lewis, Z.-g. Si, and Y.-F. Zhou, Phys. Rev. D **82**, 115020 (2010); R. M. Godbole, K. Rao, S. D. Rindani, and R. K. Singh, J. High Energy Phys. 11 (2010) 144; C. Kao and D. Wackeroth, Phys. Rev. D **61**, 055009 (2000); K.-i. Hikasa, J. M. Yang, and B.-L. Young, Phys. Rev. D **60**, 114041 (1999); P.-Y. Li, G.-R. Lu, J. M. Yang, and H. Zhang, Eur. Phys. J. C **51**, 163 (2007); J. Cao, L. Wu, and J. M. Yang, Phys. Rev. D **83**, 034024 (2011).
[33] D. Chang, S.-C. Lee, and A. Soumarokov, Phys. Rev. Lett. **77**, 1218 (1996); S. Fajfer, J. F. Kamenik, and B. Melic, arXiv:1205.0264.
[34] T. Banks and A. Zaks, Nucl. Phys. B **196**, 189 (1982).
[35] H. Davoudiasl, Phys. Rev. Lett. **99**, 141301 (2007); A. Freitas and D. Wyler, J. High Energy Phys. 12 (2007) 033.
[36] V. Barger, Y. Gao, W.-Y. Keung, D. Marfatia, and V. N. Senoguz, Phys. Lett. B **661**, 276 (2008).
[37] H. Georgi, Phys. Lett. B **650**, 275 (2007).
[38] T. M. Aliev, A. S. Cornell, and N. Gaur, J. High Energy Phys. 07 (2007) 072; Phys. Lett. B **657**, 77 (2007); K. Cheung, W.-Y. Keung, and T.-C. Yuan, Phys. Rev. D **76**, 055003 (2007); Y. Liao and J.-Y. Liu, Phys. Rev. Lett. **99**, 191804 (2007); Y. Liao, Phys. Rev. D **76**, 056006 (2007); T. G. Rizzo, J. High Energy Phys. 10 (**2007**) 044; K. Cheung, W.-Y. Keung, and T.-C. Yuan, Phys. Rev. Lett. **99**, 051803 (2007); T. Kikuchi, N. Okada, and M. Takeuchi, Phys. Rev. D **77**, 094012 (2008); T. Kikuchi and N. Okada, Phys. Lett. B **661**, 360 (2008); C. H. Chen and C. Q. Geng, Can. J. Phys. **86**, 641 (2008); J. Bergstrom and T. Ohlsson, Phys. Rev. D **80**, 115014 (2009); A. Moyotl, A. Rosado, and G. Tavares-Velasco, Phys. Rev. D **84**, 073010 (2011); CMS Collaboration, Report No. CMS-PAS-EXO-09-011; G. A. Kozlov, arXiv:1002.2859; L.-G. Bian, arXiv:1108.1538; E. O. Iltan, Int. J. Mod. Phys. A **27**, 1250055 (2012).
[39] I. Lewis, arXiv:0710.4147; P. K. Das, Phys. Rev. D **76**, 123012 (2007); A. Freitas and D. Wyler, J. High Energy Phys. 12 (2007) 033; S. Hannestad, G. Raffelt, and Y. Y. Y. Wong, Phys. Rev. D **76**, 121701 (2007); T. Kikuchi and N. Okada, Phys. Lett. B **665**, 186 (2008); G. L. Alberghi, A. Y. Kamenshchik, A. Tronconi, G. P. Vacca, and G. Venturi, Phys. Lett. B **662**, 66 (2008); H. Goldberg and P. Nath, Phys. Rev. Lett. **100**, 031803 (2008); J. R. Mureika, Phys. Lett. B **660**, 561 (2008); S. Dutta and A. Goyal, Phys. Lett. B **664**, 25 (2008); S.-L. Chen, X.-G. He, X.-P. Hu, and Y. Liao, Eur. Phys. J. C **60**, 317 (2009); J. McDonald, J. Cosmol. Astropart. Phys. 03 (2009) 019; R. A. de Souza and J. E. Horvath, Phys. Rev. D **86**, 027502 (2012).
[40] M. Bander, J. L. Feng, A. Rajaraman, and Y. Shirman, Phys. Rev. D **76**, 115002 (2007); M. A. Stephanov, Phys. Rev. D **76**, 035008 (2007); M. J. Strassler, arXiv:0801.0629; N. G. Deshpande, S. D. H. Hsu, and J. Jiang, Phys. Lett. B **659**, 888 (2008); Y. Liao, Eur. Phys. J. C **55**, 483 (2008); M. Perez-Victoria, J. High Energy Phys. 01 (2009) 011; A. Rajaraman, AIP Conf. Proc. **1078**, 63 (2008).
[41] B. Grinstein, K. A. Intriligator, and I. Z. Rothstein, Phys. Lett. B **662**, 367 (2008); G. Mack and K. Symanzik, Commun. Math. Phys. **27**, 247 (1972).
[42] J.-P. Lee, arXiv:0911.5382.
[43] G. Cacciapaglia, G. Marandella, and J. Terning, J. High Energy Phys. 01 (2008) 070.
[44] P. Gaete and E. Spallucci, Phys. Lett. B **661**, 319 (2008); J. Galloway, D. Martin, and D. Stancato, arXiv:0802.0313; A. L. Licht and W.-Y. Keung, arXiv:0806.3596; Y. Liao, Eur. Phys. J. C **60**, 125 (2009); R. Basu, D. Choudhury, and H. S. Mani, Eur. Phys. J. C **61**, 461 (2009); A. Ilderton, Phys. Rev. D **79**, 025014 (2009); G. A. Kozlov, Phys. Part. Nucl. **41**, 957 (2010).
[45] M. Bahr, S. Gieseke, M. A. Gigg, D. Grellscheid, K. Hamilton, O. Latunde-Dada, S. Platzer, P. Richardson *et al.*, Eur. Phys. J. C **58**, 639 (2008).
[46] A. Belyaev, N. D. Christensen, and A. Pukhov, arXiv:1207.6082.
[47] J. Alwall, P. Demin, S. de Visscher, R. Frederix, M. Herquet, F. Maltoni, T. Plehn, D. L. Rainwater, and T. Stelzer, J. High Energy Phys. 09 (2007) 028; J. Alwall, M. Herquet, F. Maltoni, O. Mattelaer, and T. Stelzer, J. High Energy Phys. 06 (2011) 128.
[48] T. Aaltonen *et al.* (CDF Collaboration), Phys. Rev. D **79**, 112002 (2009).
[49] N. Agarwal, M. C. Kumar, P. Mathews, V. Ravindran, and A. Tripathi, Phys. Rev. D **80**, 035015 (2009).

[50] D. Choudhury, D. K. Ghosh, and Mamta, Phys. Lett. B **658**, 148 (2008).
[51] J. A. Aguilar-Saavedra and M. Perez-Victoria, Phys. Lett. B **701**, 93 (2011).
[52] S. Chatrchyan *et al.* (CMS Collaboration), J. High Energy Phys. 08 (2011) 005.
[53] CDF Collaboration, Report No. 10466, 2011, http://www-cdf.fnal.gov.
[54] V. M. Abazov *et al.* (D0 Collaboration), Phys. Rev. Lett. **106**, 022001 (2011).
[55] T. Aaltonen *et al.* (CDF Collaboration), Phys. Rev. Lett. **101**, 192002 (2008).
[56] V. M. Abazov *et al.* (D0 Collaboration), Phys. Lett. B **701**, 313 (2011).
[57] R. Mohanta and A. K. Giri, Phys. Lett. B **660**, 376 (2008).
[58] J. K. Parry, Phys. Rev. D **78**, 114023 (2008).
[59] G. Aad *et al.* (ATLAS Collaboration), J. High Energy Phys. 09 (2012) 041.
[60] S. Chatrchyan *et al.* (CMS Collaboration), arXiv:1209.4397 [J. High Energy Phys. (to be published)].
[61] CMS Collaboration, CMS, Report No. PASS EXO-10-001, http://cms-physics.web.cern. ch/cms-physics/public/EXO-10-001-pas.pdf.
[62] CMS Collaboration, CMS, Report No. PASS QCD-10-011, http://cdsweb.cern.ch/record/1280682/files/QCD-10-011-pas.pdf.
[63] ATLAS Collaboration, Report No. ATLAS-CONF-2012-134, http://cdsweb.cern.ch/record/1478422/files/ATLAS-CONF-2012-134.pdf.
[64] G. Aad *et al.* (ATLAS Collaboration), J. High Energy Phys. 09 (2012) 139.
[65] S. Chatrchyan *et al.* (CMS Collaboration), arXiv:1208.0957 [Phys. Lett. B (to be published)].